

Harnessing the Role of HDAC6 in Idiopathic Pulmonary Fibrosis: Design, Synthesis, Structural Analysis, and Biological Evaluation of Potent Inhibitors

Giuseppe Campiani,* Caterina Cavella, Jeremy D. Osko, Margherita Brindisi, Nicola Relitti, Simone Brogi, A. Prasanth Saraswati, Stefano Federico, Giulia Chemi, Samuele Maramai, Gabriele Carullo, Benedikt Jaeger, Alfonso Carleo, Rosaria Benedetti, Federica Sarno, Stefania Lamponi, Paola Rottoli, Elena Bargagli, Carlo Bertucci, Daniele Tedesco, Daniel Herp, Johanna Senger, Giovina Ruberti, Fulvio Saccoccia, Simona Saponara, Beatrice Gorelli, Massimo Valoti, Breándan Kennedy, Husvinee Sundaramurthi, Stefania Butini,* Manfred Jung, Katy M. Roach, Lucia Altucci, Peter Bradding, David W. Christianson, Sandra Gemma,^{|||} and Antje Prasse^{|||}

 Cite This: *J. Med. Chem.* 2021, 64, 9960–9988

 Read Online

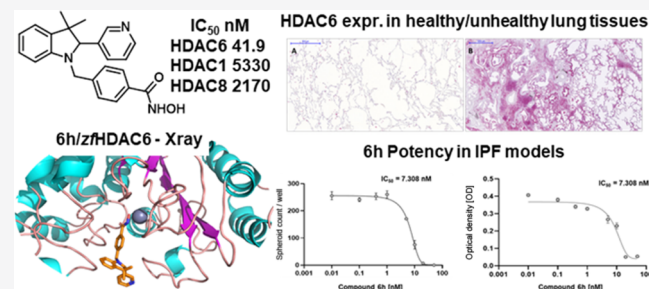
ACCESS |

 Metrics & More

 Article Recommendations

 Supporting Information

ABSTRACT: Idiopathic pulmonary fibrosis (IPF) is an interstitial lung disease characterized by a progressive-fibrosing phenotype. IPF has been associated with aberrant HDAC activities confirmed by our immunohistochemistry studies on HDAC6 overexpression in IPF lung tissues. We herein developed a series of novel *h*HDAC6 inhibitors, having low inhibitory potency over *h*HDAC1 and *h*HDAC8, as potential pharmacological tools for IPF treatment. Their inhibitory potency was combined with low *in vitro* and *in vivo* toxicity. Structural analysis of **6h** and structure–activity relationship studies contributed to the optimization of the binding mode of the new molecules. The best-performing analogues were tested for their efficacy in inhibiting fibrotic sphere formation and cell viability, proving their capability in reverting the IPF phenotype. The efficacy of analogue **6h** was also determined in a validated human lung model of TGF- β 1-dependent fibrogenesis. The results highlighted in this manuscript may pave the way for the identification of first-in-class molecules for the treatment of IPF.



INTRODUCTION

Millions of people worldwide suffer from lung diseases that affect the whole respiratory system including the airways, air sacs (alveoli), lung interstitium, blood vessels, and pleura. Interstitial lung diseases (ILDs) are a numerous and heterogeneous group of diseases that affect the lung interstitium, a thin layer of cells, and the tissue matrix between the alveoli, which contain blood vessels and cells that help support the alveoli, allowing efficient gas exchange. The pathological deposition of collagen and other connective tissue proteins causes progressive scarring and fibrosis. This disorganized damaged tissue impairs the vital role of the lungs in respiration with devastating consequences in terms of functional capacity, quality of life, and increased mortality.¹ The most relevant ILDs may be associated with a progressive-fibrosing phenotype, and these ILDs are classified with a term known as progressive-fibrosing rare diseases. Among these progressive-fibrosing ILDs, the most common is idiopathic pulmonary fibrosis (IPF), characterized by a very poor prognosis.

IPF accounts for 25% of all ILDs with about 35 000 new cases diagnosed every year in Europe and 5 000 000 worldwide. IPF has an annual incidence of 0.22–7.4 per 100 000 people with a prevalence of 1.25–23.4 cases per 100 000 population.² The contribution of inflammation to the fibrotic process in IPF is controversial, but conventional anti-inflammatory therapies (e.g., glucocorticoids) are not efficacious.^{3,4} In the past decades, many clinical trials have been designed to determine the safety and efficacy of pharmacotherapies for patients with IPF. However, so far, only two drugs (pirfenidone **1** and nintedanib **2**, Figure 1) were found to have an impact on disease progression. These two drugs have been approved for the

Received: February 1, 2021

Published: July 12, 2021



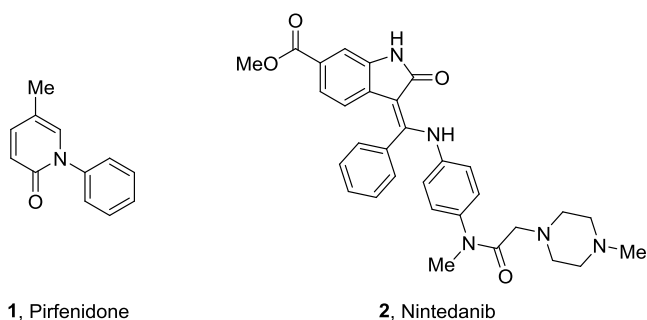


Figure 1. Representative structures of the FDA-approved drugs for the treatment of IPF.

treatment of IPF by regulatory agencies and are currently in clinical use worldwide.^{5,6} Even though these drugs possess an acceptable safety profile, they only delay disease progression and fail to reverse lung damage.^{2,6,7}

Epigenetic regulation modulates many cellular processes and greatly influences key disease mechanisms. Histone deacetylase (HDAC) enzymes play a crucial role either as biomarkers or therapeutic targets owing to their involvement in specific pathophysiological pathways. HDACs are a class of enzymes responsible for the removal of acetyl groups from histones leading to decreased gene transcription and are mostly involved in biological processes related to chromatin.⁸ HDACs can deacetylate both histone and nonhistone substrates, including transcription factors such as p53, Rb, and others. They also regulate key protein substrates such as α -tubulin, actin, and cortactin and can thereby influence many cellular processes, namely, apoptosis, cell signaling, and DNA repair, replication, and recombination.⁹ HDACs represent a family of 11 zinc-dependent enzymes (HDAC1–11) clustered into three groups (classes I, II, and IV). Class I comprises nuclear enzymes HDAC1–3 and HDAC8, while class II contains HDAC4–7 and

HDAC9–10 possessing nucleocytoplasmic shuttling ability, also observed in class IV HDAC (HDAC11). Class III HDAC contains nonzinc-dependent enzymes, called sirtuins (SIRT1–7), requiring NAD⁺ for their activity.¹⁰ Overexpression of HDACs is implicated in many pathological conditions including cancer, neurodegeneration, and rare diseases such as IPF as confirmed by us (see below).^{7,11–13} Currently, four pan-HDAC inhibitors (HDACis) have been approved by the FDA for the treatment of hematological malignancies, and many other HDACis are under clinical investigation for cancer and other diseases.^{14,15} However, none of them have been approved for fibrotic diseases yet.

Aberrant HDAC activities are observed in fibrotic diseases; mounting evidence indicates the involvement of HDACs in the initiation and progression of fibrosis occurring in organs such as the lungs, heart, liver, and kidneys; preliminary studies performed on animal models have shown that HDACi can ameliorate various forms of fibrosis.^{16,17} Due to the limitations of pirfenidone (1) and nintedanib (2) in IPF, and a lack of promising clinical candidates, an unprecedented effort is required to enrich the therapeutic arsenal available to tackle IPF and other rare fibrotic disorders.¹⁸ In particular, the regulation of transforming growth factor β 1 (TGF- β 1) by HDAC6, a microtubule-associated deacetylase, is significant in the pathogenesis and progression of fibrotic diseases through epithelial–mesenchymal transitions (EMT).¹⁹ Fibrotic lesions are associated with an aberrant expression of TGF- β 1, which is a potent EMT inducer.²⁰ Recent reports suggest that HDAC6 inhibition by siRNA or tubacin (3, Figure 2) reduces the TGF- β 1-induced EMT markers and impairs SMAD3 activation in response to TGF- β 1. Since SMAD3 is a core element for TGF- β 1 signaling, its inactivation impairs HDAC6-dependent deacetylation of α -tubulin highlighting the role of HDAC6 in EMT through the TGF- β 1–SMAD3 signaling pathway.¹⁷ Several reports highlighted the efficacy of pan-HDACi (such as SAHA (4) and panobinostat (5), Figure 2) against IPF and fibrotic lung

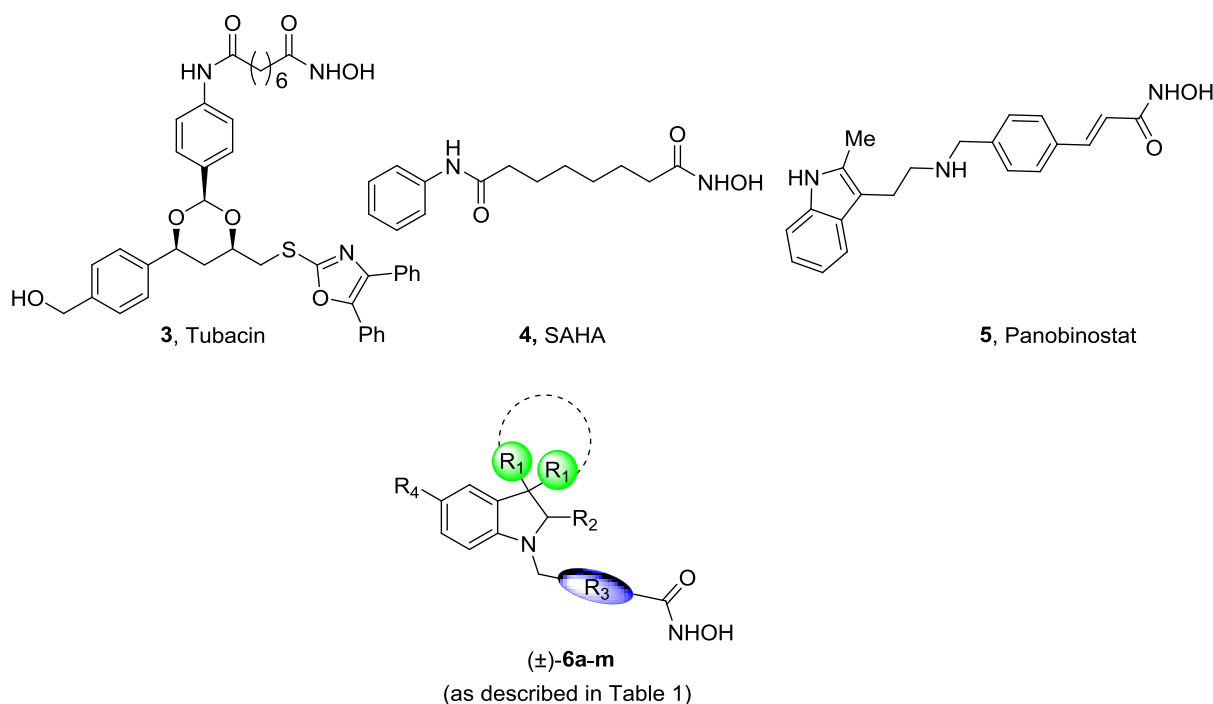


Figure 2. Representative structures of some HDACis as antifibrotic agents and title compounds (±)-6a–m (as described in Table 1).

diseases,²¹ mainly based on the reduction in fibroblast-myofibroblast differentiation and fibroblast proliferation induced by TGF- β 1.^{22,23} Recently, HDAC6 inhibitors showed to protect mice from lung fibrosis by repressing TGF- β 1-induced collagen expression and diminished Akt phosphorylation.²⁴

For many decades, HDACs have drawn widespread attention as therapeutic agents for different diseases. However, due to reports indicating several challenges encountered with the use of pan-HDACi and their off-target effects, there is an urgent need to develop isoform-selective inhibitors to be investigated in fibrotic diseases.^{25,26} Based on these observations, further studies pointed out how only HDAC6 enzyme could be selectively targeted, mostly because of its cytoplasmic localization.²⁷

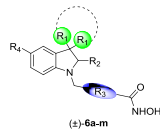
The general pharmacophoric model of HDACi comprises (i) a cap-group, which interacts with the amino acid residues on the surface of the enzyme, (ii) a zinc-binding group (ZBG), usually a hydroxamic acid group, chelating the Zn²⁺ necessary for the inhibitory activity, and (iii) a linker group between these portions. Our research group has been actively involved in the development of potent HDACi as therapeutic agents for the treatment of cancers, rare disorders, and infectious diseases.^{28–31} Based on reports outlining the HDACi (compound 3)-mediated impairment of the TGF- β 1-EMT pathway, we designed and synthesized novel HDAC6is (6a–m, Table 1) selective over *h*HDAC1 and *h*HDAC8, as promising pharmaceutical tools for the treatment of IPF, with the aim of investigating also the role of this enzyme isoform in fibrotic processes. In this strategy, a key challenge was the rational improvement of HDAC6 selectivity over other specific isoforms, such as HDAC1 and HDAC8, class I nuclear HDACs. While HDAC1 deacetylates histones and transcriptional regulators, HDAC8 is fundamentally distinct from HDAC1–3 and is the only isoform for which the gene lies in the X chromosome. Moreover, because of similarities in the active site of HDAC6 and HDAC8, discriminating between these two isoforms is challenging.

Following our previous experience on HDAC6 inhibition by small molecules, we decided to investigate the effect of introducing a bulkier cap-group to increase the number of interactions with the lipophilic pocket of the HDAC6 enzyme minimizing interactions with the catalytic sites of *h*HDAC1 and *h*HDAC8 isoforms.^{31,32} This was achieved by decorating the indoline scaffold with different aromatic and aliphatic moieties at the C2 and C3 positions, respectively. Thereafter, we determined the affinity of the newly developed series of compounds on *h*HDAC6, *h*HDAC8, and *h*HDAC1. To establish the binding mode on HDAC6 of the new series, we cocrystallized compound **6h** with zebrafish HDAC6 (*zf*HDAC6) (2.04 Å). The best-performing compounds were then evaluated for their antifibrotic and pharmacokinetic profiles. In addition, their potential toxicity, cytotoxicity, cardiotoxicity, and mutagenicity were also evaluated in different *in vitro* and *in vivo* models.

RESULTS AND DISCUSSION

Chemistry. The synthetic approach for the development of the new molecules is based on three key steps: (i) the formation of the suitable ketones to be subjected to interrupt Fischer indolization and subsequent indolenine reduction, (ii) reductive amination on the indoline nitrogen, and (iii) the conversion of the methyl ester to hydroxamic acid.

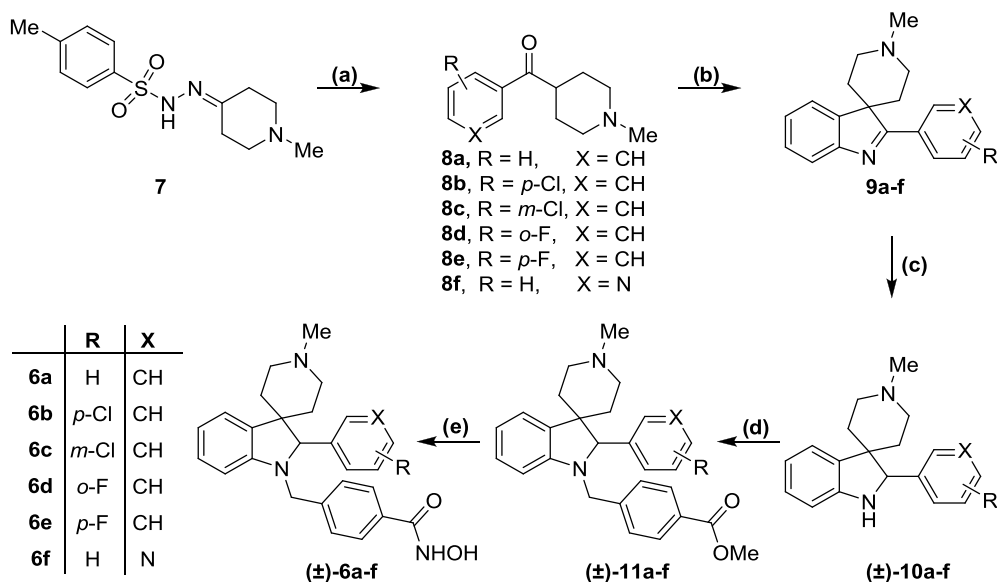
Table 1. Inhibitory Activity of Compounds 6a–m toward *h*HDAC1 and *h*HDAC6 (as IC₅₀, nM)^a



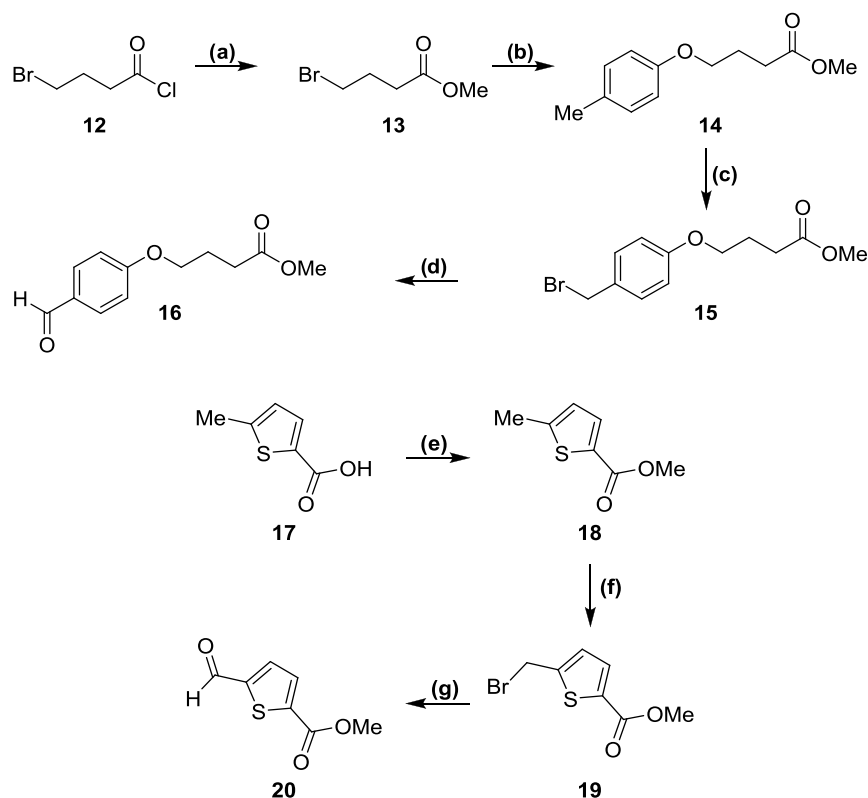
Cmpd	R ₁	R ₂	R ₃	R ₄	<i>h</i> HDAC1 (IC ₅₀ nM)	<i>h</i> HDAC6 (IC ₅₀ nM)	HDAC1/6
(±)-6a				H	4290	73.2 ± 11.6	59
(±)-6b				H	3650	164.8 ± 30.7	22
(±)-6c				H	8100	110.6 ± 15.5	73
(±)-6d				H	4850	28.5 ± 3.8	170
(±)-6e				H	6160	141.9 ± 38.6	43
(±)-6f				H	7600	111.7 ± 19.4	68
(±)-6g	Me			H	18680	166.2 ± 31.3	112
(±)-6h	Me			H	5330	41.9 ± 6.0	127
(R)-(+)-6h	Me			H	16190	90.6 ± 15.5	178
(S)-(–)-6h	Me			H	3380	71.3 ± 8.4	47
(±)-6i	Me			OMe	5320	67.2 ± 15.3	79
(±)-6j	Me			H	6320	810.8 ± 59.6	8
(±)-6k	Me			H	1630	616.3 ± 40.7	3
(±)-6l	Me			H	10790	61.1 ± 12.9	177
(±)-6m				H	8100	151.6 ± 26.4	53
Tubacin, 3 ⁷	-	-	-	-	1400	4	350
SAHA, 4 ⁷	-	-	-	-	33	33	1

^aEach value is the mean of at least three determinations; results are expressed with \pm standard deviation (SD). When not specified, SD is <10% of the IC₅₀.

The synthesis of tosylhydrazones **7**, **21**, and **26** was achieved following the procedure applied in our previous work starting from commercially available supplies.³⁰ In Scheme 1, the synthesis of the final compounds **6a–f** is reported. The tosylhydrazone **7** was converted to ketones **8a–f** after treatment with the opportune aldehyde and Cs₂CO₃. **8a–f** were subjected

Scheme 1. Synthesis of Compounds (\pm)-6a–f^a

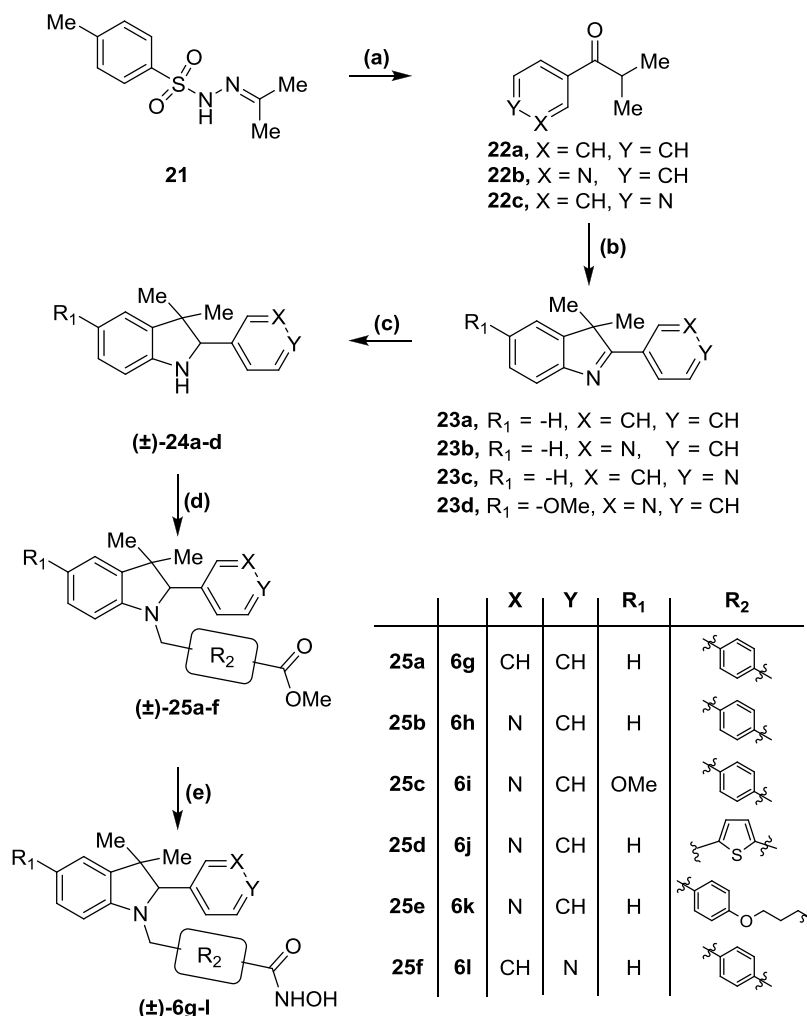
^aReagents and conditions: (a) Appropriate aryl aldehyde, Cs₂CO₃, 1,4-dioxane, 110 °C, 14 h, 40–100%; (b) phenylhydrazine, H₂SO₄, 1,4-dioxane, 70 °C, 2 h, then 25 °C, 14 h, 30–66%; (c) NaBH₄, MeOH, 25 °C, 12 h or H₂/Pd, MeOH, 25 °C, 12 h, 40–100%; (d) methyl 4-formylbenzoate, NaBH₃CN, EtOH, AcOH, 70 °C, 14 h, 25–43%; (e) NH₂OH (50% in H₂O), KOH, DCM/MeOH from 0 to 25 °C, 12 h, 33–73%.

Scheme 2. Synthesis of Aldehydes 16 and 20^a

^aReagents and conditions: (a) MeOH, from 0 to 25 °C, 12 h, 100%; (b) *p*-cresol, Cs₂CO₃, MeCN, 90 °C, 14 h, 74%; (c) NBS, AIBN, CCl₄, 90 °C, 1 h; (d) NBS, DMSO, 100 °C, 2 h, 30% over two steps; (e) SOCl₂, MeOH, 0–25 °C, 12 h, 100%; (f) NBS, AIBN, CCl₄, 80 °C, 4 h, 60%; (g) NMO, MeCN, 25 °C, 12 h, 70%.

to a Fischer protocol with phenylhydrazine and sulfuric acid affording spiroindolenines **9a–f**. Catalytic hydrogenation of the metastable indolenine followed by reductive amination with methyl 4-formylbenzoate afforded spiroindolines **11a–f**. These

intermediates were converted to their corresponding hydroxamic acids (\pm)-**6a–f** after treatment with KOH and aqueous NH₂OH. All of the products were obtained as racemic mixtures.

Scheme 3. Synthesis of Compounds (\pm)-6g–l^a

^aReagents and conditions: (a) Appropriate aryl aldehyde, Cs₂CO₃, dioxane, 110 °C, 14 h, 89–100%; (b) for **23a–c**: phenylhydrazine, AcOH, 80 °C, 14 h; for **23d**: 4-methoxyphenylhydrazine, AcOH, 80 °C, 14 h, 30–48%; (c) NaBH₄, MeOH, 25 °C, 12 h or H₂, Pd/C, MeOH, 25 °C, 12 h, 50–79%; (d) for (\pm)-**25a–c** and **25f**: methyl 4-formylbenzoate, EtOH, AcOH, NaBH₃CN, 40 °C, 14 h; for (\pm)-**25d**: **20**, EtOH, AcOH, NaBH₃CN, 40 °C, 14 h; for (\pm)-**25e**: **16**, NaBH(OAc)₃, DCM, 40 °C, 14 h, 20–84%; (e) NH₂OH (50% in H₂O), KOH, DCM/MeOH from 0 to 25 °C, 12 h, 18–79%.

The synthesis of the linker moieties **16** and **20** is described in Scheme 2. 4-Bromobutyl chloride was converted to its corresponding methyl ester and then used to alkylate *p*-cresol in the presence of Cs₂CO₃. The resulting compound **14** was subjected to radical bromination, leading to the formation of unstable intermediate **15** that was immediately oxidized by NBS in the presence of DMSO. This reaction provided aldehyde **16** in good yields.

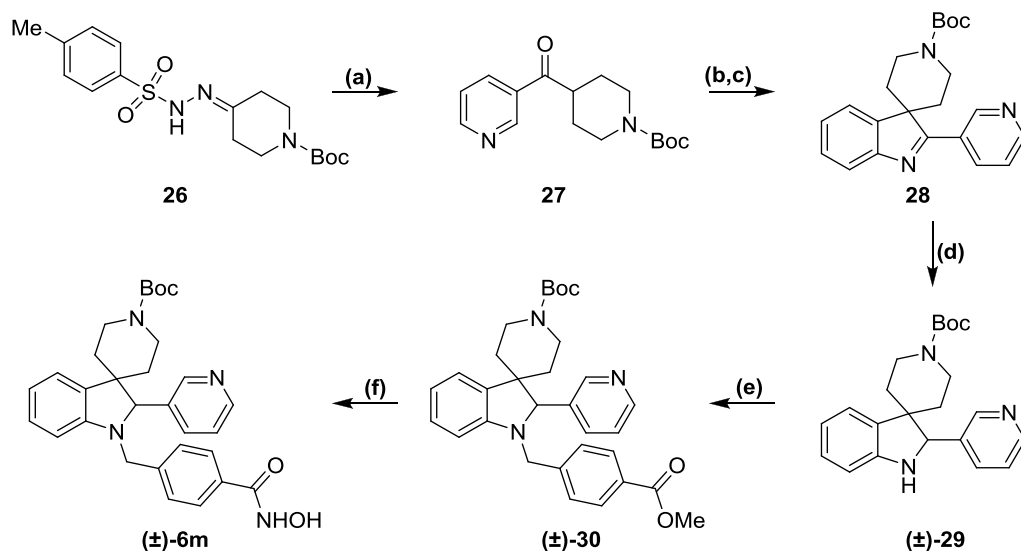
For the synthesis of lateral chain **20**, 5-methylthiophene-2-carboxylic acid was converted into its corresponding methyl ester **18**. Compound **18** was subjected to a radical bromination with NBS and AIBN affording the bromo-derivative **19**. The aldehyde **20** was obtained from intermediate **19** upon reaction with 4-methylmorpholine *N*-oxide (NMO) in MeCN.

In Scheme 3, the synthesis of compounds **6g–l** is described. Following the synthetic approach previously shown in Scheme 1, tosylhydrazones **21** were reacted with suitable arylaldehydes to obtain ketones **22b–c**. The cyclization reaction between phenylhydrazine and compounds **22a–c** provided derivatives **23a–c**. **22b** was reacted with 4-methoxyphenylhydrazine to furnish compound **23d**. These intermediates were reduced with

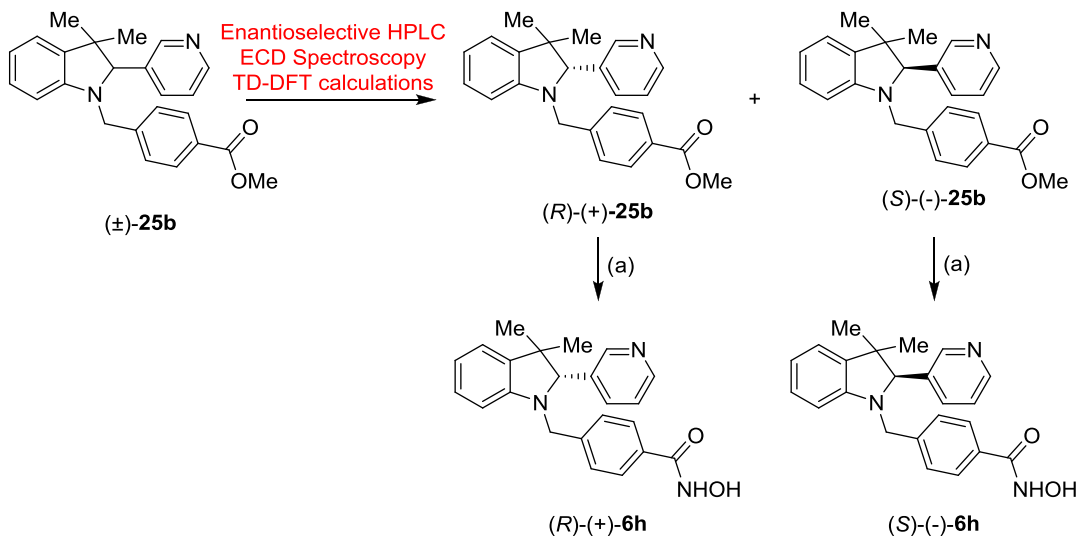
NaBH₄ or by catalytic hydrogenation affording **24a–d**. Indoline derivatives were subjected to a reductive amination protocol with the appropriate aldehydes generating the compounds (\pm)-**25a–f** that were reacted with KOH and NH₂OH to provide hydroxamic acids (\pm)-**6g–l** as racemic mixtures.

In Scheme 4, the synthesis of compound **6m** is reported. Following the previously described procedure, tosylhydrazone **26** was reacted with 3-pyridinecarboxaldehyde and Cs₂CO₃ to afford compound **27**. This intermediate was subjected to a Fischer reaction to get the corresponding indolenine. The loss of the Boc protecting group due to the acidic conditions of the Fischer reaction required subsequent treatment with Boc₂O for its reinstallation, providing indolenine **28**. The reduction of this intermediate by catalytic hydrogenation followed by a reductive amination with methyl 4-formylbenzoate afforded (\pm)-**30** as a racemic mixture. This compound was converted to hydroxamic acid (\pm)-**6m** after treatment with KOH and NH₂OH.

To evaluate the stereoselective interaction with *h*HDAC6, we decided to resolve the racemic mixture of (\pm)-**6h**. Analogue **6h** successfully cocrystallized with the enzyme (Figure 4). To this end, we resolved the racemic mixture of esters (\pm)-**25b** by chiral

Scheme 4. Synthesis of Compound (\pm)-6m^a

^aReagents and conditions: (a) 3-Pyridinecarboxaldehyde, Cs₂CO₃, dioxane, 110 °C, 14 h, 100%; (b) phenylhydrazine, H₂SO₄, dioxane, 70 °C, 2 h, 14%; (c) Boc₂O, THF, NaOH, 25 °C, 2 h, 100%; (d) H₂, Pd/C, MeOH, 25 °C, 12 h, 100%; (e) methyl 4-formylbenzoate, NaBH₃CN, EtOH, AcOH, 70 °C, 14 h, 30%; (f) NH₂OH (50% in H₂O), KOH, DCM/MeOH from 0 to 25 °C, 12 h, 51%.

Scheme 5. Synthesis of (*R*)-(+)-6h and (*S*)-(-)-6h^a

^aReagents and conditions: (a) NH₂OH (50% in H₂O), KOH, DCM/MeOH from 0 to 25 °C, 12 h, 34–38%.

high-performance liquid chromatography (HPLC) (see the Supporting Information (SI)). The two enantiomers, (+)-25b and (−)-25b, were isolated with an enantiomeric excess of >99% (Figure S1 of the Supporting Information) and underwent the final reaction giving the two enantiomers of 6h; in particular, (+)-25b and (−)-25b yielded (+)-6h and (−)-6h, respectively (Scheme 5). The absolute configuration of (−)-25b was established by electronic circular dichroism (ECD) spectroscopy and time-dependent density functional theory (TD-DFT) calculations. The comparison between the experimental and theoretical spectra (Figure 3) allowed us to assign the (*S*)-absolute configuration to (−)-25b ($r = 0.7345$ for the ECD spectra) and, consequently, to (−)-6h.

Crystal Structure Determination of the zfHDAC6–6h Complex. The 2.04 Å-resolution crystal structure of the zfHDAC6–6h complex containing two monomers in the

asymmetric unit of a monoclinic unit cell was obtained. There are no major conformational changes between the liganded and unliganded (PDB SEEM) enzyme structures, and the root-mean-square deviation (RMSD) is 0.15 Å for 309 Cα atoms in monomer A. By soaking experiments with racemic 6h, we obtained cocrystallization of the (*S*)-enantiomer only. The inhibitor hydroxamate group coordinates to the catalytic Zn²⁺ ion through only the ionized N–O[−] moiety (Figure 4). The Zn²⁺-bound oxyanion also accepts a hydrogen bond from the phenolic hydroxyl group of Y745. Weak electron density for a Zn²⁺-bound water molecule is also observed. This water molecule forms hydrogen bonds with H573, H574, and the carbonyl group of the hydroxamate moiety.

The inhibitor capping group consists of a 3,3-dimethyl-2-(pyridine-3-yl)indoline, and the pyridine nitrogen forms a hydrogen bond with N645 at the mouth of the active site cleft.

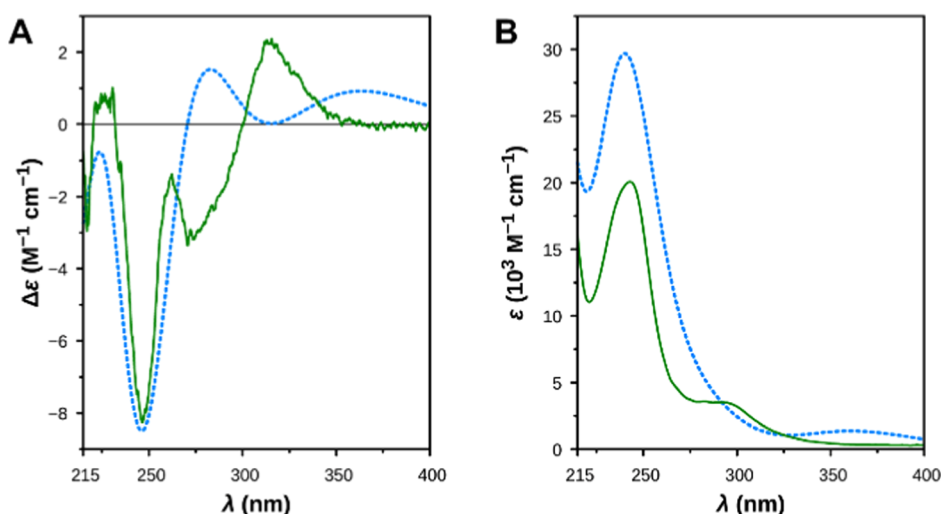


Figure 3. Comparison between the experimental spectra of (–)-25b (solid lines) and the theoretical spectra of (S)-25b, as determined by TD-DFT calculations (dashed lines). (A) ECD spectra. (B) UV spectra.

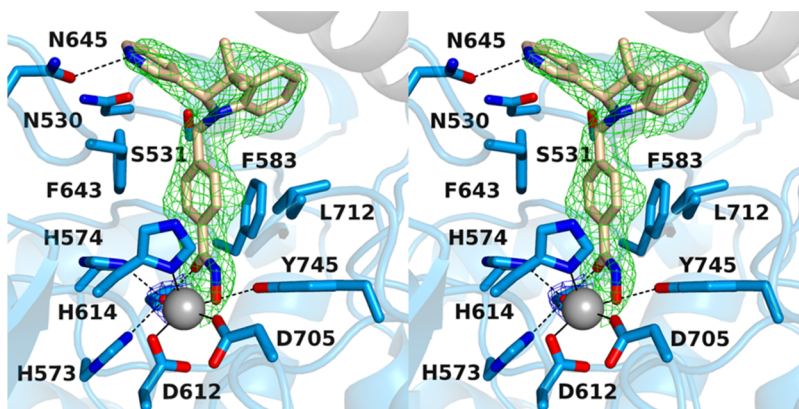


Figure 4. Stereoview of a Polder omit map of the zfHDAC6/(S)-6h complex (PDB 6V79; contoured at 2.5 σ). The Zn²⁺-bound water molecule is contoured at 3.5 σ . Atoms are color-coded as follows: C = light blue (zfHDAC6 monomer A), light gray (zfHDAC6 monomer B), or wheat (inhibitor), N = blue, O = red, Zn²⁺ = gray sphere, and Zn²⁺-bound water molecule = small red sphere. Metal coordination and hydrogen bond interactions are indicated by solid and dashed black lines, respectively.

The pyridine NH group is presumably protonated in this environment to donate the hydrogen bond to the side chain carbonyl group of N645. The orientation of N645 is fixed by other hydrogen bond interactions with the protein. This hydrogen bond may rationalize the orientation of the capping group into the L2 pocket, where relatively few HDAC6 inhibitors orient unless they possess bifurcated capping groups.³³ Notably, however, hHDAC6 has a methionine residue at position 645 instead of an asparagine, so this interaction is specific only to the zebrafish enzyme. No other hydrogen bond interactions with the protein, either direct or water-mediated, are observed for the inhibitor capping group.

Docking Studies and Structure–Activity Relationship (SARs). Computational investigations were performed using the crystal structure of zfHDAC6 in comparison with hHDAC6 applying the docking protocol described in the [Experimental Section](#), evaluating the performance of our docking protocol. All molecules were docked on HDAC1 and HDAC6 by their (S) and (R) enantiomers (see the [Supporting Information](#)). The most relevant docking results are herein discussed for selected molecules/enantiomers. Aiming at investigating the binding modes of the developed compounds into the catalytic sites of hHDAC1 and hHDAC6 enzymes and performing the SAR

analysis, we combined experimental data ([Table 1](#)) with *in silico* investigation (human enzymes, [Figures 5](#) and [S3–S15](#)).^{28,29} Generally, for the selected compounds, we observed a common trend in their binding mode with the HDAC6 enzyme, establishing a higher number of contacts compared to HDAC1.

In particular, taking into account (S)-(–)-6h, complexed with zfHDAC6, when docked into hHDAC6 and zfHDAC6, it similarly accommodates in both enzymes,^{28–30} see the SI for details ([Figure S2](#)). This study confirms that zfHDAC6 could be a valuable model for translating the results of potential inhibitors to hHDAC6.³¹

When docked in zfHDAC6, both enantiomers of 6a, besides the metal coordination, with their hydroxamate moiety target G619 and Y782, the benzyl linker forms π – π stacking with H651 and F680, while the benzyl substituent establishes π – π stacking with F679. The cap-group establishes hydrophobic contacts with F620 and L749. The higher number of contacts of 6a reflects its higher affinity for HDAC6 over HDAC1 (IC₅₀ values: HDAC1 = 4290 nM; HDAC6 = 73.2 nM) (see the [SI](#) for a detailed discussion of the docking results for HDAC1). The introduction of Cl at the *p*- or *m*-position of the phenyl ring (6b and 6c, respectively) does not substantially modify the binding

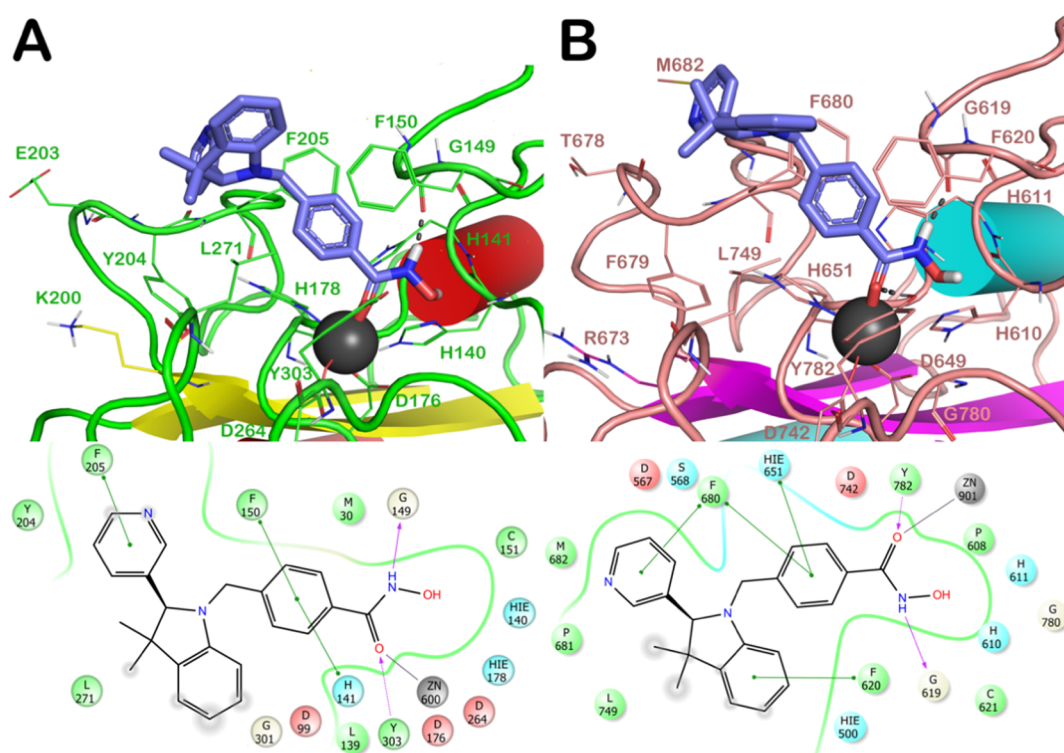


Figure 5. Docked poses of (S)-(-)-**6h** (light blue sticks) into HDAC1 (PDB ID 4BKX; panel A) and HDAC6 (PDB ID SEDU; panel B). The residues in the active sites are represented as lines, and the proteins are represented as cartoons. Zn^{2+} is represented as a gray sphere. H-bonds are represented as black dotted lines, while the metal coordination bond is represented by a red stick.

mode retrieved for **6a**. The same was true after the introduction of a *p*-F-phenyl (**6e**) or a pyridin-3-yl (**6f**) at C2 (see the SI).

Among the halogenated analogues, the *o*-F-phenyl substituent at the chiral C2 of **6d** (Figure S6) favored beneficial interactions with F679 and H651 residues when in the R configuration. The replacement of the spiro *N*-methylpiperidine moiety by two geminal methyl groups at the 3-position of the indoline system of **6a** led to analogue **6g**. **6g** showed similar contacts to spiro-fused analogues (**6a–f**, **m**) for both enantiomers ((S)-**6g**: π - π stacking with H651 and F680; the cap-group with F620; (R)-**6g** lacks the contact with F620). The introduction of a pyridin-3-yl substituent at the 2-position of the indoline core of **6g** led to analogue **6h**. The docking output for the **6h** S-enantiomer on HDAC1/6 isoforms is reported in Figure 5 (R-enantiomer in Figure S10). In HDAC1 active site, **6h** established critical π - π stackings involving the benzyl linker (H141 and F150) and the cap-group (F205) (Figure 5A). The R-enantiomer (Figure S10A) establishes, in addition to the contacts of the hydroxamate moiety, π - π stacking with H141 (benzyl linker) and Y204 (cap-group). Figure 5B highlights the contacts of (S)-**6h** with HDAC6: the benzyl linker interacts with H651 and F680 (π - π stacking), while the pyridine at C2 interacts with F680. Interactions of (R)-**6h** are shown in Figure S10B. Docking data support the higher affinity of **6h** for HDAC6 (IC_{50} HDAC1 = 5330 nM; IC_{50} HDAC6 = 41.9 nM).

A similar result was obtained when a methoxy substituent was introduced on the cap-group of **6h**, obtaining compound **6i** (Figure S11, IC_{50} : HDAC1 = 5320 nM and HDAC6 = 67.2 nM).

The replacement of the benzyl linker of **6h** with a thienylmethyl linker (**6j**) or a propyloxybenzyl system (**6k**) caused a large decrease in potency against the HDAC6 enzyme (Figures S12–S13). The introduction of pyridin-4-yl at C2 (**6l**) confirmed the same interactions observed for **6h**.

The *N*-Me group of **6f** was also replaced by a Boc group (**6m**), establishing contacts into HDAC1 and HDAC6 similar to those identified for other analogues (Figure S15), indicating that the protonatable function is not critical for binding HDAC enzymes.

In addition to *h*HDAC1 and *h*HDAC6, the potency of three representative inhibitors (**6d**, **h**, **l**, Table 2) was assessed on the

Table 2. Inhibitory Activity of Compounds **6d**, **h**, **l**, as IC_{50} (μM), against the *h*HDAC8 Enzyme^a

compound	6d	6h	6l	TubA ²⁸
IC_{50} (μM) ^a	3.49 ± 1.54	2.17 ± 0.70	4.64 ± 1.28	0.695

^aThe concentration range of all compounds (40 nM–50 μM) was determined using the reference compound TubA and the results are expressed as standard deviations.

*h*HDAC8 isoform, which represents a unique member of the class I HDAC family. HDAC8 is endowed with the ability to recognize both histone and nonhistone substrates. This isoform is ubiquitously expressed, and it is localized either in the nucleus or in the cytoplasm.³⁴ Discrimination between *h*HDAC6 and *h*HDAC8 binding sites was achieved and analogues **6d**, **6h**, and **6l** demonstrated low potency against HDAC8 (IC_{50} in the range of 2.17–4.64 μM , Table 2).

HDAC6 is a Privileged Target of This New Series: Western Blot Analysis. The selectivity issues for HDACi is a crucial point in HDAC research; however, the reliability of *in vitro* enzymatic tests on all of the 11 HDAC isoforms is debatable, as recently pointed out.³⁵ Accordingly, for assessing HDAC6 preferential interaction, the most potent and interesting analogues (**6a**, **6d**, **6e**, **6h**, and **6l**) were engaged in experiments in living cells. We performed our cell-based assays using three cancer cell lines including hematological (NB4,

acute promyelocytic leukemia) and solid (U2OS, osteosarcoma and U87, glioblastoma) cancer cells. In all of these cells, the levels of tubulin acetylation (the client protein of HDAC6) and acetylation of histone H3 (the primary substrate of HDAC1 and other nuclear HDACs) were evaluated after incubation of our compounds at 5 μ M for 30 h (Figure 6). Under these conditions,

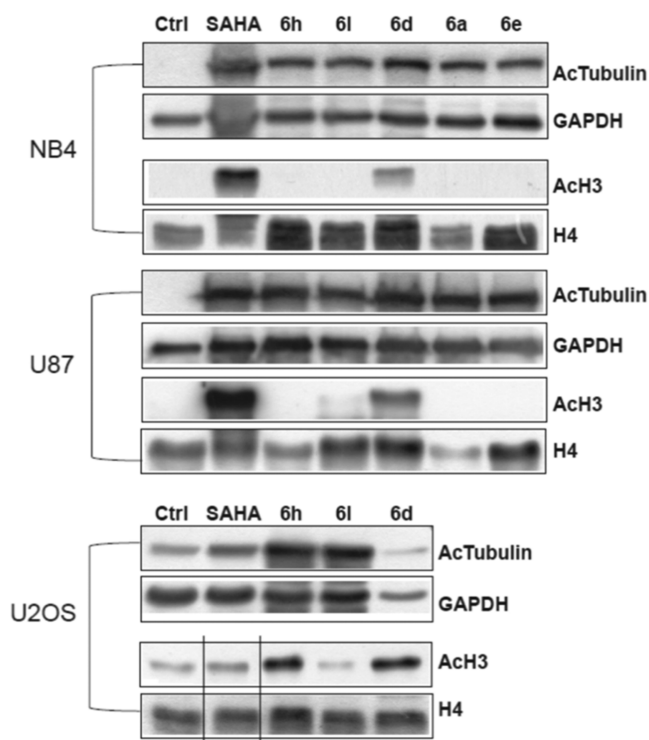


Figure 6. Western blot experiments to evaluate HDAC6 selectivity over HDAC1. Acetylation levels of the α -tubulin (AcTub) and histone H3 in NB4, U87, and U2OS cell lines treated with compounds **6a**, **6d**, **6e**, **6h**, and **6l** at 5 μ M for 30 h. SAHA was used as a positive control at the same time and concentration. GAPDH and H4 were used as loading controls.

in NB4 and U87 cells, the analogues **6a**, **6e**, **6h**, and **6l** efficiently inhibited HDAC6, inducing marked acetylation of tubulin. At the same dose, histone H3 acetylation was unchanged, hinting to the preferential interaction of this set of compounds toward the HDAC6 enzyme, with respect to HDACs1/8. Conversely, compound **6d**, although equally effective in inhibiting HDAC6, also induced the acetylation of histone H3, proving to be slightly less selective. When compounds **6h**, **6l**, and **6d** were tested in the U2OS cell line, we observed different results and only **6l** demonstrated to preferentially promote acetylation of α -tubulin. In this case, it cannot be excluded that the specific characteristics of the U2OS cell line (e.g., the alternative lengthening of telomeres)³⁶ may play a role in the response to HDACi.

HDAC6 Overexpression in IPF Lung Tissues. It was recently demonstrated that the accumulation of airway basal cells (ABCs) in lung tissues from IPF patients was associated with a lower survival rate, suggesting that these cells play an important profibrotic role in IPF progression.³⁷ By the bronchoalveolar lavage (BAL) transcriptome analysis of three independent cohorts of IPF patients, we have recently shown that genes, exclusively expressed by ABC, are enriched in the BAL of patients with poor outcome.^{37,38} Lung tissue data demonstrated the accumulation of ABC in IPF, and our own data suggest a profibrotic role of these cells. Recent single-cell

RNAseq analyses and immunohistochemistry data of IPF tissues showed that ABC is shifted toward an EMT phenotype and HDAC6 is crucial to TGF- β -induced EMT.³⁷ Accordingly, analysis of the BAL transcriptome from IPF patients showed a marked increase in the expression of genes exclusively expressed by ABC.³⁷ Immunohistochemistry highlighted HDAC6 expression in three-dimensional (3D) organoids derived from ABC from IPF patients, which build bronchospheres. HDAC6 is highly expressed by the outer rim of ABC of the bronchosphere structure. Immunohistochemistry for HDAC6 expression also revealed high HDAC6 expression of ABC derived from IPF patients. These data and cell RNA sequencing analyses of IPF tissues showed that ABCs were shifted toward an EMT phenotype that is induced by TGF- β , which in turn is regulated by the activity of the HDAC6 enzyme.¹⁹ Further studies showed a profibrotic effect of ABC derived from IPF patients,³⁹ which prompted us to analyze the expression of HDAC6 in normal and lung tissues derived from IPF patients. Immunohistochemistry of lung tissues derived from IPF patients confirmed HDAC6 overexpression in fibrotic lungs (Figure 7).

To investigate the potential of the new HDAC6 inhibitors, functional and gene expression studies were performed on ABC obtained by routine bronchoscopy using bronchial brushes in accordance with a standardized protocol and lung tissues derived from explants. In addition, we investigated the functional role of TGF- β , EMT, and HDAC6 in our recently established 3D organoid assay.³⁹ Further details on 3D organoid culture preparation are shown in Figure S16. Sphere formation was counted by bright-field microscopy, and cell viability was quantified with the aid of the MTT assay.

HDAC6 Overexpression as a Key Element in Cell Migration, Proliferation, and Fibrotic Remodeling by ABC. The best-performing compounds (**6a**, **6d**, **6h**, and **6l**) resulting from the enzymatic assay were chosen as potential hit compounds for IPF treatment and tested in the 3D organoid assay (Figure 8). The molecules were tested in the concentration range of 0.1 to 50 nM for 14 days with ABC derived from IPF patients ($n = 3$). The sphere counts (dots) and the MTT assay demonstrated a strong reduction in sphere formation and cell proliferation at 50 and 20 nM (Figures 9 to 10). The best compounds of the series **6a** ($IC_{50} = 1.73$ nM), **6d** ($IC_{50} = 3.31$ nM), **6h** ($IC_{50} = 5.15$ nM), and **6l** ($IC_{50} = 4.61$ nM) were highly effective in reverting the IPF phenotype and determined the complete inhibition of sphere formation (Figure 9, A–D) and in the cell proliferation assay (Figure 9, E–H). These data indicate the pivotal role of HDAC6 inhibitors, such as **6a**, **6d**, **6h**, and **6l**, that may represent promising hit compounds for the development of novel small molecules as useful pharmacological tools for IPF treatment.

6h Attenuates TGF- β 1-Dependent Fibrogenesis in Human Lung Tissue. Having identified HDAC6 expression in healthy and IPF human lung tissue *ex vivo*, we tested the efficacy of **6h** in a validated human lung model of TGF- β 1-dependent fibrogenesis.⁴⁰ mRNA RIN values were >8 in all experimental conditions. As previously described, TGF- β 1 significantly upregulated mRNA for the fibrosis-associated molecules α -SMA, collagens I, and collagen III in *ex vivo* human lung parenchyma over 7 days of culture ($n = 6$ donors, Figure 11A–C). TGF- β 1 also significantly upregulated mRNA for the matrix protein fibronectin (Figure 11D). There was a trend toward increased expression of HDAC6 with TGF- β 1 stimulation, but this did not reach statistical significance ($n = 3$ donors, Figure 11E). Compound **6h** at a concentration of 4.1

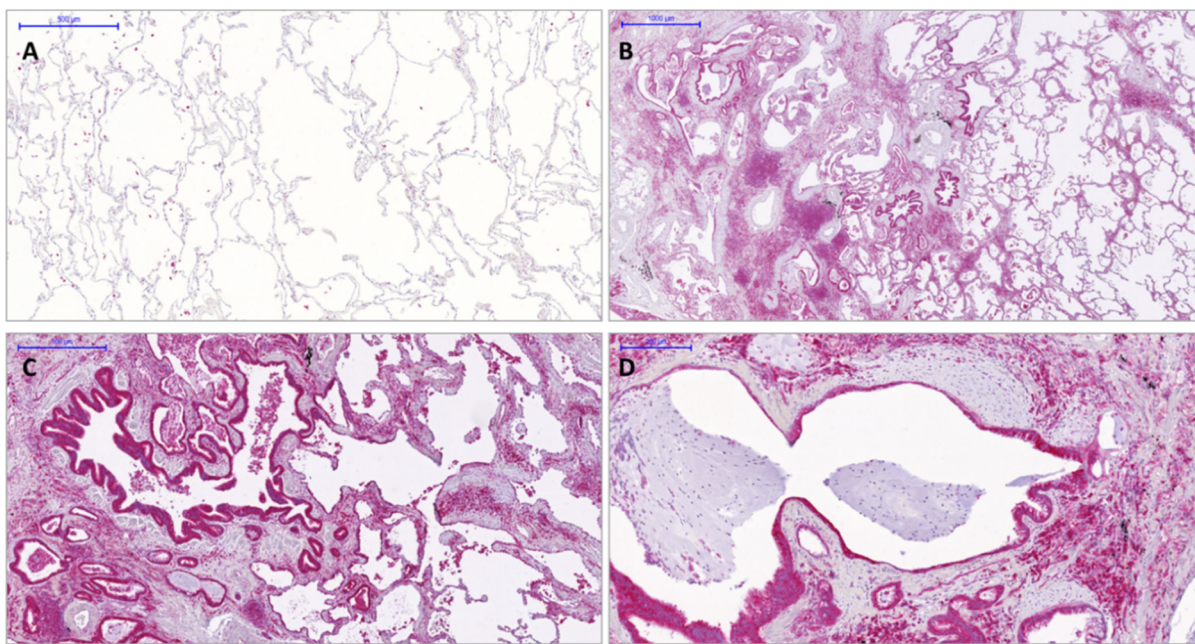


Figure 7. HDAC6 overexpression in IPF lung tissues. Immunohistochemistry of HDAC6 in normal (A) and IPF lung tissues (B–D). In IPF lungs, HDAC6 is highly expressed in ABC covering fibroblasts foci or honeycomb cysts as well as by macrophages and lymphocytes. Notably, in normal lungs, alveolar macrophages expressed HDAC6.

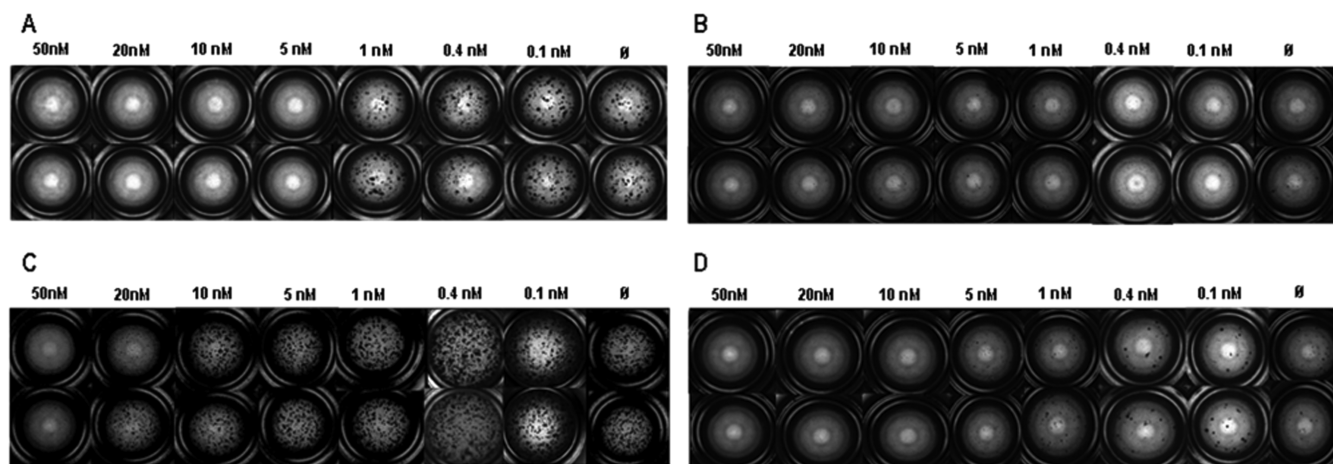


Figure 8. Newly generated HDAC6 inhibitors showed a concentration-dependent inhibitory effect on bronchosphere formation in 3D organoid cultures derived from IPF ABC. (A–D) ABC of IPF patients ($n = 3$) in 3D organoid cultures were stimulated for 14 days with the newly developed HDAC6 inhibitors **6a** (A), **6d** (B), **6h** (C), and **6l** (D) in the concentration range from 0.1 to 50 nM. Bright-field microscopy mosaic images of one representative experiment were taken with an Observer.Z1 Zeiss microscope, and exemplary registrations are depicted.

μM significantly inhibited the mRNA expression for $\alpha\text{-SMA}$, collagen types I and III, fibronectin, and HDAC6 in TGF- β 1-stimulated lung tissue (Figure 11A–D,F). Taken together, these data suggest that HDAC6 plays a critical role in profibrotic TGF- β 1-dependent signaling human lung parenchyma and that **6h** may be an effective tool for the treatment of IPF.

Preliminary *In Vitro* Physicochemical Property Assessment and Determination of Geno- and Cytotoxicity and Metabolic Stability. We assessed the solubility and chemical stability of compounds **6d** and **6h**. The solubility (at pH = 3 and 7.4, Table 2) and the chemical stability (at pH = 3, Table 3) of these compounds were measured by HPLC methods, as previously reported.^{41,42} From our analysis, it emerged that both **6d** and **6h** exhibited favorable chemical stability and solubility profile at acidic pH. Instead, a significant difference in

solubility at neutral pH was observed between the two compounds, with compound **6h** being less soluble. This fact could be explained by the absence of the polar *N*-methyl-piperidyl moiety on the structure of this compound. However, both the solubility and chemical stability of these compounds can be considered satisfactory.

In vitro studies were conducted to assess the metabolic stability of **6d** and **6h** in human liver microsomal (HLM) preparations. The plot of nonmetabolized compound [natural logarithm of % of compound recovery (100% at time 0 min)] as a function of incubation time showed a monoexponential decay relationship (first-order kinetics) for both substrates (Figure 12). The apparent decay constants (k), half-life time ($t_{1/2}$), and intrinsic clearance (CL_{int}) are reported in Table 4. The incubation of both compounds in HLM showed different

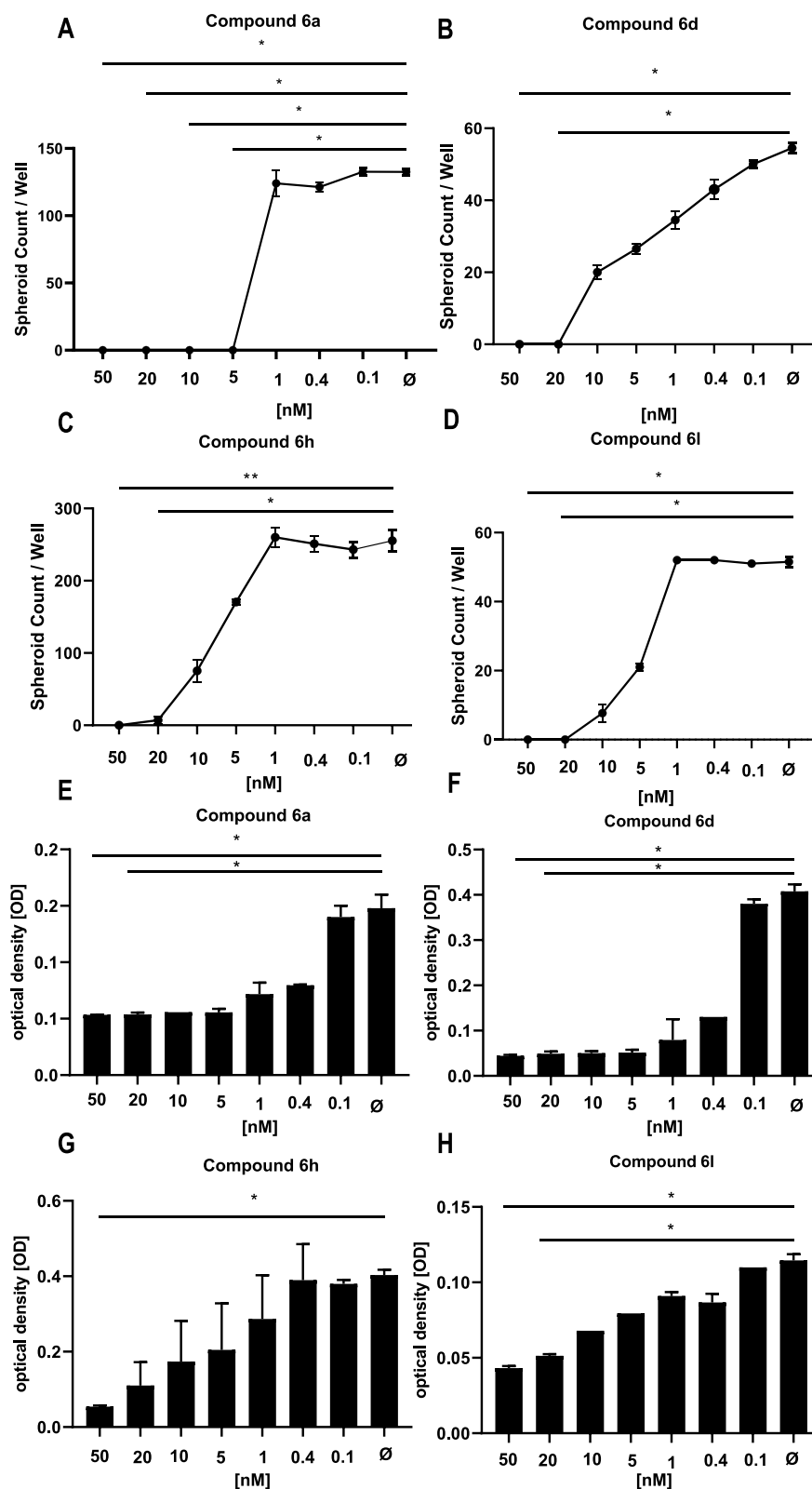


Figure 9. Bronchosphere generation was completely blocked by newly developed HDAC6 inhibitors. Bronchosphere counts derived from ABC from IPF patients ($n = 3$) were obtained (A–D, 6a, 50 nM: $p = 0.044$, 20 nM: $p = 0.044$; 6d, 50 nM: $p = 0.0161$, 20 nM: $p = 0.0161$; 6h, 50 nM: $p = 0.0229$, 20 nM: $p = 0.0229$; 6l, 50 nM: $p = 0.0047$, 20 nM: $p = 0.0307$), and cell proliferation was tested by the MTT assay (E–H, 6a, 50 nM: $p = 0.023$ 20 nM: $p = 0.044$; 6d, 50 nM: $p = 0.0113$, 20 nM: $p = 0.0228$; 6h, 50 nM: $p = 0.0163$; 6l, 50 nM: $p = 0.0053$, 20 nM: $p = 0.0441$) in the presence of several HDAC6 inhibitors such as compounds 6a (A, E), 6d (B, F), 6h (C, G), and 6l (D, H) in the concentration range of 1–50 nM. Bronchosphere counts and optical density values derived from the MTT assay correlated well. The data indicate mean \pm standard error of the mean (SEM) from triplicate measurements, $n = 3$. For statistical comparison, repeated measures analysis of variance (ANOVA) followed by Friedman multiple comparisons test was used.

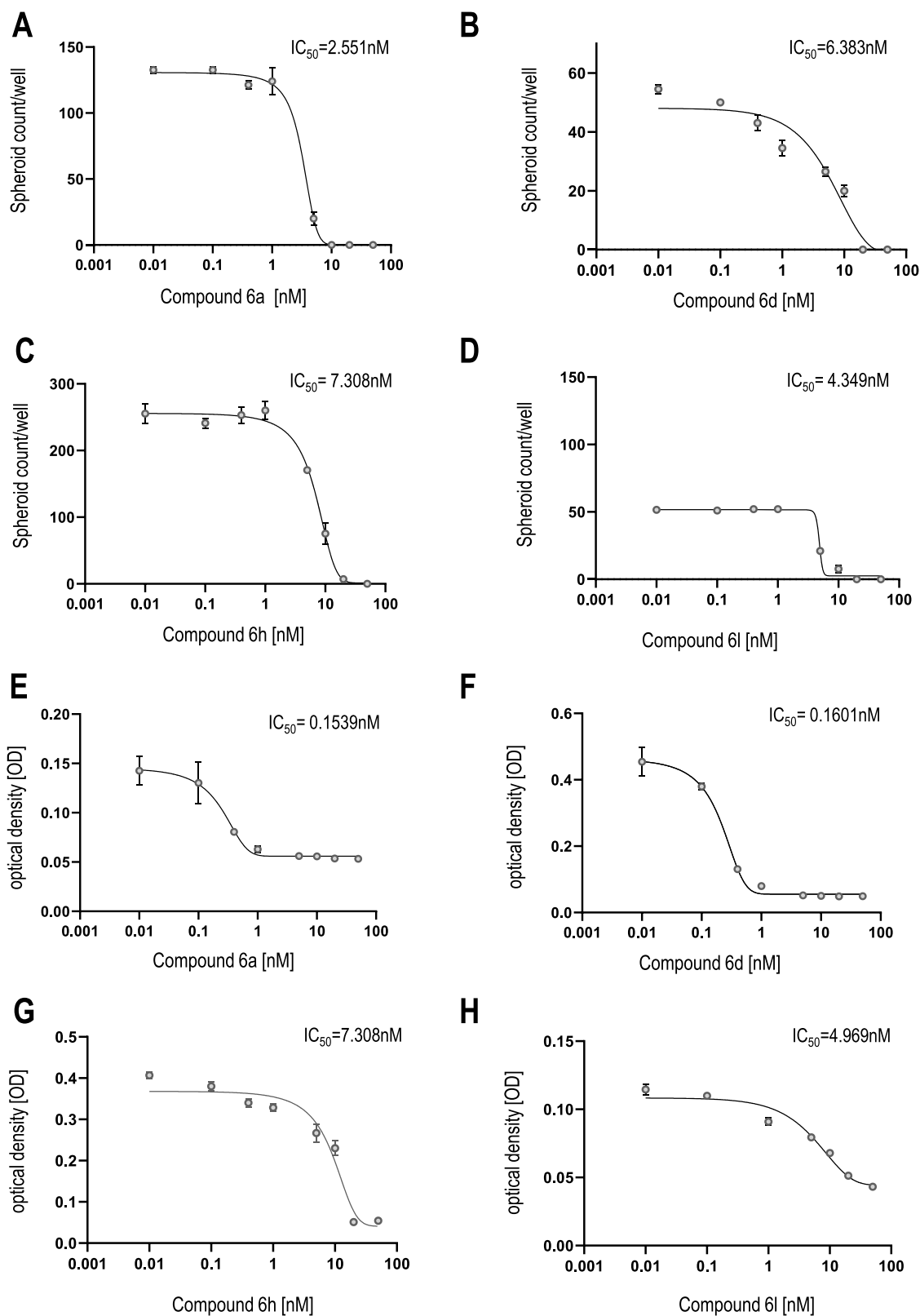


Figure 10. HDAC6 inhibitors show a concentration-dependent inhibitory effect on bronchosphere formation. IC_{50} values were determined from bronchosphere counts and bronchosphere cell proliferation by GraphPad Prism 9 (mean \pm SEM, $n = 3$). The mean value is determined from the IC_{50} value of the organoid counts and the MTT assay. Calculated IC_{50} values represent the concentration of the best HDAC6 inhibitor compounds **6a**, **6d**, **6h**, and **6l** at which they exert their half-maximal inhibitory effect on bronchosphere formation in the 3D organoid assay.

behavior as confirmed by the $t_{1/2}$ values (51.68 and 53.47 min for **6d** and **6h**, respectively). The similar values of CL_{int} indicate that

both **6d** and **6h** can be considered to possess intermediate properties in terms of metabolic stability.

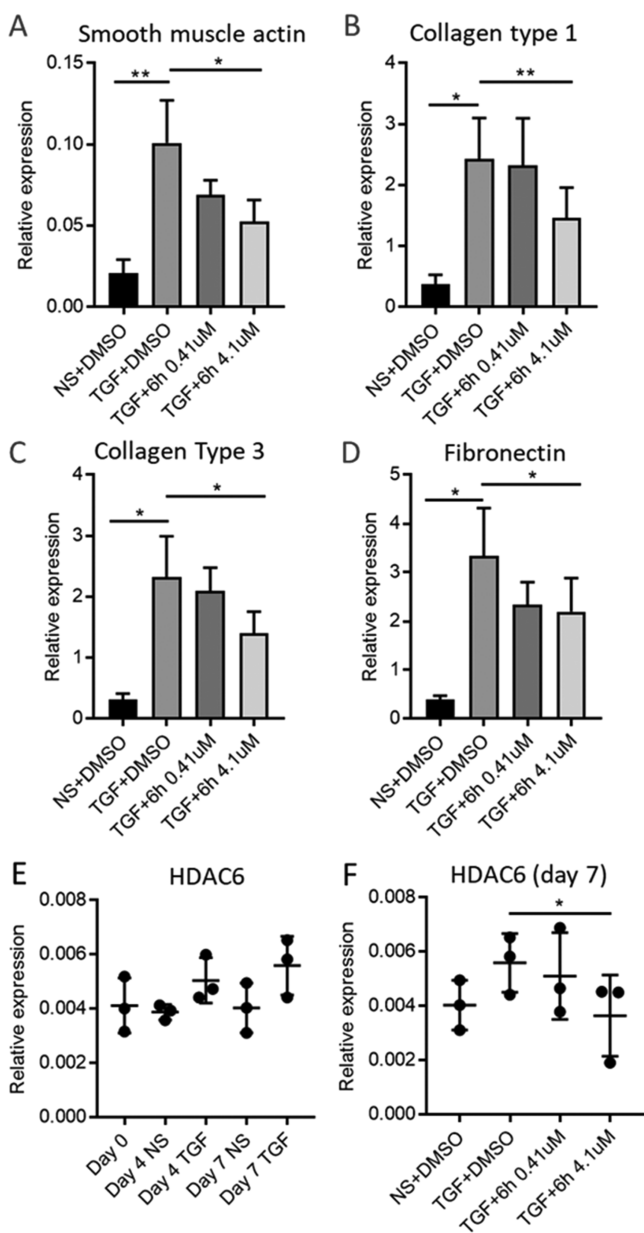


Figure 11. HDAC6 inhibition attenuates TGF- β 1-dependent profibrotic gene expression in *ex vivo* cultured human lung parenchyma. (A) α -SMA actin mRNA expression is upregulated by TGF- β 1 and inhibited by 4.1 μ M **6h** ($n = 6$). $^{**}p < 0.01$, $^{*}p < 0.05$, paired t -test. (B) Collagen type I mRNA expression is upregulated by TGF- β 1 and inhibited by 4.1 μ M ($n = 6$). $^{**}p < 0.01$, $^{*}p < 0.05$, paired t -test. (C) Collagen type III mRNA expression is upregulated by TGF- β 1 and inhibited by 4.1 μ M ($n = 6$). $^{*}p < 0.05$, paired t -test. (D) Fibronectin mRNA expression is upregulated by TGF- β 1 and inhibited by 4.1 μ M ($n = 6$). $^{*}p < 0.05$, paired t -test. (E) HDAC6 mRNA is expressed in human lung parenchyma ($n = 3$). (F) HDAC6 mRNA expression is inhibited by 4.1 μ M ($n = 3$), $^{*}p < 0.05$, paired t -test. NS = nonstimulated.

In silico analysis by means of MetaSite software,⁴³ for predicting the site of CYP-dependent metabolism, revealed that the hydroxylation of the aromatic ring is the most probable metabolite of both compounds. Moreover, these metabolites seem to be formed, preferentially, by CYP3A4 and CYP2D6. The other CYP isoforms, such as CYP belonging to the 2C family, seem to drive the metabolism toward *N*-oxide formation.

Table 3. Solubility and Chemical Stability of Compounds **6d** and **6h**

compound	solubility (μ M) after 24 h		chemical stability (%) after 24 h
	pH = 3	pH = 7.4	
6d	456	285	98
6h	459	97	89
TubA	244	231	nc ^a

^anc: not calculated.

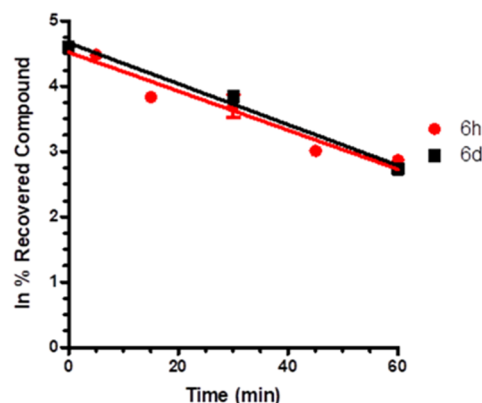


Figure 12. CYP-dependent metabolic depletion of 5 μ M **6d** (red line, three time points, at 0, 30, and 60 min) and **6h** (black line, six time points, at 0, 5, 15, 30, 45, and 60 min) in HLM preparation. Results are presented graphically as a percentage of compound recovery (100% at time 0 min) as a function of incubation time. Data are presented as mean \pm SEM of three different experiments.

Table 4. Kinetic Parameters and Metabolic Stability of Compounds **6d** and **6h**

compound	k (min^{-1})	$t_{1/2}$ (min)	CL_{int} ($\mu\text{L}/\text{min}/\text{mg prot}$)
6d	0.01297	51.68	27.43
6h	0.01357	53.47	25.46
SAHA ⁴⁴		60	

Potential mutagenicity associated with the use of hydroxamic acid-based compounds poses a significant challenge in terms of their druglike profile.⁴⁵ To date, Givinostat is the only compound under clinical evaluation that has exhibited no mutagenic effect, while the FDA-approved drugs have shown mutagenicity.⁴⁶ Therefore, we confirmed for compound **6h** a lack of mutagenic effect in TA98 and TA100 strains of *Salmonella typhimurium*. The Ames test was employed to detect potential risks of mutagenicity at the early stages of drug development. The assay can be performed with or without the S9 fraction of the rat liver. This latter condition allows an in-depth investigation for evaluating the risk of mutagenicity derived from the metabolites of the compounds under study. After applying both the experimental conditions, no mutagenic effect was observed for compound **6h** at all tested concentrations (1–75 μ M) (Figure 13). Besides the physicochemical parameters of the compounds, we experimentally determined additional features that might contribute to designate the most promising compound **6h** as the potential hit of the series. Accordingly, we evaluated its potential cytotoxicity profile after incubation with mouse embryonic fibroblasts (NIH3T3 cell line). The viability of these cells, after incubation with **6h**, is reported in Table 4 and expressed as IC_{50} (μ M). We observed

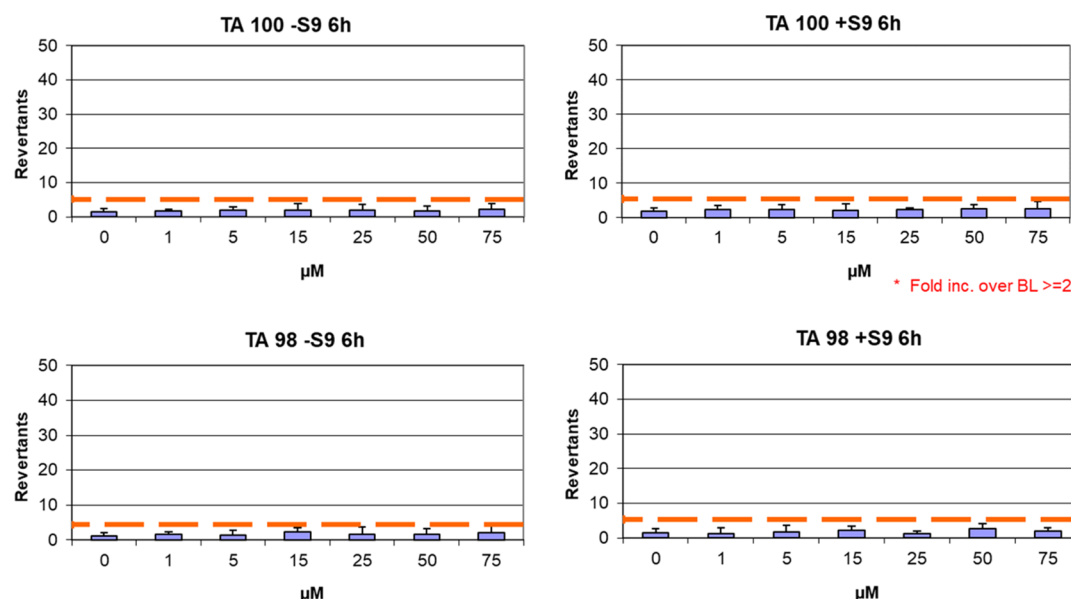


Figure 13. Ames test performed on *S. Typhimurium* TA98 and TA100 strains for compound 6h.

Table 5. Viability of Mouse Fibroblasts NIH3T3 after Incubation with Different Concentrations of 6h and Reference HDAC Inhibitor SAHA (%)^a

[μ M]	1	2	2.5	5	7.5	10	15	20	25	50	75
6h				98 \pm 6			94 \pm 9		*87 \pm 5	*71 \pm 9	*53 \pm 10
SAHA	*83 \pm 6	*62 \pm 5	*49 \pm 3	*31 \pm 5	*22 \pm 3	*17 \pm 6		*7 \pm 6			

^aCell viability was measured by the neutral red uptake (NRU) test, and data were normalized as % control. Data are expressed as mean \pm s.d. of three experiments repeated in six replicates. *Values are statistically different versus control, $p \leq 0.05$.

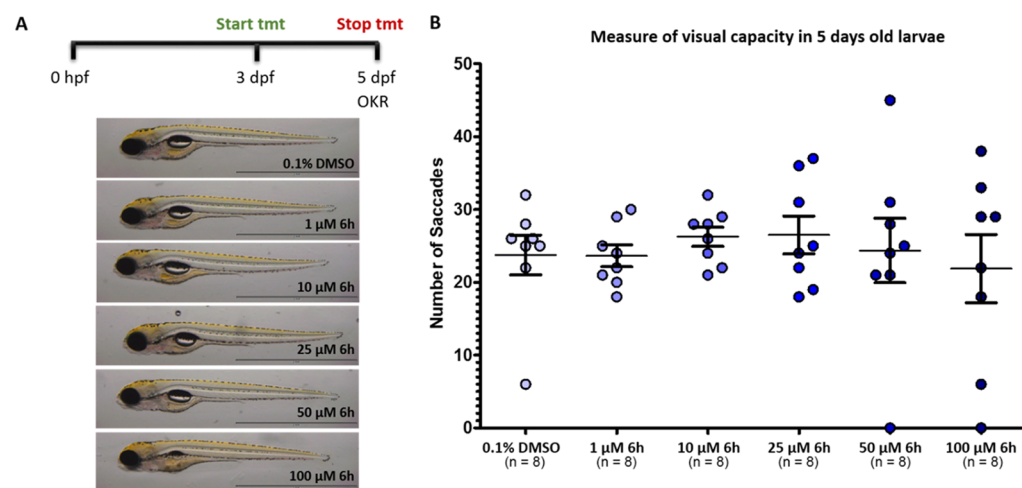


Figure 14. (A) Toxicity screening of 6h in the zebrafish model and (B) measurement of visual capacity in 5-day postfertilization (dpf) old larvae at different concentrations (1–100 μ M).

that 6h showed toxicity only in the μ M range with a TC_{50} of 75 μ M, resulting in a highly safe profile for this compound (Table 5).

Safety of 6h in a Zebrafish Model and in Langendorff-Perfused Rat Hearts. There is a clear potential for zebrafish to provide valuable new insights into chemical toxicity, useful in the drug discovery trajectory, and human disease using recent advances in forward and reverse genetic techniques coupled with large-scale, high-throughput screening. Recently, there is increasing use of zebrafish in toxicology.⁴⁷ Since zebrafish could provide a sound basis for the risk assessment of drug

administration in humans, we decided to use this model to assess the toxic potential of 6h. Three-day-old zebrafish larvae were treated for 2 days with increasing doses of this compound (Figure 14A). 6h was well tolerated up to 50 μ M instead, and only at 100 μ M, some larvae failed to inflate their swim bladder and presented mild cardiac edema, thus confirming the safety profile of this compound. Additionally, visual behavior analysis conducted on five-day-old larvae revealed that there were no significant changes in larvae treated with compound 6h in comparison to vehicle control (0.1% DMSO)-treated larvae, thus confirming that the drug is well tolerated (Figure 14B).

Table 6. Effects of 6h on HR, RR, PQ, QRS, QT, and QTc in Langendorff-Perfused Rat Hearts^a

6h (μ M)	HR (BPM)	RR (ms)	PQ (ms)	QRS (ms)	QT (ms)	QTc (ms)
none	235.7 \pm 8.3	257.2 \pm 8.1	43.6 \pm 2.5	15.2 \pm 0.2	76.2 \pm 2.9	150.5 \pm 5.5
0.01	235.4 \pm 9.2	255.9 \pm 9.3	44.1 \pm 2.6	15.6 \pm 0.5	78.1 \pm 3.2	154.6 \pm 5.8
0.1	238.1 \pm 10.5	253.7 \pm 10.0	44.6 \pm 3.2	15.4 \pm 0.4	78.0 \pm 3.3	155.1 \pm 6.6
1	235.4 \pm 12.0	257.7 \pm 11.2	44.5 \pm 3.0	15.8 \pm 0.4	76.4 \pm 3.1	150.8 \pm 6.1
10	207.9 \pm 17.1**	294.1 \pm 20.9**	50.4 \pm 2.2**	18.0 \pm 0.5**	78.3 \pm 3.4	145.3 \pm 5.7

^aEach value represents mean \pm SEM ($n = 5$). ** $P < 0.01$, repeated measures ANOVA and Dunnett's post-test. HR, frequency; RR, cycle length; PQ, atrioventricular conduction time; QRS, intraventricular conduction time; QT, duration of ventricular depolarization and repolarization, i.e., the action potential duration; QTc, corrected QT.

Cardiovascular adverse effects contribute disproportionately to drug withdrawals from the market and represent one of the major hurdles in the development of new drugs. To evaluate the potential cardiovascular toxicity of compound **6h**, its effect on cardiac mechanical function and the electrocardiogram (ECG) in Langendorff-isolated rat hearts was assessed, as previously described.^{48,49} Under control conditions, left ventricle pressure (LVP) and coronary perfusion pressure (CPP) values of 57.53 ± 7.19 and 52.30 ± 5.65 mmHg ($n = 5$), respectively, were obtained. At the maximum concentration tested (10μ M), **6h** significantly increased LVP to 70.99 ± 10.15 mmHg and decreased CPP to 44.11 ± 3.53 mmHg. Moreover, at 10μ M, **6h** significantly increased RR, PQ, and QRS, though not QT_c ECG intervals (Table 6). Therefore, these findings highlight that at the maximum concentration tested, which was however three orders of magnitude higher than that effective in hDAC6 inhibition, **6h** exhibited positive inotropic, negative chronotropic, and coronary vasodilating activity and prolonged the cardiac cycle length as well both the atrioventricular and intraventricular conduction time.

CONCLUSIONS

Combining structural analysis, bioinformatics, and molecular modeling efforts, we generated a series of new HDAC6 inhibitors, selective over hHDAC1 and hHDAC8. Synthetic accessibility, high potency, and interesting preliminary pharmacokinetic profile, including low geno/cardio/cytotoxicity, characterize the novel heterocyclic inhibitors of isoform 6, exemplified by **6h**. Using **6h**, we confirmed the lack of a stereoselective inhibition of HDAC6 since both enantiomers of **6h** showed similar inhibition properties ((*R*)-**6h** IC₅₀ hHDAC6 = 91 nM vs (*S*)-**6h** IC₅₀ hHDAC6 = 71 nM), with the (*R*)-enantiomer much more selective over hHDAC1 (Table 1). The binding mode on HDAC6 was determined by X-ray crystallography using **6h** in complex with zfHDAC6. SARs of the new inhibitors were analyzed by docking protocols using human enzymes. Selected analogues were not mutagenic; moreover, they were not cardiotoxic in Langendorff-isolated rat hearts and not toxic *in vivo*. Additionally, selected analogues **6d** and **6h** showed favorable solubility, chemical stability at both neutral and acidic pH, and metabolic stability to hCYP3A4. By an immunohistochemistry analysis, we confirmed the overexpression of HDAC6 in human IPF lung tissues. Our data suggest that this fact may confer hyperproliferative and profibrotic effects of ABC on IPF. Consecutively, we tested our best-performing compounds, resulting from enzymatic assay (**6a**, **6d**, **6h**, and **6l**), in 3D organoid and MTT assays to evaluate their efficacy in reverting the IPF phenotype and their antifibrotic activity. The results emphasized the important role that HDAC6 inhibition plays in the treatment of IPF. This evidence was further confirmed by the attenuation of TGF- β 1-

dependent fibrogenesis in human lung tissue with compound **6h**. Overall, this work provides robust proof for HDAC6 inhibitors as potential therapeutic tools for the treatment of IPF. In conclusion, we identified **6h** as a promising and optimized HDAC6i hit, with efficacy in reverting the IPF phenotype, which may pave the way to the development of druglike leads.

EXPERIMENTAL SECTION

Chemistry. Unless otherwise specified, materials were purchased from commercial suppliers and used without further purification. Reaction progress was monitored by TLC using silica gel 60 F254 (0.040–0.063 mm) with detection by UV (254 nm). Silica gel 60 (0.040–0.063 mm) or aluminum oxide 90 (0.063–0.200 mm) were used for column chromatography. ¹H NMR and ¹³C NMR spectra were recorded on a Varian 300 MHz or Bruker 400 MHz spectrometer using the residual signal of the deuterated solvent as the internal standard. Splitting patterns are described as singlet (s), doublet (d), triplet (t), quartet (q), quintet (p), and broad (br); the value of chemical shifts (δ) is given in ppm, and coupling constants (*J*) are given in hertz (Hz). Electrospray ionization mass spectrometry (ESI-MS) spectra were performed by an Agilent 1100 series LC/MSD spectrometer. Optical rotation values were measured at room temperature using a PerkinElmer model 343 polarimeter operating at 589 nm, corresponding to the sodium D line. Yields refer to purified products and are not optimized. All moisture-sensitive reactions were performed under an argon atmosphere using oven-dried glassware and anhydrous solvents. ESI-MS spectra for exact mass determination were recorded on an LTQ Orbitrap Thermo Fischer Scientific instrument. All final compounds were purified by flash column chromatography. The purity of final products (>95%) was determined by an analytical HPLC Merk Purospher STAR RP-18e (5 μ m) LiChroCART 250-4 column; detection at 254 nm; flow rate = 1.0 mL/min; mobile phase A, 0.01% trifluoroacetic acid (TFA) (v/v) in water; mobile B, acetonitrile; gradient, 90/10–10/90 A/B in 20 min. The gradient was optimized based on compound polarity.

(1-Methylpiperidin-4-yl)(phenyl)methanone (8a). Tosylhydrazide **7** (538 mg, 1.91 mmol) and Cs₂CO₃ (932 mg, 2.86 mmol) were placed in a tube. The tube was backfilled with nitrogen, before the addition of 1,4-dioxane (7 mL) followed by the addition of benzaldehyde (194 μ L, 1.91 mmol). The tube was sealed with a silicone/poly(tetrafluoroethylene) (PTFE) cap and heated to 110 °C for 12 h. The reaction was cooled to 25 °C, quenched with a saturated solution of NH₄Cl (20 mL), and extracted with DCM (3 \times 20 mL). The combined organic layers were dried over Na₂SO₄, and the solvents were removed *in vacuo* to give a residue that was purified by flash column chromatography on silica gel (MeOH/DCM 1:15) to give **8a** (155 mg, 40% yield); ¹H NMR (400 MHz, CDCl₃) δ 7.90 (d, *J* = 7.2 Hz, 2H), 7.58–7.47 (m, 1H), 7.43 (t, *J* = 7.8 Hz, 2H), 3.28–3.11 (m, 1H), 2.92 (m, 2H), 2.29 (s, 3H), 2.17–2.00 (m, 2H), 1.97–1.73 (m, 4H); ESI-MS *m/z*: [M + H]⁺ 204.

(4-Chlorophenyl)(1-methylpiperidin-4-yl)methanone (8b). Starting from **7** (1.0 g, 3.56 mmol) and 4-chlorobenzaldehyde (500 mg, 3.56 mmol), compound **8b** was obtained following the procedure described for the preparation of **8a**. Purification by column chromatography on silica gel (MeOH/DCM 1:15) afforded **8b** (432 mg, 51% yield); ¹H NMR (300 MHz, CDCl₃) δ 7.86 (d, *J* = 8.6 Hz, 2H), 7.43 (d, *J* = 8.8 Hz,

2H), 3.19–3.10 (m, 1H), 2.96–2.94 (m, 2H), 2.32 (s, 3H), 2.17–2.03 (m, 2H), 1.91–1.80 (m, 4H); ESI-MS m/z : $[M + H]^+$ 239.

(3-Chlorophenyl)(1-methylpiperidin-4-yl)methanone (8c). Starting from **7** (1.0 g, 3.56 mmol) and 3-chlorobenzaldehyde (500 mg, 3.56 mmol), compound **8c** was obtained following the procedure described for the preparation of **8a**. Purification by column chromatography on silica gel (MeOH/DCM 1:15) afforded the title compound (633 mg, 75% yield); ^1H NMR (300 MHz, CDCl_3) δ 7.83–7.69 (m, 2H), 7.44 (s, 1H), 7.27–7.17 (m, 1H), 3.12 (m, 1H), 2.88 (m, 2H), 2.40 (t, J = 5.0 Hz, 2H), 2.25 (s, 3H), 1.88–1.70 (m, 4H); ESI-MS m/z : $[M + H]^+$ 238.

(2-Fluorophenyl)(1-methylpiperidin-4-yl)methanone (8d). Starting from **7** (1.0 g, 3.56 mmol) and 2-fluorobenzaldehyde (442 mg, 3.56 mmol), compound **8d** was obtained following the procedure described for the preparation of **8a**. Purification by column chromatography on silica gel (MeOH/DCM 1:15) afforded the title compound (598 mg, 76% yield); ^1H NMR (300 MHz, CDCl_3) δ 7.78–7.65 (m, 1H), 7.70–7.56 (m, 1H), 7.48–7.31 (m, 1H), 7.07–6.93 (m, 1H), 3.06–2.90 (m, 1H), 2.86–2.68 (m, 2H), 2.39–2.22 (m, 2H), 2.18 (s, 3H), 2.05–1.86 (m, 1H), 1.86–1.74 (m, 2H), 1.74–1.55 (m, 1H); ESI-MS m/z : $[M + H]^+$ 222.

(4-Fluorophenyl)(1-methylpiperidin-4-yl)methanone (8e). Starting from **7** (1.0 g, 3.56 mmol) and 4-fluorobenzaldehyde (440 mg, 3.56 mmol), compound **8e** was obtained following the procedure described for the preparation of **8a**. Purification by column chromatography on silica gel (MeOH/DCM 1:20) afforded the title compound (597 mg, 75% yield); ^1H NMR (300 MHz, CDCl_3) δ 8.02–7.89 (m, 2H), 7.14 (t, J = 8.6 Hz, 2H), 3.28–3.11 (m, 1H), 3.00–2.88 (m, 2H), 2.34 (s, 3H), 2.22–2.06 (m, 2H), 1.95–1.77 (m, 4H); ESI-MS m/z : $[M + H]^+$ 222.

(1-Methylpiperidin-4-yl)(pyridin-3-yl)methanone (8f). Starting from **7** (500 mg, 1.78 mmol) and 3-pyridinecarboxaldehyde (107 mg, 1.78 mmol), compound **8f** was obtained following the procedure described for the preparation of **8a**. Title compound was obtained as pure without any further purification (quantitative yield); ^1H NMR (300 MHz, CDCl_3) δ 9.14 (s, 1H), 8.77 (d, J = 4.8 Hz, 1H), 8.20 (d, J = 8.0 Hz, 1H), 7.48–7.36 (m, 1H), 3.26–3.11 (m, 1H), 3.02–2.89 (m, 2H), 2.33 (s, 3H), 2.22–2.05 (m, 4H), 1.95–1.83 (m, 2H); ESI-MS m/z : $[M + H]^+$ 205.

1'-Methyl-2-phenylspiro[indole-3,4'-piperidine] (9a). Phenylhydrazine (143 μL , 1.45 mmol) and **8a** (295 mg, 1.45 mmol) were dissolved in 1,4-dioxane (5 mL) and cooled to 0 °C. Concentrated sulfuric acid (700 μL) was added dropwise to the reaction at 0 °C. The reaction was then heated at 70 °C for 2 h and stirred for an additional 12 h at 25 °C. The mixture was then treated with a saturated solution of NaHCO_3 (20 mL) and extracted with DCM (3×20 mL). The combined organic layers were dried over Na_2SO_4 , and solvents were removed *in vacuo* to give a residue that was purified by flash column chromatography on silica gel (MeOH/DCM 1:15) to give the title compound (120 mg, 30% yield); ^1H NMR (300 MHz, CDCl_3) δ 8.27–7.99 (m, 2H), 7.85 (d, J = 7.5 Hz, 2H), 7.73 (d, J = 7.7 Hz, 2H), 7.61–7.32 (m, 4H), 7.22 (t, J = 8.1 Hz, 1H), 2.95 (br, 2H), 2.75 (br, 4H), 2.49 (s, 3H), 1.45 (br, 2H); ESI-MS m/z : $[M + H]^+$ 277.

2-(4-Chlorophenyl)-1'-methylspiro[indole-3,4'-piperidine] (9b). Compound **9b** was obtained from **8** (268 mg, 1.13 mmol) following the procedure described for the preparation of **9a**. Purification by column chromatography on silica gel (MeOH/DCM 1:30) afforded the title compound (112 mg, 32% yield); ^1H NMR (300 MHz, CDCl_3) δ 8.16 (d, J = 8.6 Hz, 2H), 7.86 (d, J = 7.1 Hz, 1H), 7.73 (d, J = 7.8 Hz, 1H), 7.44 (d, J = 8.5 Hz, 2H), 7.41 (m, 1H), 7.29–7.16 (m, 1H), 3.02–2.97 (m, 2H), 2.81–2.62 (m, 4H), 2.51 (s, 3H), 1.53–1.21 (m, 2H); ESI-MS m/z : $[M + H]^+$ 311.

2-(3-Chlorophenyl)-1'-methylspiro[indole-3,4'-piperidine] (9c). Compound **9c** was obtained from **8c** (476 mg, 2.0 mmol) following the procedure described for the preparation of **9a**. Purification by column chromatography on silica gel (MeOH/DCM 1:20) afforded the title compound (187 mg, 30% yield); ^1H NMR (300 MHz, CDCl_3) δ 8.16 (s, 1H), 7.97 (d, J = 7.1 Hz, 1H), 7.85 (d, J = 7.7 Hz, 1H), 7.74 (d, J = 7.7 Hz, 1H), 7.50–7.36 (m, 3H), 7.30–7.20 (m, 1H), 3.00–2.92 (m, 2H), 2.81–2.59 (m, 4H), 2.51 (s, 3H), 1.50–1.42 (m, 2H); ESI-MS m/z : $[M + H]^+$ 311.

2-(2-Fluorophenyl)-1'-methylspiro[indole-3,4'-piperidine] (9d). Compound **9d** was obtained from **8d** (300 mg, 1.36 mmol) following the procedure described for the preparation of **9a**. Purification by column chromatography on silica gel (MeOH/DCM 1:20) afforded the title compound (120 mg, 30% yield); ^1H NMR (300 MHz, CDCl_3) δ 7.83 (d, J = 7.5 Hz, 1H), 7.72 (d, J = 7.7 Hz, 1H), 7.46–7.38 (m, 2H), 7.32–7.23 (m, 3H), 7.23–7.07 (m, 1H), 2.81 (s, 1H), 2.69 (t, J = 11.6 Hz, 2H), 2.42 (s, 3H), 2.23 (t, J = 12.6 Hz, 2H), 1.57 (d, J = 13.2 Hz, 2H); ESI-MS m/z : $[M + H]^+$ 295.

2-(4-Fluorophenyl)-1'-methylspiro[indole-3,4'-piperidine] (9e). Compound **9e** was obtained from **8e** (627 mg, 2.8 mmol) following the procedure described for the preparation of **9a**. Purification by column chromatography on silica gel (acetone/DCM 1:20) afforded the title compound (412 mg, 50% yield); ^1H NMR (300 MHz, CDCl_3) δ 8.26–8.11 (m, 1H), 7.85 (d, J = 7.5 Hz, 2H), 7.71 (d, J = 7.9 Hz, 2H), 7.41 (t, J = 7.7 Hz, 1H), 7.27–7.06 (m, 2H), 3.06–2.87 (m, 2H), 2.79–2.60 (m, 4H), 2.50 (s, 3H), 1.51–1.39 (m, 2H); ESI-MS m/z : $[M + H]^+$ 295.

1'-Methyl-2-(pyridin-3-yl)spiro[indole-3,4'-piperidine] (9f). Starting from **8f** (200 mg, 0.98 mmol), the title compound **9f** was obtained following the procedure described for the preparation of **9a**. Purification by column chromatography on silica gel (MeOH/DCM 1:10) afforded the title compound (180 mg, 66% yield); ^1H NMR (300 MHz, CDCl_3) δ 9.37 (s, 1H), 8.71–8.62 (m, 1H), 8.40 (d, J = 8.1 Hz, 1H), 7.83 (d, J = 6.3 Hz, 1H), 7.76–7.63 (m, 1H), 7.47–7.32 (m, 2H), 7.28–7.14 (m, 1H), 3.03–2.91 (m, 2H), 2.80–2.56 (m, 4H), 2.50 (s, 3H), 1.46 (d, J = 12.6 Hz, 2H); ESI-MS m/z : $[M + H]^+$ 279.

(\pm)-1'-Methyl-2-phenylspiro[indoline-3,4'-piperidine] ((\pm)-10a). To a solution of **9a** (110 mg, 0.40 mmol) in MeOH (5 mL), NaBH_4 (76 mg, 2.00 mmol) was added. The reaction was kept stirring for 12 h at 50 °C. Then, the reaction was quenched with a saturated solution of NaHCO_3 (10 mL) and MeOH was removed under reduced pressure. The residue was dissolved with EtOAc and washed with H_2O (3×10 mL). The organic phase was dried over Na_2SO_4 , and solvents were removed *in vacuo* to give a residue that was purified by flash column chromatography on silica gel (MeOH/DCM 1:20) affording the title compound (60 mg, 40% yield); ^1H NMR (300 MHz, CDCl_3) δ 7.32–7.20 (m, 6H), 7.09 (td, J = 7.6, 1.1 Hz, 1H), 6.77 (td, J = 7.4, 0.8 Hz, 1H), 6.66 (d, J = 7.7 Hz, 1H), 4.59 (s, 1H), 4.14 (br, 1H), 2.85–2.73 (m, 1H), 2.66–2.55 (m, 1H), 2.52–2.41 (m, 1H), 2.30 (s, 3H), 2.13–1.74 (m, 4H), 1.42 (m, 1H); ESI-MS m/z : $[M + H]^+$ 279.

(\pm)-2-(4-Chlorophenyl)-1'-methylspiro[indoline-3,4'-piperidine] ((\pm)-10b). Starting from **9b** (110 mg, 0.35 mmol), compound (\pm)-10b was obtained following the procedure described for the preparation of (\pm)-10a. Purification by column chromatography on silica gel (MeOH/DCM 1:20) afforded the title compound (45 mg, 40% yield); ^1H NMR (300 MHz, CDCl_3) δ 7.31–7.17 (m, 5H), 7.11 (t, J = 7.6 Hz, 1H), 6.78 (t, J = 7.5 Hz, 1H), 6.68 (d, J = 7.7 Hz, 1H), 4.07 (s, 1H), 2.82 (br, 1H), 2.65–2.52 (m, 2H), 2.35 (s, 3H), 2.19–1.90 (m, 4H), 1.41 (t, J = 9.8 Hz, 2H); ESI-MS m/z : $[M + H]^+$ 313.

(\pm)-2-(3-Chlorophenyl)-1'-methylspiro[indoline-3,4'-piperidine] ((\pm)-10c). Starting from **9c** (102 mg, 0.33 mmol), compound (\pm)-10c was obtained following the procedure described for the preparation of (\pm)-10a. The title compound was used in the next step without any further purification. (Quantitative yield); ^1H NMR (300 MHz, CDCl_3) δ 7.36–7.17 (m, 5H), 7.10 (t, J = 8.4 Hz, 1H), 6.77 (t, J = 7.4 Hz, 1H), 6.68 (d, J = 7.8 Hz, 1H), 4.56 (s, 1H), 4.09 (br, 1H), 2.80–2.71 (m, 1H), 2.67–2.52 (m, 1H), 2.51–2.36 (m, 1H), 2.31 (s, 3H), 2.19–1.85 (m, 4H), 1.83–1.65 (m, 1H); ESI-MS m/z : $[M + H]^+$ 313.

(\pm)-2-(2-Fluorophenyl)-1'-methylspiro[indoline-3,4'-piperidine] ((\pm)-10d). A mixture of **9d** (113 mg, 0.38 mmol) and a catalytic amount of 10% palladium on carbon in MeOH (2 mL) was stirred under a hydrogen atmosphere at 25 °C. The disappearance of the starting material was monitored by TLC, and the Pd/C was filtered and washed with MeOH (5 mL). The solvent was removed *in vacuo*, and the title compound was used in the next step without any further purification (quantitative yield); ^1H NMR (300 MHz, CDCl_3) δ 7.35–7.20 (m, 4H), 7.15–6.96 (m, 2H), 6.79 (t, J = 7.5 Hz, 1H), 6.68 (d, J = 7.8 Hz, 1H), 5.10 (s, 1H), 4.00 (br, 1H), 3.06–2.87 (m, 1H), 2.80–2.55 (m,

2H), 2.44 (s, 3H), 2.28–1.93 (m, 4H), 1.62–1.43 (m, 2H); ESI-MS m/z : $[M + H]^+$ 297.

(\pm)-2-(4-Fluorophenyl)-1'-methylspiro[indoline-3,4'-piperidine] ((\pm)-**10e**). Starting from **9e** (300 mg, 1.02 mmol), compound (\pm)-**10e** was obtained following the procedure described for the preparation of (\pm)-**10a**. Purification by column chromatography on silica gel (acetone/DCM 1:20) afforded the title compound (176, 58% yield); ^1H NMR (300 MHz, CDCl_3) δ 7.31–7.20 (m, 3H), 7.10 (t, J = 7.6 Hz, 1H), 6.96 (t, J = 8.7 Hz, 2H), 6.77 (t, J = 7.5 Hz, 1H), 6.67 (d, J = 7.9 Hz, 1H), 4.58 (s, 1H), 4.09 (br, 1H), 2.89–2.73 (m, 1H), 2.70–2.55 (m, 1H), 2.55–2.41 (m, 1H), 2.33 (s, 3H), 2.15–2.04 (m, 1H), 2.04–1.89 (m, 2H), 1.84–1.79 (m, 1H), 1.45–1.29 (m, 1H); ESI-MS m/z : $[M + H]^+$ 297.

(\pm)-1'-Methyl-2-(pyridin-3-yl)spiro[indoline-3,4'-piperidine] ((\pm)-**10f**). Starting from **9f** (180 mg, 0.64 mmol), compound (\pm)-**10f** was obtained following the procedure described for the preparation of (\pm)-**10a**. The title compound was used in the next step without any further purification (quantitative yield); ^1H NMR (300 MHz, CDCl_3) δ 8.56 (d, J = 2.3 Hz, 1H), 8.54–8.48 (m, 1H), 7.59 (d, J = 7.9 Hz, 1H), 7.28 (d, J = 7.9 Hz, 1H), 7.25–7.14 (m, 1H), 7.11 (t, J = 7.6 Hz, 1H), 6.79 (t, J = 7.4 Hz, 1H), 6.69 (d, J = 7.7 Hz, 1H), 4.62 (d, J = 1.4 Hz, 1H), 4.10 (br, 1H), 2.87–2.72 (m, 1H), 2.69–2.54 (m, 1H), 2.54–2.40 (m, 1H), 2.31 (s, 3H), 2.16–1.86 (m, 4H), 1.88–1.71 (m, 1H), 1.42–1.24 (m, 1H); ESI-MS m/z : $[M + H]^+$ 280.

(\pm)-Methyl 4-((1'-Methyl-2-phenylspiro[indoline-3,4'-piperidin]-1-yl)methyl)benzoate ((\pm)-**11a**). To a solution of (\pm)-**10a** (121 mg, 0.438 mmol) and methyl 4-formylbenzoate (72 mg, 0.438 mmol) in EtOH (5 mL), AcOH (700 μL) and NaBH_3CN (55 mg, 0.876 mmol) were added. The reaction was then heated to 70 $^\circ\text{C}$ for 2 h and stirred for additional 12 h at 25 $^\circ\text{C}$. The mixture was then treated with a saturated solution of NaHCO_3 (20 mL) and extracted with EtOAc (3 \times 20 mL). The combined organic phases were dried over Na_2SO_4 , and solvents were removed *in vacuo* to give a residue that was purified by flash column chromatography on silica gel (MeOH/DCM 1:15) (65 mg, 35% yield); ^1H NMR (300 MHz, CDCl_3) δ 7.95 (d, J = 8.2 Hz, 2H), 7.32–6.97 (m, 9H), 6.73 (t, J = 7.4 Hz, 1H), 6.35 (d, J = 7.8 Hz, 1H), 4.43–4.28 (m, 2H), 3.96–3.79 (m, 4H), 2.98–2.81 (m, 1H), 2.75–2.46 (m, 2H), 2.36 (s, 3H), 2.18–1.84 (m, 4H), 1.60–1.40 (m, 1H); ESI-MS m/z : $[M + H]^+$ 427.

(\pm)-Methyl 4-((2-(4-Chlorophenyl)-1'-methylspiro[indoline-3,4'-piperidin]-1-yl)methyl)benzoate ((\pm)-**11b**). Starting from (\pm)-**10b** (40 mg, 0.13 mmol), compound (\pm)-**11b** was obtained following the procedure described for the preparation of **11a**. Purification by column chromatography on silica gel (acetone/DCM 1:30) afforded the title compound (26 mg, 43% yield); ^1H NMR (300 MHz, CDCl_3) δ 7.96 (d, J = 8.0 Hz, 2H), 7.34–7.20 (m, 5H), 7.10 (t, J = 7.6 Hz, 3H), 6.75 (t, J = 7.4 Hz, 1H), 6.38 (d, J = 7.8 Hz, 1H), 4.43–4.31 (m, 2H), 3.91 (s, 3H), 3.85 (d, J = 16.1 Hz, 1H), 2.89 (q, J = 5.8, 5.4 Hz, 2H), 2.68–2.54 (m, 2H), 2.38 (s, 3H), 2.18–1.91 (m, 2H), 1.58–1.39 (m, 2H); ESI-MS m/z : $[M + H]^+$ 461.

(\pm)-Methyl 4-((2-(3-Chlorophenyl)-1'-methylspiro[indoline-3,4'-piperidin]-1-yl)methyl)benzoate ((\pm)-**11c**). Starting from (\pm)-**10c** (100 mg, 0.32 mmol), compound (\pm)-**11c** was obtained following the procedure described for the preparation of (\pm)-**11a**. Purification by column chromatography on silica gel (MeOH/DCM 1:20) afforded the title compound (47 mg, 32% yield); ^1H NMR (300 MHz, CD_3OD) δ 7.94 (d, J = 7.5 Hz, 2H), 7.33 (d, J = 8.2 Hz, 2H), 7.32–7.17 (m, 4H), 7.14–7.00 (m, 2H), 6.73 (t, J = 7.5 Hz, 1H), 6.50–6.35 (m, 1H), 4.47 (s, 1H), 4.40 (d, J = 16.3 Hz, 1H), 3.93 (d, J = 16.8 Hz, 1H), 3.88 (s, 3H), 2.96–2.81 (m, 1H), 2.73–2.52 (m, 2H), 2.34 (s, 3H), 2.18–1.98 (m, 2H), 1.97–1.82 (m, 2H), 1.39 (d, J = 30.0 Hz, 1H); ESI-MS m/z : $[M + H]^+$ 461.

(\pm)-Methyl 4-((2-(2-Fluorophenyl)-1'-methylspiro[indoline-3,4'-piperidin]-1-yl)methyl)benzoate ((\pm)-**11d**). Starting from (\pm)-**10d** (156 mg, 0.53 mmol), compound (\pm)-**11d** was obtained following the procedure described for the preparation of (\pm)-**11a**. Purification by column chromatography on silica gel (MeOH/DCM 1:20) afforded the title compound (59 mg, 25% yield); ^1H NMR (300 MHz, CDCl_3) δ 7.97 (d, J = 8.3 Hz, 2H), 7.31–7.19 (m, 4H), 7.17–6.90 (m, 3H), 6.78–6.68 (m, 2H), 6.35 (d, J = 7.8 Hz, 1H), 4.95 (s, 1H), 4.34 (d, J =

16.1 Hz, 1H), 3.87 (s, 3H), 3.86 (d, J = 16.3 Hz, 1H), 2.87–2.73 (m, 1H), 2.59–2.45 (m, 2H), 2.31 (s, 3H), 2.11–1.87 (m, 4H), 1.56–1.43 (m, 1H); ESI-MS m/z : $[M + H]^+$ 445.

(\pm)-Methyl 4-((2-(4-Fluorophenyl)-1'-methylspiro[indoline-3,4'-piperidin]-1-yl)methyl)benzoate ((\pm)-**11e**). Starting from (\pm)-**10e** (178 mg, 0.60 mmol), (\pm)-**11e** was obtained following the procedure described for the preparation of (\pm)-**11a**. Purification by column chromatography on silica gel (MeOH/DCM 1:20) afforded the title compound (122 mg, 46% yield); ^1H NMR (300 MHz, CD_3OD) δ 7.92 (d, J = 6.7 Hz, 2H), 7.30 (d, J = 6.7 Hz, 2H), 7.26–7.11 (m, 3H), 7.07–6.98 (m, 3H), 6.70 (t, J = 7.4 Hz, 1H), 6.43–6.34 (m, 1H), 4.46 (s, 1H), 4.37 (d, J = 16.1 Hz, 1H), 3.91 (d, J = 11.0 Hz, 1H), 3.86 (s, 3H), 2.92–2.77 (m, 1H), 2.68–2.45 (m, 2H), 2.30 (s, 3H), 2.13–1.95 (m, 2H), 1.95–1.75 (m, 2H), 1.46–1.33 (m, 1H); ESI-MS m/z : $[M + H]^+$ 445.

(\pm)-Methyl 4-((1'-Methyl-2-(pyridin-3-yl)spiro[indoline-3,4'-piperidin]-1-yl)methyl)benzoate ((\pm)-**11f**). Starting from (\pm)-**10f** (189 mg, 0.68 mmol), compound (\pm)-**11f** was obtained following the procedure described for the preparation of (\pm)-**11a**. Purification by column chromatography on silica gel (EtOAc/*n*-hexane 1:2) afforded the title compound (73 mg, 25% yield); ^1H NMR (300 MHz, CDCl_3) δ 8.53 (d, J = 6.4 Hz, 1H), 8.36 (m, 1H), 7.96 (d, J = 8.3 Hz, 2H), 7.48–7.37 (m, 1H), 7.32–7.21 (m, 3H), 7.19 (d, J = 6.5 Hz, 1H), 7.09 (t, J = 7.7 Hz, 1H), 6.76 (t, J = 6.9 Hz, 1H), 6.39 (d, J = 7.8 Hz, 2H), 4.45–4.29 (m, 1H), 3.90 (s, 3H), 2.88–2.68 (m, 2H), 2.57–2.40 (m, 2H), 2.09–1.80 (m, 4H), 1.46–1.30 (m, 2H); ESI-MS m/z : $[M + H]^+$ 428.

(\pm)-N-Hydroxy-4-((1'-methyl-2-phenylspiro[indoline-3,4'-piperidin]-1-yl)methyl)benzamide (**6a**). To a solution of (\pm)-**11a** (66 mg, 0.155 mmol) in DCM/MeOH 1:2 cooled at 0 $^\circ\text{C}$, NH_2OH (50% H_2O solution, 1.02 mL, 15.50 mmol) and a 4 M solution of KOH (1.94 mL, 7.75 mmol) were added, and the reaction mixture was left stirring at 25 $^\circ\text{C}$ for 4 h. Then, the pH was adjusted to 7 with 6 N HCl and the solvent was removed under reduced pressure. The residue was purified by column chromatography on silica gel (MeOH/DCM 1:20) affording the final product (45 mg, 68% yield); ^1H NMR (300 MHz, CD_3OD) δ 7.68 (d, J = 8.2 Hz, 2H), 7.40–7.16 (m, 8H), 7.08 (t, J = 7.7 Hz, 1H), 6.73 (t, J = 7.3 Hz, 1H), 6.45 (d, J = 7.9 Hz, 1H), 4.53–4.36 (m, 2H), 3.90 (d, J = 15.9 Hz, 1H), 3.18 (m, 1H), 3.05 (m, 1H), 2.86 (m, 1H), 2.57 (s, 3H), 2.43 (m, 1H), 2.15 (m, 1H), 1.97 (m, 2H), 1.53 (m, 1H). ^{13}C NMR (75 MHz, DMSO) δ 164.7, 151.4, 142.5, 138.1, 136.9, 132.2, 128.8, 128.6, 128.4, 127.7, 124.0, 118.0, 106.8, 77.2, 52.4, 49.9, 46.2, 46.1, 31.4; ESI-MS m/z : $[M + H]^+$ 428; HPLC RT: 13.0 min.

(\pm)-4-((2-(4-Chlorophenyl)-1'-methylspiro[indoline-3,4'-piperidin]-1-yl)methyl)-N-hydroxybenzamide (**6b**). Compound **6b** was obtained from (\pm)-**11b** (26 mg, 0.056 mmol) following the procedure described for the preparation of **6a**. Purification by column chromatography on silica gel (NH_4OH /MeOH/DCM 0.1:1:10) afforded the title compound as a transparent oil (9 mg, 33% yield); ^1H NMR (300 MHz, CD_3OD) δ 11.13 (br, 1H), 8.98 (br, 1H), 7.67 (d, J = 8.3 Hz, 2H), 7.44–7.30 (m, 2H), 7.28 (d, J = 8.3 Hz, 2H), 7.19 (d, J = 7.2 Hz, 2H), 6.99 (t, J = 7.7 Hz, 1H), 6.63 (t, J = 6.9 Hz, 1H), 6.34 (d, J = 6.9 Hz, 2H), 4.51 (s, 1H), 4.31 (d, J = 16.3 Hz, 1H), 3.83 (d, J = 16.3 Hz, 1H), 2.68–2.53 (m, 2H), 2.14 (s, 3H), 1.76–1.63 (m, 4H), 1.22–1.08 (m, 2H); ^{13}C NMR (75 MHz, DMSO) δ 164.7, 151.1, 142.3, 137.2, 136.9, 133.0, 132.2, 128.9, 128.4, 127.8, 127.7, 124.1, 118.1, 106.8, 76.2, 52.4, 52.1, 49.9, 46.6, 46.2, 37.6, 31.5; ESI-MS m/z : $[M + H]^+$ 462; calcd for $\text{C}_{27}\text{H}_{29}\text{N}_3\text{O}_2\text{Cl}$ 462.1943; found 462.1929; HPLC RT: 12.2 min.

(\pm)-4-((2-(3-Chlorophenyl)-1'-methylspiro[indoline-3,4'-piperidin]-1-yl)methyl)-N-hydroxybenzamide (**6c**). Compound **6c** was obtained from (\pm)-**11c** (37 mg, 0.08 mmol) following the procedure described for the preparation of **6a**. Purification by column chromatography on silica gel (NH_4OH /MeOH/DCM 0.1:1:10) afforded the title compound (21 mg, 57% yield); ^1H NMR (300 MHz, CD_3OD) δ 11.15 (br, 1H), 8.99 (br, 1H), 7.67 (d, J = 8.2 Hz, 2H), 7.34 (s, 1H), 7.29 (d, J = 6.5 Hz, 2H), 7.20 (d, J = 7.4 Hz, 2H), 7.00 (t, J = 7.6 Hz, 2H), 6.64 (t, J = 8.1 Hz, 1H), 6.43–6.22 (m, 2H), 4.54 (s, 1H), 4.32 (d, J = 14.0 Hz, 1H), 3.86 (d, J = 16.3 Hz, 1H), 2.74–2.58 (m, 1H), 2.49–2.32 (m, 1H), 2.17 (s, 3H), 2.00–1.82 (m, 2H), 1.79–1.57 (m, 2H), 1.29–1.09 (m, 2H); ^{13}C NMR (75 MHz, CD_3OD) δ 164.9, 149.5, 139.6, 138.3, 137.7, 132.9, 130.6, 128.9, 128.5,

127.8, 127.7, 126.5, 124.2, 121.3, 110.3, 84.4, 52.1, 51.3, 50.6, 46.0, 34.7; ESI-MS m/z : $[M + H]^+$ 462; HPLC RT: 10.4 min.

(\pm)-4-((2-(2-Fluorophenyl)-1'-methylspiro[indoline-3,4'-piperidin]-1-yl)methyl)-N-hydroxybenzamide (**6d**). Compound **6d** was obtained from (\pm)-**11d** (30 mg, 0.07 mmol) following the procedure described for the preparation of **6a**. Purification by column chromatography on silica gel ($\text{NH}_4\text{OH}/\text{MeOH}/\text{DCM}$ 0.1:1:10) afforded the title compound (12 mg, 40%); ^1H NMR (300 MHz, CD_3OD) δ 11.15 (br, 1H), 8.99 (br, 1H), 7.66 (d, J = 8.3 Hz, 2H), 7.41–7.27 (m, 2H), 7.31–7.15 (m, 2H), 7.17–7.04 (m, 2H), 7.02 (t, J = 8.3 Hz, 2H), 6.65 (t, J = 6.9 Hz, 1H), 6.43 (d, J = 7.8 Hz, 1H), 4.84 (s, 1H), 4.41 (d, J = 16.0 Hz, 1H), 3.78 (d, J = 16.0 Hz, 1H), 2.74–2.57 (m, 1H), 2.44–2.24 (m, 2H), 2.15 (s, 3H), 1.91–1.67 (m, 4H), 1.29–1.09 (m, 1H); ^{13}C NMR (75 MHz, DMSO) δ 164.7, 162.5, 159.2, 151.2, 141.9, 136.5, 132.2, 130.5, 129.4, 128.6, 127.9, 127.7, 125.1, 124.8, 124.1, 118.2, 116.7, 116.4, 106.8, 67.5, 52.4, 51.9, 49.7, 46.5, 46.4, 37.7, 31.7; ESI-MS m/z : $[M + H]^+$ 446; HRMS-ESI m/z : $[M + H]^+$ calcd for $\text{C}_{27}\text{H}_{29}\text{FN}_3\text{O}_2$ 446.2238; found 446.2225; HPLC RT: 10.6 min.

(\pm)-4-((2-(4-Fluorophenyl)-1'-methylspiro[indoline-3,4'-piperidin]-1-yl)methyl)-N-hydroxybenzamide (**6e**). Compound **6e** was obtained from (\pm)-**11e** (60 mg, 0.13 mmol) following the procedure described for the preparation of **6a**. Purification by column chromatography on silica gel ($\text{NH}_4\text{OH}/\text{MeOH}/\text{DCM}$ 0.1:1:10) afforded the title compound (32 mg, 56% yield); ^1H NMR (300 MHz, CD_3OD) δ 11.12 (br, 1H), 8.99 (br, 1H), 7.67 (d, J = 8.0 Hz, 2H), 7.28 (d, J = 8.0 Hz, 2H), 7.21–7.04 (m, 4H), 6.98 (t, J = 7.6 Hz, 2H), 6.63 (t, J = 7.3 Hz, 1H), 6.33 (d, J = 7.8 Hz, 1H), 4.50 (s, 1H), 4.30 (d, J = 16.2 Hz, 1H), 3.83 (d, J = 16.3 Hz, 1H), 2.60 (s, 1H), 2.35–2.23 (m, 1H), 2.12 (s, 3H), 1.95–1.79 (m, 2H), 1.79–1.53 (m, 2H), 1.33–1.07 (m, 2H); ^{13}C NMR (75 MHz, CD_3OD) δ 166.7, 164.4, 161.1, 150.9, 142.7, 136.0, 133.4, 132.0, 131.2, 129.1, 127.9, 127.6, 127.1, 123.3, 117.8, 114.7, 106.4, 76.2, 51.9, 51.8, 49.6, 45.6, 44.9, 36.6, 30.8; ESI-MS m/z : $[M + H]^+$ 446; HRMS-ESI m/z : $[M + H]^+$ calcd for $\text{C}_{27}\text{H}_{29}\text{FN}_3\text{O}_2$ 446.2238; found 446.2227; HPLC RT: 11.4 min.

(\pm)-N-Hydroxy-4-((1'-methyl-2-(pyridin-3-yl)spiro[indoline-3,4'-piperidin]-1-yl)methyl)benzamide (**6f**). Compound **6f** was obtained from (\pm)-**11f** (45 mg, 0.11 mmol) following the procedure described for the preparation of **6a**. Purification by column chromatography on silica gel ($\text{NH}_4\text{OH}/\text{MeOH}/\text{DCM}$ 0.1:1:10) afforded the title compound (34 mg, 73% yield); ^1H NMR (300 MHz, CD_3OD) δ 11.16 (br, 1H), 8.99 (br, 1H), 8.53 (s, 1H), 7.68 (d, J = 7.9 Hz, 2H), 7.35 (s, 2H), 7.29 (d, J = 8.0 Hz, 2H), 7.07 (t, J = 7.6 Hz, 1H), 6.71 (t, J = 7.4 Hz, 1H), 6.44 (d, J = 7.8 Hz, 1H), 4.59 (s, 1H), 4.36 (d, J = 16.1 Hz, 1H), 3.85 (d, J = 16.1 Hz, 2H), 3.05–2.87 (m, 1H), 2.64 (s, 3H), 2.14–1.86 (m, 4H), 1.30–1.16 (m, 2H); ^{13}C NMR (75 MHz, CD_3OD) δ 166.6, 150.7, 149.3, 142.1, 136.3, 133.8, 133.4, 131.3, 128.8, 127.7, 127.3, 124.2, 123.3, 118.7, 107.4, 73.9, 51.4, 49.9, 44.9, 42.9, 34.2, 34.1, 29.1; ESI-MS m/z : $[M + H]^+$ 429; HRMS-ESI m/z : $[M + H]^+$ calcd for $\text{C}_{26}\text{H}_{29}\text{N}_4\text{O}_2$ 429.2285; found 429.2271; HPLC RT: 7.1 min.

Methyl 4-Bromobutanoate (**13**). 4-Bromobutyl chloride (1.6 mL, 13.82 mmol) was treated with MeOH (7 mL) at 0 °C. The reaction mixture was stirred at 0 °C for 2 h and then at 25 °C for 12 h. The solvent was removed under reduced pressure. The title compound was obtained as pure compound without further purification (quantitative yield); ^1H NMR (300 MHz, CDCl_3) δ 3.65 (s, 3H), 3.43 (t, J = 5.7 Hz, 2H), 2.48 (t, J = 6.4 Hz, 2H), 2.22–2.04 (m, 2H).

Methyl 4-(*p*-Tolyloxy)butanoate (**14**). To a solution of *p*-cresol (500 mg, 2.76 mmol) in dry MeCN (2.5 mL), Cs_2CO_3 (900 mg, 2.76 mmol) and the mixture were stirred at 95 °C for 30 min. Then, a solution of **13** (149 mg, 1.38 mmol) in dry MeCN (2.5 mL) was added and the reaction mixture was left at 95 °C for 12 h. The reaction was cooled down to 25 °C; then, the solvent was removed under reduced pressure. The residue was dissolved in EtOAc , washed with a saturated solution of NaHCO_3 , dried over Na_2SO_4 , and evaporated *in vacuo*. Purification by column chromatography on silica gel (EtOAc/n -hexane 1:8) afforded the title compound (425 mg, 74% yield); ^1H NMR (300 MHz, CDCl_3) δ 7.07 (d, J = 8.1 Hz, 2H), 6.78 (d, J = 8.6 Hz, 2H), 3.97 (t, J = 6.1 Hz, 2H), 3.68 (s, 3H), 2.52 (t, J = 7.3 Hz, 2H), 2.28 (s, 3H), 2.17–1.99 (m, 2H).

Methyl 4-(4-Formylphenoxy)butanoate (**16**). Methyl 4-(4-(Bromomethyl)phenoxy)butanoate (**15**). To a solution of **14** (420 mg, 2.01 mmol) in CCl_4 were added NBS (77 mg, 0.9 mmol) and AIBN (33 mg, 0.20 mmol), and the reaction mixture was kept stirring at 80 °C for 4 h. The solvent was evaporated to obtain compound **15** that was immediately used in the next reaction without further purification.

To a solution of **15** (100 mg, 0.35 mmol) in DMSO (1.5 mL) was added NBS (87 mg, 0.49 mmol), and the reaction mixture was kept stirring at 60 °C for 1 h and then at 100 °C for an additional hour. After cooling, H_2O was added (15 mL) and organic products were extracted with EtOAc (3 \times 15 mL). The organic phase was dried over Na_2SO_4 and reduced *in vacuo*. Purification by column chromatography on silica gel (EtOAc/n -hexane 1:4) afforded the title compound (23 mg, 30% yield over two steps); ^1H NMR (300 MHz, CDCl_3) δ 9.87 (s, 1H), 7.87 (d, J = 7.6 Hz, 2H), 7.15 (d, J = 7.5 Hz, 2H), 4.02 (t, J = 7.5 Hz, 2H), 3.64 (s, 3H), 2.48 (t, J = 8.1 Hz, 2H), 2.16–2.06 (m, 2H).

Methyl 5-Methylthiophene-2-carboxylate (**18**). To a solution of 5-methyl-2-thiophenecarboxylic acid (1.0 g, 7.0 mmol) in MeOH (15 mL), SOCl_2 (2 mL) was added dropwise at 0 °C. The reaction mixture was allowed to reach 25 °C and then was left stirring for 12 h. The solvent was removed, and the residue was dissolved in EtOAc and washed with a saturated solution of NaHCO_3 . The title compound was used in the next step without any further purification (quantitative yield). ^1H NMR (300 MHz, CDCl_3) δ 7.60 (d, J = 3.7 Hz, 1H), 6.76 (d, J = 3.7 Hz, 1H), 3.85 (s, 3H), 2.51 (s, 3H). ESI-MS m/z : $[M + H]^+$ 157.

Methyl 5-(Bromomethyl)thiophene-2-carboxylate (**19**). To a solution of **18** (570 mg, 3.65 mmol) in CCl_4 (8 mL), NBS (584 mg, mmol) and AIBN (60 mg, 0.37 mmol) were added and the reaction mixture was stirred at 80 °C for 4 h. CCl_4 was removed under reduced pressure, and the residue was diluted with DCM and purified by column chromatography on silica gel (EtOAc/n -hexane 1:30) (512 mg, 60% yield); ^1H NMR (300 MHz, CDCl_3) δ 7.63 (d, J = 3.8 Hz, 1H), 7.08 (d, J = 3.8 Hz, 1H), 4.66 (s, 3H), 3.87 (s, 3H); ESI-MS m/z : $[M + H]^+$ 235.

Methyl 5-Formylthiophene-2-carboxylate (**20**). To a solution of 4-methylmorpholine *N*-oxide (449 mg, 3.83 mmol) in MeCN (5 mL), cooled at 0 °C and in the presence of 3 Å molecular sieves, a solution of **19** (300 mg, 1.28 mmol) in MeCN was added. The reaction mixture was stirred at 25 °C for 12 h, and then, it was purified by column chromatography on silica gel (EtOAc/n -hexane 1:20) obtaining the title compound (152 mg, 70% yield); ^1H NMR (300 MHz, CDCl_3) δ 9.96 (s, 1H), 7.82 (d, J = 1.1 Hz, 1H), 7.72 (d, J = 2.8 Hz, 1H), 3.93 (s, 3H); ESI-MS m/z : $[M + H]^+$ 171.

2-Methyl-1-(pyridin-3-yl)propan-1-one (**22b**). Starting from **21** (513 mg, 2.27 mmol) and 3-pyridinecarboxaldehyde (214 μL , 2.27 mmol), compound **22b** was obtained following the procedure described for the preparation of **8a**. Purification by column chromatography on silica gel ($\text{EtOAc}/\text{EtPet}$ 1:2) afforded the title compound (301 mg, 89% yield); ^1H NMR (300 MHz, CDCl_3) δ 9.11 (s, 1H), 8.72 (d, J = 4.8 Hz, 1H), 8.23–8.13 (m, 1H), 7.44–7.33 (m, 1H), 3.60–3.36 (m, 1H), 1.20 (s, 3H), 1.18 (s, 3H); ESI-MS m/z : $[M + H]^+$ 150.

2-Methyl-1-(pyridin-4-yl)propan-1-one (**22c**). Starting from **21** (1.0 g, 4.41 mmol) and 4-pyridinecarboxaldehyde (474 μL , 4.41 mmol), compound **22c** was obtained following the procedure described for the preparation of **8a**. The title compound was used in the next step without any further purification (quantitative yield); ^1H NMR (300 MHz, CDCl_3) δ 8.79 (d, J = 4.5 Hz, 2H), 7.70 (d, J = 4.5 Hz, 2H), 3.53–3.43 (m, 1H), 1.23 (s, 3H), 1.21 (s, 3H); ESI-MS m/z : $[M + H]^+$ 150.

3,3-Dimethyl-2-phenyl-3H-indole (**23a**). To a solution of the commercially available 2-methyl-1-phenylpropan-1-one (**22a**, 506 μL , 3.37 mmol) in AcOH (5 mL), phenylhydrazine (331 μL , 3.37 mmol) was added. The reaction was heated at 80 °C for 12 h; then, it was concentrated to dryness, extracted with EtOAc , and washed with Na_2CO_3 . The organic layer was dried over Na_2SO_4 , evaporated, and purification by column chromatography on silica gel (EtOAc/n -hexane 1:30) afforded the title compound (357 mg, 48% yield); ^1H NMR (300 MHz, CDCl_3) δ 8.22–8.09 (m, 2H), 7.77–7.65 (m, 1H), 7.55–7.45 (m, 3H), 7.40–7.21 (m, 3H), 1.60 (s, 6H); ESI-MS m/z : $[M + \text{Na}]^+$ 222.

3,3-Dimethyl-2-(pyridin-3-yl)-3H-indole (23b). Starting from **22b** (300 mg, 2.01 mmol), compound **23b** was obtained following the procedure described for the preparation of **23a**. Purification by column chromatography on silica gel (EtOAc/*n*-hexane 1:2) afforded the title compound (134 mg, 30% yield); ^1H NMR (300 MHz, CDCl_3) δ 9.31 (s, 1H), 8.70 (d, J = 4.7 Hz, 1H), 8.48 (d, J = 8.1 Hz, 1H), 7.70 (d, J = 7.6 Hz, 1H), 7.45–7.25 (m, 4H), 1.59 (s, J = 0.6 Hz, 6H); ESI-MS m/z : $[\text{M} + \text{H}]^+ 223$.

3,3-Dimethyl-2-(pyridin-4-yl)-3H-indole (23c). Compound **23c** was obtained from **22c** (745 mg, 5.0 mmol) following the procedure described for the preparation of **23a**. Purification by column chromatography on silica gel (EtOAc/*n*-hexane 1:1) afforded the title compound (333 mg, 30% yield); ^1H NMR (300 MHz, CDCl_3) δ 8.76 (d, J = 4.7 Hz, 2H), 7.96 (d, J = 6.2 Hz, 2H), 7.79–7.69 (m, 1H), 7.48–7.29 (m, 3H), 1.59 (s, 6H); ESI-MS m/z : $[\text{M} + \text{H}]^+ 223$.

5-Methoxy-3,3-dimethyl-2-(pyridin-3-yl)-3H-indole (23d). Starting from **22b** (500 mg, 3.36 mmol) and 4-methoxyphenylhydrazine (587 mg, 3.36 mmol), compound **23d** was obtained following the procedure described for the preparation of **23b**. Purification by column chromatography on silica gel (EtOAc/*n*-hexane 1:1) afforded the title compound (322 mg, 38% yield); ^1H NMR (300 MHz, CDCl_3) δ 9.27 (s, 1H), 8.67 (d, J = 3.2 Hz, 1H), 8.51–8.36 (m, 1H), 7.61 (d, J = 9.2 Hz, 1H), 7.46–7.34 (m, 1H), 6.95–6.80 (m, 2H), 3.87 (s, 3H), 1.58 (s, 6H); ESI-MS m/z : $[\text{M} + \text{H}]^+ 253$.

(\pm)-3,3-Dimethyl-2-phenylindoline ((\pm)-24a). To a solution of **23a** (500 mg, 2.26 mmol) in MeOH (25 mL), NaBH_4 (513 mg, 13.56 mmol) was added. The reaction was stirred for 12 h at 50 °C. Then, the reaction was quenched with a saturated solution of NaHCO_3 (10 mL), MeOH was removed under reduced pressure, and the residue was dissolved with EtOAc and washed with H_2O (3×20 mL). The organic phase was dried over Na_2SO_4 , and solvents were removed *in vacuo* to give a residue that was purified by flash column chromatography on silica gel (MeOH/DCM 1:30) (304 mg, 60% yield); ^1H NMR (300 MHz, CDCl_3) δ 7.45–7.38 (m, 1H), 7.34–7.26 (m, 3H), 7.26–7.13 (m, 2H), 6.80–6.71 (m, 1H), 6.63–6.56 (m, 1H), 4.69 (s, 1H), 3.71 (br, 1H), 1.36 (s, 3H), 0.98 (s, 3H).

(\pm)-3,3-Dimethyl-2-(pyridin-3-yl)indoline ((\pm)-24b). Starting from **23b** (500 mg, 2.26 mmol), (\pm)-**24a** was obtained following the procedure described for (\pm)-**24a**. Purification by column chromatography on silica gel (MeOH/DCM 1:30) (305 mg, 60% yield); ^1H NMR (300 MHz, CDCl_3) δ 8.67 (s, 1H), 8.56 (d, J = 6.4 Hz, 1H), 7.92–7.80 (m, 1H), 7.84–7.73 (m, 1H), 7.36–7.21 (m, 1H), 7.14–6.99 (m, 1H), 6.81 (t, J = 8.0 Hz, 1H), 6.74 (d, J = 7.4 Hz, 1H), 4.61 (s, 1H), 4.08 (br, 1H), 1.44 (s, 3H), 0.74 (s, 3H).

(\pm)-3,3-Dimethyl-2-(pyridin-4-yl)indoline ((\pm)-24c). Starting from **23c** (300 mg, 1.02 mmol), compound (\pm)-**24c** was obtained following the procedure described for the preparation of (\pm)-**24a**. Purification by column chromatography on silica gel (MeOH/DCM 1:20) afforded the title compound (115 mg, 50% yield); ^1H NMR (300 MHz, CDCl_3) δ 8.57 (d, J = 4.9 Hz, 2H), 7.39 (d, J = 5.1 Hz, 2H), 7.17–6.96 (m, 2H), 6.85–6.77 (m, 1H), 6.73 (d, J = 7.7 Hz, 1H), 4.57 (s, 1H), 4.10 (br, 1H), 1.46 (s, 3H), 0.72 (s, 3H); ESI-MS m/z : $[\text{M} + \text{H}]^+ 225$.

(\pm)-5-Methoxy-3,3-dimethyl-2-(pyridin-3-yl)indoline ((\pm)-24d). Starting from **23d** (327 mg, 1.29 mmol), compound (\pm)-**24d** was obtained following the procedure described for the preparation of (\pm)-**24a**. Purification by column chromatography on silica gel (MeOH/DCM 1:30) afforded the title compound (259 mg, 79% yield); ^1H NMR (300 MHz, CDCl_3) δ 8.67 (s, 1H), 8.56 (d, J = 5.5 Hz, 2H), 7.85 (d, J = 7.9 Hz, 1H), 7.44–7.31 (m, 1H), 6.90–6.80 (m, 1H), 6.73–6.52 (m, 2H), 4.59 (s, 1H), 3.87 (s, 3H), 1.42 (s, 3H), 0.74 (s, 3H); ESI-MS m/z : $[\text{M} + \text{H}]^+ 255$.

(\pm)-Methyl 4-((3,3-Dimethyl-2-phenylindolin-1-yl)methyl)benzoate ((\pm)-25a). Starting from (\pm)-**24a** (506 mg, 3.37 mmol), compound (\pm)-**25a** was obtained following the procedure described for the preparation of (\pm)-**11a**. Purification by column chromatography on silica gel (EtOAc/*n*-hexane 1:20) afforded the title compound (1050 mg, 84% yield); ^1H NMR (300 MHz, CDCl_3) δ 7.99 (d, J = 8.3 Hz, 2H), 7.44–7.15 (m, 6H), 7.14–6.88 (m, 2H), 6.79 (t, J = 7.9 Hz, 1H), 6.39 (d, J = 7.8 Hz, 1H), 4.43 (d, J = 16.4 Hz, 1H), 4.29 (s, 1H),

4.05 (d, J = 16.4 Hz, 1H), 3.92 (s, 3H), 1.41 (s, 3H), 0.84 (s, 3H); ESI-MS m/z : $[\text{M} + \text{H}]^+ 372$, $[\text{M} + \text{Na}]^+ 394$.

(\pm)-Methyl 4-((3,3-Dimethyl-2-(pyridin-3-yl)indolin-1-yl)methyl)benzoate ((\pm)-25b). Starting from (\pm)-**24b** (130 mg, 0.585 mmol), compound (\pm)-**25b** was obtained following the procedure described for the preparation of (\pm)-**11a**. Purification by column chromatography on silica gel (EtOAc/*n*-hexane 1:3) (43 mg, 20% yield); ^1H NMR (300 MHz, CDCl_3) δ 8.57 (br, 1H), 7.97 (d, J = 8.2 Hz, 2H), 7.70 (br, 1H), 7.33 (d, J = 8.0 Hz, 2H), 7.06 (dd, J = 12.1, 4.4 Hz, 2H), 6.82 (t, J = 7.4 Hz, 1H), 6.43 (d, J = 7.9 Hz, 1H), 4.37 (d, J = 16.2 Hz, 1H), 4.28 (s, 1H), 4.04 (d, J = 16.4 Hz, 1H), 3.91 (s, 3H), 1.40 (s, 3H), 0.83 (s, 3H); ESI-MS m/z : $[\text{M} + \text{H}]^+ 372$, $[\text{M} + \text{Na}]^+ 394$;

(+)-Methyl 4-((3,3-Dimethyl-2-(pyridin-3-yl)indolin-1-yl)methyl)benzoate ((+)-25b). ^1H NMR data are identical to those of the racemic mixture (\pm)-**25b**; $[\alpha]_D^{20}$ = +51.0 (c 0.58, CHCl_3);

(–)-Methyl 4-((3,3-Dimethyl-2-(pyridin-3-yl)indolin-1-yl)methyl)benzoate ((–)-25b). ^1H NMR data are identical to those of the racemic mixture (\pm)-**25b**; $[\alpha]_D^{20}$ = –52.0 (c 0.63, CHCl_3).

(\pm)-Methyl 4-((5-Methoxy-3,3-dimethyl-2-(pyridin-3-yl)indolin-1-yl)methyl)benzoate ((\pm)-25c). Starting from (\pm)-**24c** (102 mg, 0.40 mmol), compound (\pm)-**25c** was obtained following the procedure described for the preparation of (\pm)-**11a**. Purification by column chromatography on silica gel (EtOAc/*n*-hexane 1:2) afforded the title compound (39 mg, 24% yield); ^1H NMR (300 MHz, CDCl_3) δ 8.57 (s, 1H), 7.97 (d, J = 8.4 Hz, 2H), 7.36 (d, J = 7.9 Hz, 2H), 7.33–7.18 (m, 2H), 6.70 (d, J = 2.5 Hz, 1H), 6.61–6.53 (m, 1H), 6.30 (d, J = 8.5 Hz, 2H), 4.28 (d, J = 16.4 Hz, 1H), 4.22 (s, 1H), 3.98 (d, J = 16.2 Hz, 1H), 3.91 (s, 3H), 3.76 (s, 3H), 1.39 (s, 3H), 0.83 (s, 3H); ESI-MS m/z : $[\text{M} + \text{H}]^+ 403$, $[\text{M} + \text{Na}]^+ 426$.

(\pm)-Methyl 5-((3,3-Dimethyl-2-(pyridin-3-yl)indolin-1-yl)methyl)thiophene-2-carboxylate ((\pm)-25d). To a solution of (\pm)-**24b** (140 mg, 0.63 mmol) in dry DCM (3 mL) was added a solution of **20** (106 mg, 0.63 mmol) in dry DCM (3 mL). After 1 h at 25 °C, $\text{NaBH}(\text{OAc})_3$ (668 mg, 2.52 mmol) was added and the reaction mixture was stirred at 50 °C for 12 h. The reaction was treated with a saturated solution of NaHCO_3 , and organic products were extracted with DCM. The combined organic layers were washed with brine, dried over Na_2SO_4 , and concentrated *in vacuo*. Purification by column chromatography on silica gel (PetEt/ Et_2O 2:1) afforded the title compound (126 mg, 53% yield); ^1H NMR (300 MHz, CDCl_3) δ 8.64–8.49 (m, 2H), 7.81 (br, 1H), 7.62 (d, J = 3.8 Hz, 1H), 7.39–7.28 (m, 1H), 7.15–6.98 (m, 2H), 6.87–6.75 (m, 2H), 6.61 (d, J = 7.8 Hz, 1H), 4.50 (d, J = 16.2 Hz, 1H), 4.22 (s, 1H), 4.16 (d, J = 16.3 Hz, 1H), 1.35 (s, 3H), 0.79 (s, 3H); ESI-MS m/z : $[\text{M} + \text{H}]^+ 379$.

(\pm)-Methyl 4-((4-((3,3-Dimethyl-2-(pyridin-3-yl)indolin-1-yl)methyl)phenoxy)butanoate ((\pm)-25e). Starting from (\pm)-**24b** (61 mg, 0.27 mmol) and **16** (60 mg, 0.27 mmol), compound (\pm)-**25f** was obtained following the procedure described for the preparation of (\pm)-**25e**. Purification by column chromatography on silica gel (PetEt/ Et_2O 1:1) and afforded the title compound (23 mg, 20% yield); ^1H NMR (300 MHz, CDCl_3) δ 8.56 (d, J = 4.8 Hz, 2H), 7.71 (br, 1H), 7.32–7.18 (m, 2H), 7.16–6.99 (m, 4H), 6.85–6.71 (m, 2H), 6.55 (d, J = 7.8 Hz, 1H), 4.35 (d, J = 15.5 Hz, 1H), 4.22 (s, 1H), 3.97 (t, J = 6.1 Hz, 2H), 3.90 (d, J = 15.5 Hz, 1H), 3.69 (s, 3H), 2.52 (t, J = 7.3 Hz, 2H), 2.15–2.01 (m, 2H), 1.37 (s, 3H), 0.79 (s, 3H); ESI-MS m/z : $[\text{M} + \text{H}]^+ 431$.

(\pm)-Methyl 4-((3,3-Dimethyl-2-(pyridin-4-yl)indolin-1-yl)methyl)benzoate ((\pm)-25f). Starting from (\pm)-**24d** (150 mg, 0.67 mmol), compound (\pm)-**25d** was obtained following the procedure described for the preparation of (\pm)-**11a**. Purification by column chromatography on silica gel (EtOAc/*n*-hexane 1:2) afforded the title compound (62 mg, 25% yield); ^1H NMR (300 MHz, CDCl_3) δ 8.57 (d, J = 5.1 Hz, 2H), 7.98 (d, J = 8.4 Hz, 2H), 7.38–7.21 (m, 4H), 7.11–6.96 (m, 2H), 6.88–6.72 (m, 1H), 6.43 (d, J = 8.2 Hz, 1H), 4.39 (d, J = 16.4 Hz, 1H), 4.25 (s, 1H), 4.05 (d, J = 16.4 Hz, 1H), 3.91 (s, 3H), 1.42 (s, 3H), 0.81 (s, 3H); ESI-MS m/z : $[\text{M} + \text{Na}]^+ 395$.

(\pm)-4-((3,3-Dimethyl-2-phenylindolin-1-yl)methyl)-N-hydroxybenzamide (6g). Starting from (\pm)-**25a** (100 mg, 0.27 mmol), compound **6g** was obtained following the procedure described for the preparation of **6a**. Purification by column chromatography on silica gel (MeOH/DCM NH_4OH 1:20:0.1) afforded the title compound (18

mg, 18% yield); ^1H NMR (300 MHz, DMSO) δ 7.67 (d, J = 8.2 Hz, 2H), 7.43–7.21 (m, 7H), 7.12–6.84 (m, 2H), 6.71 (t, J = 7.4 Hz, 1H), 6.43 (d, J = 7.8 Hz, 1H), 4.45 (d, J = 16.2 Hz, 1H), 4.24 (s, 1H), 4.00 (d, J = 16.3 Hz, 1H), 1.35 (s, 3H), 0.76 (s, 3H); ^{13}C NMR (75 MHz, DMSO) δ 164.2, 150.8, 141.7, 138.7, 137.9, 132.4, 129.0, 128.4, 127.4, 127.9, 127.6, 122.7, 119.0, 108.7, 79.7, 50.7, 44.6, 27.2, 25.8; ESI-MS m/z : $[\text{M} + \text{H}]^+$ 373, $[\text{M} + \text{Na}]^+$ 395; HRMS-ESI m/z : $[\text{M} + \text{Na}]^+$ calcd for $\text{C}_{24}\text{H}_{24}\text{N}_3\text{O}_3\text{Na}$ 395.1730; found 395.1727; HPLC RT: 19.0 min.

(\pm)-4-((3,3-Dimethyl-2-(pyridin-3-yl)indolin-1-yl)methyl)-*N*-hydroxybenzamide (**6h**). Starting from (\pm)-**25b** (40 mg, 0.114 mmol), compound (\pm)-**6h** was obtained following the procedure described for the preparation of **6a**. Purification by column chromatography on silica gel (MeOH/DCM/NH₄OH 1:8:0.1) afforded the title compound (14 mg, 33% yield); ^1H NMR (300 MHz, CD₃OD) δ 11.01 (br, 1H), 9.06 (br, 1H), 8.52 (dd, J = 4.8, 1.5 Hz, 2H), 7.75 (d, J = 7.8 Hz, 1H), 7.67 (d, J = 8.2 Hz, 2H), 7.44–7.37 (m, 1H), 7.29 (d, J = 8.2 Hz, 2H), 7.07 (d, J = 7.2 Hz, 1H), 6.99 (dd, J = 8.2, 7.1 Hz, 1H), 6.70 (t, J = 7.3 Hz, 1H), 6.44 (d, J = 7.8 Hz, 1H), 4.46–4.29 (m, 2H), 3.97 (d, J = 16.4 Hz, 1H), 1.32 (s, 3H), 0.71 (s, 3H); ^{13}C NMR (75 MHz, CD₃OD): δ 167.3, 166.7, 150.5, 148.9, 148.4, 142.5, 138.0, 134.5, 131.2, 127.6, 127.5, 127.2, 123.9, 122.0, 119.3, 108.6, 77.8, 53.6, 44.6, 25.9, 24.5; ESI-MS m/z : $[\text{M} + \text{H}]^+$ 374; HRMS-ESI m/z : $[\text{M} + \text{H}]^+$ calcd for $\text{C}_{23}\text{H}_{24}\text{N}_3\text{O}_2$ 374.1869; found 374.1862; HPLC RT: 10.4 min.

(+)-4-((3,3-Dimethyl-2-(pyridin-3-yl)indolin-1-yl)methyl)-*N*-hydroxybenzamide ((+)-**6h**). Starting from (+)-**25b** (23 mg, 0.062 mmol), compound (+)-**6h** was obtained following the procedure described for the preparation of **6a**. Purification by column chromatography on silica gel (MeOH/DCM/NH₄OH 1:8:0.1) afforded the compound (9 mg, 38% yield); ^1H NMR data are identical to those of the racemic mixture ((\pm)-**6h**); $[\alpha]_{\text{D}}^{20}$ = +35.0 (c 0.16, CHCl₃);

(–)-4-((3,3-Dimethyl-2-(pyridin-3-yl)indolin-1-yl)methyl)-*N*-hydroxybenzamide ((–)-**6h**). Starting from (–)-**25b** (20 mg, 0.054 mmol), compound (–)-**6h** was obtained following the procedure described for the preparation of **6a**. Purification by column chromatography on silica gel (MeOH/DCM/NH₄OH 1:8:0.1) afforded the title compound (8 mg, 34% yield); ^1H NMR data are identical to those of the racemic mixture ((–)-**6h**); $[\alpha]_{\text{D}}^{20}$ = –36.0 (c 0.39, CHCl₃);

(\pm)-*N*-Hydroxy-4-((5-methoxy-3,3-dimethyl-2-(pyridin-3-yl)indolin-1-yl)methyl)benzamide (**6i**). Compound **6i** was obtained from (\pm)-**25c** (32 mg, 0.08 mmol) following the procedure described for the preparation of **6a**. Purification by column chromatography on silica gel (DCM/MeOH/NH₄OH 0.1:1:8) afforded the title compound (16 mg, 49% yield); ^1H NMR (300 MHz, CD₃OD) δ 11.12 (br, 1H), 8.98 (br, 1H), 8.61–8.44 (m, 2H), 7.67 (d, J = 8.1 Hz, 2H), 7.43–7.33 (m, 1H), 7.32 (d, J = 8.1 Hz, 2H), 6.75 (d, J = 2.5 Hz, 1H), 6.62–6.51 (m, 2H), 6.30 (d, J = 8.4 Hz, 1H), 4.32–4.21 (m, 2H), 3.90 (d, J = 16.3 Hz, 1H), 3.64 (s, 3H), 1.30 (s, 3H), 0.71 (s, 3H); ^{13}C NMR (75 MHz, CD₃OD) δ 166.7, 154.4, 148.9, 148.3, 144.6, 142.7, 139.6, 137.2, 134.5, 131.1, 127.6, 127.1, 123.8, 112.0, 109.4, 109.2, 78.6, 55.1, 52.3, 44.7, 25.2, 24.3; ESI-MS m/z : $[\text{M} + \text{H}]^+$ 404; HPLC RT: 9.5 min.

(\pm)-5-((3,3-Dimethyl-2-(pyridin-3-yl)indolin-1-yl)methyl)-*N*-hydroxythiophene-2-carboxamide (**6j**). Compound **6j** was obtained from (\pm)-**25d** (65 mg, 0.17 mmol) following the procedure described for the preparation of **6a**. Purification by column chromatography on silica gel (NH₄OH/MeOH/DCM 0.1:1:10) afforded the title compound (52 mg, 77% yield); ^1H NMR (300 MHz, DMSO) δ 11.14 (br, 1H), 8.99 (br, 1H), 8.54 (d, J = 5.2 Hz, 2H), 7.67 (d, J = 8.2 Hz, 2H), 7.37–7.22 (m, 4H), 7.06 (d, J = 7.3 Hz, 1H), 6.99 (t, J = 7.7 Hz, 1H), 6.70 (t, J = 7.4 Hz, 1H), 6.45 (d, J = 7.8 Hz, 1H), 4.40 (d, J = 16.4 Hz, 1H), 4.31 (s, 1H), 3.98 (d, J = 16.4 Hz, 1H), 1.34 (s, 3H), 0.69 (s, 3H); ^{13}C NMR (75 MHz, DMSO) δ 172.7, 164.7, 150.6, 150.3, 147.2, 141.7, 138.3, 132.2, 128.0, 127.7, 123.8, 122.7, 119.3, 108.9, 78.5, 55.5, 44.8, 27.3, 25.6; ESI-MS m/z : $[\text{M} + \text{H}]^+$ 374 $[\text{M} + \text{Na}]^+$ 396; HRMS-ESI m/z : $[\text{M} + \text{H}]^+$ calcd for $\text{C}_{23}\text{H}_{24}\text{N}_3\text{O}_2$ 374.1863; found 374.1853; HPLC RT: 10.1 min.

(\pm)-4-((3,3-Dimethyl-2-(pyridin-3-yl)indolin-1-yl)methyl)-phenoxyl)-*N*-hydroxybutanamide (**6k**). Compound **6k** was obtained from (\pm)-**25e** (74 mg, 0.20 mmol) following the procedure described

for the preparation of **6a**. Purification by column chromatography on silica gel (NH₄OH/MeOH/DCM 0.1:1:12) afforded the title compound (48 mg, 63% yield); ^1H NMR (300 MHz, CD₃OD) δ 8.61–8.45 (m, 2H), 7.92 (br, 1H), 7.50–7.45 (m, 1H), 7.43–7.35 (m, 1H), 7.08–7.01 (m, 2H), 6.86–6.74 (m, 2H), 6.70 (d, J = 7.8 Hz, 1H), 4.60 (d, J = 16.3 Hz, 1H), 4.25 (s, 1H), 4.17 (d, J = 16.3 Hz, 1H), 1.33 (s, 3H), 0.74 (s, 3H); ^{13}C NMR (75 MHz, CD₃OD) δ 161.7, 149.4, 149.0, 148.5, 145.9, 138.2, 137.2, 134.9, 134.0, 128.1, 127.5, 126.4, 124.3, 122.0, 119.2, 109.1, 76.9, 45.7, 44.7, 25.4, 24.6. ESI-MS m/z : $[\text{M} + \text{H}]^+$ 380; HRMS-ESI m/z : $[\text{M} + \text{H}]^+$ calcd for $\text{C}_{21}\text{H}_{22}\text{N}_3\text{O}_2\text{S}$ 380.1427; found 380.1422; HPLC RT: 11.7 min.

(**6l**). Compound **6l** was obtained from (\pm)-**25f** (20 mg, 0.047 mmol) following the procedure described for the preparation of **6a**. Purification by column chromatography on silica gel (NH₄OH/MeOH/DCM 0.1:1:12) afforded the title compound (16 mg, 79% yield); ^1H NMR (300 MHz, CD₃OD) δ 8.47 (d, J = 4.9 Hz, 2H), 7.81 (s, 1H), 7.48–7.33 (m, 1H), 7.15–6.94 (m, 4H), 6.80 (d, J = 8.6 Hz, 2H), 6.73 (t, J = 7.9 Hz, 1H), 6.60 (d, J = 8.8 Hz, 1H), 4.36 (d, J = 15.4 Hz, 1H), 4.23 (s, 1H), 4.06–3.80 (m, 3H), 2.27 (t, J = 7.3 Hz, 2H), 2.10–1.99 (m, 2H), 1.34 (s, 3H), 0.74 (s, 3H); ^{13}C NMR (75 MHz, CD₃OD) δ 171.1, 158.3, 150.6, 148.9, 148.1, 137.9, 137.1, 134.7, 129.9, 128.9, 127.4, 123.8, 121.8, 118.8, 114.3, 108.6, 77.0, 66.7, 50.4, 44.4, 29.1, 25.9, 25.2, 24.5; ESI-MS m/z : $[\text{M} + \text{H}]^+$ 432; HRMS-ESI m/z : $[\text{M} + \text{Na}]^+$ calcd for $\text{C}_{26}\text{H}_{29}\text{N}_3\text{O}_3\text{Na}$ 454.2101; found 454.2099; HPLC RT: 10.0 min.

tert-Butyl 4-Nicotinoylpiperidine-1-carboxylate (**27**). Compound **27** was obtained from **26** (1.9 g, 5.09 mmol) following the procedure described for the preparation of **8a**. Purification by column chromatography on silica gel (DCM/MeOH 30:1) afforded the title compound (quantitative yield); ^1H NMR (300 MHz, CDCl₃) δ 9.23–9.03 (m, 1H), 8.79 (dd, J = 4.8, 1.7 Hz, 1H), 8.22 (dt, J = 8.0, 2.0 Hz, 1H), 7.52–7.33 (m, 1H), 4.36–3.89 (m, 2H), 3.52–3.20 (m, 1H), 2.91 (t, J = 12.7 Hz, 2H), 1.97–1.79 (m, 2H), 1.79–1.64 (m, 2H), 1.46 (s, 9H); ESI-MS m/z : $[\text{M} + \text{H}]^+$ 291.

tert-Butyl 2-(Pyridin-3-yl)spiro[indole-3,4'-piperidine]-1'-carboxylate (**28**). Compound **28** was obtained from **27** (116 mg, 0.40 mmol) following the procedure described for the preparation of **9a**. The crude of this reaction was immediately dissolved in THF (5 mL) and 0.5 M NaOH (5 mL) and then treated with Boc₂O (134 mg, 0.62 mmol). The mixture was stirred at 25 °C for 2 h and then H₂O was added, and the crude was extracted with EtOAc (3 \times 10 mL). The combined organic layers were dried over Na₂SO₄, evaporated, and purified by column chromatography on alumina (EtOAc/*n*-hexane 1:4) affording the title compound (20 mg, 14% yield, over two steps); ^1H NMR (300 MHz, CDCl₃) δ 9.26 (dd, J = 2.3, 1.0 Hz, 1H), 8.70 (dd, J = 4.8, 1.5 Hz, 1H), 8.46–8.23 (m, 1H), 7.78 (t, J = 8.0 Hz, 2H), 7.55–7.35 (m, 2H), 7.35–7.13 (m, 1H), 4.25 (br, 2H), 3.47 (t, J = 13.4 Hz, 2H), 2.61–2.29 (m, 2H), 1.63–1.31 (m, 1H); ESI-MS m/z : $[\text{M} + \text{H}]^+$ 364.

tert-Butyl 2-(Pyridin-3-yl)spiro[indoline-3,4'-piperidine]-1'-carboxylate ((\pm)-**29**). Compound (\pm)-**29** was obtained from **28** (24 mg, 0.29 mmol) following the procedure described for the preparation of **10d**. The crude material was used in the next step without further purification, affording the title compound (24 mg, quantitative yield); ^1H NMR (300 MHz, CDCl₃) δ 8.69–8.42 (m, 2H), 7.64 (d, J = 8.1 Hz, 1H), 7.35–7.18 (m, 2H), 7.12 (td, J = 7.6, 1.2 Hz, 1H), 6.90–6.54 (m, 2H), 4.61 (s, 1H), 4.19 (br, 1H), 3.88–3.53 (m, 2H), 3.48–3.27 (m, 1H), 3.27–2.97 (m, 1H), 1.98–1.75 (m, 2H), 1.75–1.55 (m, 1H), 1.42 (s, 10H); ESI-MS m/z : $[\text{M} + \text{H}]^+$ 366.

tert-Butyl 1-(4-(Methoxycarbonyl)benzyl)-2-(pyridin-3-yl)spiro[indoline-3,4'-piperidine]-1'-carboxylate ((\pm)-**30**). Compound (\pm)-**30** was obtained from (\pm)-**29** (24 mg, 0.07 mmol) following the procedure described for the preparation of **11a**. Purification by column chromatography on silica gel (PetEt/EtOAc 4:1) afforded the title compound (10 mg, 30% yield); ^1H NMR (300 MHz, CDCl₃) δ 8.56 (dd, J = 4.9, 1.7 Hz, 1H), 8.34 (br, 1H), 7.97 (d, J = 8.3 Hz, 2H), 7.52 (br, 1H), 7.37–7.16 (m, 4H), 7.11 (td, J = 7.7, 1.2 Hz, 1H), 6.78 (td, J = 7.5, 1.0 Hz, 1H), 6.42 (d, J = 7.8 Hz, 1H), 4.50–4.21 (m, 2H), 4.02–3.83 (m, 4H), 3.83–3.66 (m, 1H), 3.66–3.50 (m, 1H), 3.50–3.31 (m, 1H), 3.09 (s, 1H), 1.97–1.80 (m, 2H), 1.80–1.60 (m, 2H), 1.42 (s, 9H); ESI-MS m/z : $[\text{M} + \text{H}]^+$ 514.

tert-Butyl 1-(4-(Hydroxycarbamoyl)benzyl)-2-(pyridin-3-yl)spiro[indoline-3,4'-piperidine]-1'-carboxylate (**6m**). Compound (\pm)-**6m** was obtained from (\pm)-**30** (10 mg, 0.02 mmol) following the procedure described for the preparation of **6a**. Purification by column chromatography on silica gel (NH₄OH/DCM/MeOH 0.1:30:1) afforded the title compound (5 mg, 51% yield); ¹H NMR (300 MHz, CD₃OD) δ 8.48 (s, 1H), 8.38 (s, 1H), 7.68 (d, J = 8.1 Hz, 3H), 7.50–7.17 (m, 4H), 7.09 (t, J = 7.7 Hz, 1H), 6.75 (t, J = 7.4 Hz, 1H), 6.48 (d, J = 7.9 Hz, 1H), 4.57 (s, 1H), 4.41 (d, J = 16.1 Hz, 1H), 3.95 (d, J = 15.9 Hz, 1H), 3.87–3.68 (m, 1H), 3.68–3.40 (m, 2H), 3.13–2.86 (m, 1H), 2.06–1.63 (m, 4H), 1.41 (s, 9H); ¹³C NMR (75 MHz, CD₃OD) δ 166.5, 155.1, 150.5, 148.7, 142.2, 135.2, 134.0, 131.0, 129.5, 129.3, 128.0, 127.4, 123.4, 123.3, 118.2, 106.9, 79.7, 49.8, 36.1, 31.0, 29.4, 29.1, 27.2; ESI-MS m/z : [M + H]⁺ 515; HRMS-ESI m/z : [M + Na]⁺ calcd for C₃₀H₃₄N₄O₄Na 537.2472; found 537.2463; HPLC RT: 12.3 min.

Stereochemical Characterization of Compound 25b. *Enantioselective HPLC.* The racemic mixture of compound (\pm)-**25b** (1 mg/mL) was resolved by enantioselective HPLC using a Daicel Chiralcel OD column (cellulose tris(3,5-dimethylphenylcarbamate), 250 mm \times 10 mm I.D.), *n*-hexane/2-propanol (60:40 v/v) mixture as the mobile phase, 4.5 mL/min flow rate, and 50 μ L injection volume. The two enantiomers were collected and analyzed by polarimetry to determine their specific rotation ($[\alpha]_D^{20}$). The enantiomeric excess (e.e.) of both fractions was then determined by HPLC analysis using the same enantioselective method used for the resolution of the racemic mixture (Figure S1).

Experimental Spectroscopy. The experimental chiroptical properties of **25b** were determined by spectroscopic analysis on a sample of (–)-**25b** (300 μ M in 2-propanol). Ultraviolet (UV) absorption and ECD spectra were measured in the 400–215 nm spectral range at 25 °C on a Jasco J-810 spectropolarimeter (Tokyo, Japan) using a QS-grade quartz cell (Hellma Analytics, Germany) with a 1 mm optical pathlength, a 2 nm spectral bandwidth, a 2 s data integration time, a 50 nm/min scanning speed, a 0.2 nm data pitch, and an accumulation cycle of three runs. Spectra were then blank-corrected and converted to molar units.

Computational Spectroscopy. The theoretical chiroptical properties of **25b** were determined by quantum mechanical (QM) calculations based on TD-DFT. A preliminary conformational search on (S)-**25b** was performed by molecular mechanics (MM) calculations using the MMFF94s force field⁵⁰ and Spartan'02⁵¹ software. DFT geometry optimization was carried out on 35 conformers having relative MM energy (ΔE_{MM}) below 5 kcal mol^{–1} using Gaussian 09 software;⁵² the B97D functional,⁵³ the def2-TZVP basis set,^{54,55} and the IEFPCM solvation model⁵⁶ for 2-propanol (2-PrOH) were employed. Conformational clustering was performed with an RMSD threshold value of 0.01 Å for heavy atoms; details on the resulting 27 optimized conformers, including relative electronic energies (ΔE_{QM}), are reported in the Supporting Information (Table S1). TD-DFT calculations were performed on all optimized conformers using Gaussian 09 software;⁵² the PBE0 functional^{57,58} was used in combination with the def2-TZVP basis set and the IEFPCM(2-PrOH) solvation model. Oscillator strengths (f_j), rotational strengths in dipole length formalism (R_j), and excitation energies (expressed as wavelengths (Table S2)). The theoretical UV and ECD spectra of conformers were determined by approximation of f_j and R_j values to Gaussian bands ($\Delta\sigma$ = 0.4 eV)⁵⁹ and sum over all states; the theoretical spectra of (S)-**25b** were derived by conformational averaging, according to the Boltzmann populations of conformers at 298.15 K and 1 atm based on ΔE_{QM} values (χ_{QM}) and then compared to the experimental spectra of (–)-**25b** by means of the Pearson correlation coefficient (r).

Crystal Structure Determination of the zfHDAC6 Complex. The expression, purification, and crystallization of histone deacetylase 6 catalytic domain 2 (CD2) from *Danio rerio* (zebrafish; here, referred to simply as “zfHDAC6”) were achieved as recently described.^{33,60} Using a Mosquito crystallization robot (TTP Labtech), a 100 nL drop of protein solution [10 mg/mL zfHDAC6, 50 mM 4-(2-hydroxyethyl)-1-piperazineethanesulfonic acid (HEPES) (pH 7.5), 100 mM KCl, 5% glycerol (v/v), 1 mM tris(2-carboxyethyl)phosphine (TCEP), and 2

mM **6h**] was combined with a 100 nL drop of precipitant solution [0.2 M ammonium phosphate dibasic and 20% PEG 3350] and equilibrated against 80 μ L of precipitant solution in the well reservoir surrounding the sitting drop. Crystals formed within 2–3 days at 4 °C were soaked in mother liquor augmented with 20% ethylene glycol for cryoprotection before flash-cooling.

X-ray diffraction data were collected on the Northeastern Collaborative Access Team (NE-CAT) beamline 24-ID-C at the Advanced Photon Source (APS). The CCP4 program suite was employed for data reduction;⁶¹ iMosflm⁶² was used to index the data, and Aimless⁶³ was used to scale the data. To phase the initial electron density map of the enzyme–inhibitor complex by molecular replacement, Phaser⁶⁴ was utilized; the structure of unliganded zfHDAC6 (PDB SEEM) was used as a search probe. The atomic model of the enzyme–inhibitor complex was built and manipulated using the interactive graphics program Coot,⁶⁵ and the structure was refined using Phenix.⁶⁶ The inhibitor was added to well-defined electron density in the final stages of refinement. Occasional spurious electron density peaks were left unmodelled. MolProbity⁶⁷ was used to validate the final structure prior to deposition of the atomic coordinates in the Protein Data Bank (www.rcsb.org). All data reduction and refinement statistics are recorded in Table S3.

Molecular Docking Simulations. Molecular docking simulations were performed using a multicore workstation (72 Intel Xeon E5-2695 v4@2.10 GHz processors and two NVIDIA GeForce 1070 GTX GPU) with Ubuntu 18.04 OS, running Maestro release 2016 (Schrödinger, LLC, New York, NY, 2016). Figures illustrating docking outputs were prepared using PyMOL (The PyMOL Molecular Graphics System, v1.8.4.0, Schrödinger LLC, New York, 2015).

Protein and Ligand Preparation. Crystal structures of human HDAC1 (PDB ID 4BKX)⁶⁸ and HDAC6 (PDB ID SEDU)³³ were taken from PDB, while zfHDAC6 was provided by our co-workers. The proteins were submitted to Protein Preparation Wizard (PPW) protocol implemented in Maestro suite release 2016 to obtain suitable protein structures for molecular docking calculations as previously reported for the same proteins.^{28,29} Ligands, water molecules, and compounds used in the crystallization process were removed, maintaining the Zn²⁺.^{28,29} By following the PPW protocol, we performed a series of computational steps to (1) generate a metal-binding state for the enzymes; (2) add hydrogens; (3) optimize the orientation of hydroxyl groups, Asn, and Gln, and the protonation state of His; and (4) perform a constrained minimization refinement with the impref utility. The refined proteins were used in molecular docking calculation as reported in the next paragraph.

Ligands were built in Maestro and minimized by MacroModel (MacroModel, Schrödinger Release 2016) software using OPLS-2005 as the force field. Moreover, the resulting compounds were treated by LigPrep application (LigPrep, Schrödinger Release 2016) to generate the most probable ionization state at the cellular pH (7.4 \pm 0.2) as reported by us.^{69,70} Moreover, according to the evidence reported in the literature,^{71–74} we used a neutral hydroxamic acid moiety of the compounds since the hydroxamic acid proton should not be transferred in HDAC isoforms containing histidine residues in the binding site, close to the reactive metal center as in the case of HDAC1 and HDAC6.^{28,31}

Computational Procedure. Glide software (Glide, Schrödinger Release 2016) has been employed to perform the docking studies presented in this paper, using the ligands and proteins prepared as above-mentioned, applying Glide extra precision (XP) scoring function. Energy grids were prepared using the default value of the protein atom scaling factor (1.0 Å) within a cubic box centered on the zinc ion which roughly represents the center of the active sites.^{28,29} After grid generation with the introduction of metal constraints, the ligands were docked into the enzymes. The number of poses entered to post-docking minimization was set to 50. Glide SP score was evaluated. In order to assess the validity of the docking protocol, SAHA and Trichostatin A were used as reference compounds for a redocking procedure. The docking results revealed a similar accommodation for the above-mentioned reference compounds with respect to the previously published results (data not shown).^{33,75}

In Vitro Testing of HDAC1, HDAC6, and HDAC8. OptiPlate-96 black microplates (PerkinElmer) were employed with an assay volume of 60 μ L. Human recombinant HDAC1 (BPS Bioscience, Catalog #: 50051) or human recombinant HDAC6 (BPS Bioscience, Catalog #: 50006) was diluted in incubation buffer (50 mM Tris–HCl, pH 8.0, 137 mM NaCl, 2.7 mM KCl, 1 mM MgCl₂, and 1 mg/mL bovine serum albumin (BSA)). A total of 52 μ L of this dilution was incubated with 3 μ L of increasing concentrations of inhibitors in DMSO and 5 μ L of fluorogenic substrate ZMAL (Z-(Ac)Lys-AMC)^{76,77} (126 μ M) at 37 °C. After 90 min incubation time, 60 μ L of the stock solution (33 μ M Trichostatin A and 6 mg/mL trypsin in trypsin buffer [Tris–HCl 50 mM, pH 8.0, NaCl 100 mM]) was added. After the following incubation at 37 °C for 30 min, the fluorescence was measured on a BMG LABTECH POLARstar OPTIMA plate reader (BMG Labtechnologies, Germany) at an excitation wavelength of 390 nm and an emission wavelength of 460 nm.^{77,78}

Recombinant human HDAC8 was purchased as part of the Fluor de Lys HDAC8 fluorometric drug discovery kit (Enzo Life Sciences, No. BMLAK518). Inhibition assays were performed as previously described (Marek et al., 2018) with minor modifications.^{30,79} The DMSO concentration was kept constant to 0.5%; the enzyme incubated with DMSO only was used as the control. To keep safe from the possibility of slow-binding inhibition, the enzyme was preincubated with the selected compounds 15 min before substrate addition to the mixture. The Fluor de Lys substrate was added at a final concentration of 50 μ M, whereas the enzyme was added at a concentration of 0.45U/reaction; the reaction was allowed to proceed for 1 h at 30 °C. TSA (2 μ M) within 50 μ L of 1 \times Developer II was added to quench the reaction, and the mixture was further incubated for 1 h at 30 °C. Fluorescence was measured by a plate reader (Varioskan Lux, Thermo Fisher Scientific) with excitation wavelength at λ = 370 nm and emission wavelength at λ = 450 nm. IC₅₀ was estimated by the nonlinear regression curve fit performed by means of GNU/Octave, according to a generalized form of the dose–response curve equation, as reported by Copeland.⁸⁰

Cellular Studies. NB4 cells were grown in RPMI-1640 (Sigma-Aldrich, Milan, Italy) culture media, supplemented with 1% L-glutamine (EuroClone, Milan, Italy), 10% heat-inactivated fetal bovine serum (FBS) (GIBCO, Monza, Italy), and antibiotics (100 U/mL penicillin, 100 μ g/mL streptomycin, and 250 ng/mL amphotericin-B). The U87 cell line was maintained in Eagle's minimum essential medium (Sigma-Aldrich, Milan, Italy) in the presence of 10% FBS. U2OS cells were cultured in high-glucose Dulbecco's modified Eagle's medium (DMEM; Gibco; Thermo Fisher Scientific) enriched with 10% FBS and 1% glutamine. All cell lines were maintained in an incubator at 37 °C and 5% CO₂.

Western Blot Analysis Methods. Cancer cells were treated with 6a, 6d, 6e, 6h, and 6l at 5 μ M for 30 h. SAHA was used as a positive control at the same time and concentration. For protein extraction, lysis buffer (50 mmol/L Tris–HCl, pH 7.4, 150 mmol/L NaCl, 1% NP40, 10 mmol/L NaF, 1 mmol/L PMSF, and protease inhibitor cocktail) was used. Samples were then centrifuged at 13 000 rpm for 30 min at 4 °C, and the protein concentration quantified by the Bradford assay (Bio-Rad). For histone extraction, cells were collected and resuspended in triton extraction buffer [TEB; PBS containing 0.5% Triton X 100 (v/v), 2 mmol/L PMSF, 0.02% (w/v) NaN₃], for 10 min at 4 °C. Samples were centrifuged at 2000 rpm for 10 min at 4 °C, and pellets were washed with TEB (half-volume). Samples were then resuspended in 0.2 N HCl, and acid histone extraction was carried out overnight at 4 °C. Protein concentration was determined by the Bradford assay (Bio-Rad). Each protein extract (35 μ g) was loaded on 10% polyacrylamide gels, and 2 μ g of histone extract was instead used on 15% polyacrylamide gel. Samples were then transferred on the nitrocellulose membrane (Trans-blot turbo, Bio-Rad catalog: 1704150) and revealed with anti-acetylated tubulin (clone 6-11B-1, Sigma) and anti-acetyl-histone H3 antibody (cod: 06599, Millipore). GAPDH (cod: 14C10, Cell Signaling) and H4 (ab31830, Abcam) antibodies were used as loading controls.

3D Organoid Model Assay and MTT Assay. Study Population. ABCs from 12 patients with IPF were obtained during bronchoscopy at routine diagnostic work-up. IPF diagnosis was established by a

multidisciplinary board according to the American Thoracic Society/European Respiratory Society criteria and was later determined to be consistent with recent guidelines.^{81–83} All IPF patients signed informed consent prior to inclusion in the study. The studies were approved by the local ethics committees.

Bronchoscopy. Bronchial epithelial cells were harvested by bronchial brushes of subsegmental bronchi of the right lower lobe during flexible bronchoscopy within the routine diagnostic work-up at initial diagnosis. None of the patients received antifibrotic treatment prior to bronchoscopy. None of the included subjects was currently smoking.

Isolation of ABC. ABCs were isolated from bronchial brushes of subsegmental bronchi of the right lower lobe using a similar protocol as recently described.^{39,84,85} Bronchial brushes were placed in 2 mL of prewarmed (37 °C) Clonetics bronchial epithelial cell growth medium (BEGM) (Lonza, CC-3170). Then, airway epithelial cells were pelleted by centrifugation (250g, 5 min) and disaggregated by resuspension in trypsin/EDTA solution (0.05%/0.02%) (Merck, L2143) for 5 min at 37 °C. Afterward, the cell pellet was resuspended in 5 mL of BEGM and seeded in T25 flasks (Merck, CLS3056) in BEGM, supplemented with growth factors according to the manufacturer's instructions. Cultures were maintained in a humidified atmosphere of 5% CO₂ at 37 °C. The medium was changed every 7 days, and cells were harvested at day 21 when the cells were 90% confluent. Therefore, cells were trypsinized, harvested, and counted. The purity of the ABC was determined by immunocytology (cytokeratin-5 staining) of cytopins and always exceeded 98%.

3D Organoid Assay. The bronchosphere formation assay was performed as recently described.³⁹ Briefly, IPF-ABCs (10⁴ cells) were added to 50 μ L of ice-cold matrigel Corning matrigel matrix (Corning, 356231) in transwell inserts (Corning Lifesciences, Costar 3470) and cultured for 30 min in the incubator (5% CO₂, 37 °C) until the matrigel became stiff. Then, 600 μ L of a 1:1 ratio of BEGM and DMEM was added below the inserts and additional 100 μ L on top of the inserts. Plates (Corning Lifesciences, Costar 3470) were cultured at 5% CO₂ and 37 °C w/wo treatment with compounds 6a, 6d, 6h, and 6l. The molecules were tested in the concentration range of 1–50 nM for 14 days. Medium exchange was done every 7 days.

Detection of Organoid Counts and Measurement of Cell Proliferation. Mosaic photomicrographs were taken from HDAC6 inhibitor-treated 3D organoid assays by microscopy using an Axio Observer Inverted microscope/Zeiss and ZEN microscope navigation software. The numbers of organoids per well were counted by bright-field microscopy on day 14. Only organoids with a size of 5 μ m or larger were counted. Cell proliferation was quantified using the colorimetric MTT assay (Sigma-Aldrich, CT01) on day 14 according to the manufacturer's instructions. IC₅₀ values were determined from bronchosphere counts and the cell proliferation MTT assay by IC₅₀ Calculator software (AAT Bioquest, Inc., Sunnyvale/USA). The mean value was determined from the IC₅₀ values of the organoid counts and the MTT assay.

Immunohistochemistry. Formalin-fixed IPF lung and normal tissues were used for immunohistochemistry as described.⁸⁶ Three micrometer thick sections of paraffin blocks were deparaffinized in xylene and rehydrated with a descending alcohol row (as described above). Heat-induced antigen retrieval was performed at 110 °C for 2 min in citrate buffer (pH 6.0) using a pressure cooker. First, staining slides were washed for 5 min with Tris–NaCl buffer and then blocked for 20 min with normal goat serum blocking solution 1:20 (Vector, S1000). For the staining procedure, rabbit monoclonal anti-HDAC6 antibody [EPRI698(2)] (Abcam, ab133493) was incubated for 1 h at room temperature (1:100). Isotype control was performed with Universal Negative Control for IS-Series Rabbit Primary Antibodies (Dako/Agilent Technologies, IS60061-2) (1:1000 dilution) overnight at 4 °C.

Slides were washed with Tris–NaCl buffer. The incubation time of the Goat IgG antirabbit IgG (H + L)-biotin (Dianova, 111-065-003) (1:800 dilution) was 30 min at 25 °C. Slides were washed with Tris–NaCl buffer. Activation was done using alkaline phosphatase Strept AP (1:800 dilution) (Vector, SA-5100) for 30 min, and slides were washed

with Tris–NaCl buffer. Visualization was performed by DAKO REAL Chromogen Red (Dako Real Kit) (Dako/Agilent Technologies, K500311-2) (incubation time 20 min). Slides were washed with aqua dest.

Slides were counterstained with Mayer's hemalum solution (Merck, 109249) 1:10 for 90 s. Slides were washed shortly with aqua dest and for 90 s with Shandon Bluing Reagent (ThermoScientific, 6769001). Before mounting, slides were washed once with aqua dest followed with three short washing steps in 90% ethanol (CG Chemikalien), six short washing steps in 100% ethanol (CG Chemikalien), and six short washing steps in xylol (CG Chemikalien). Finally, coverslips were placed over slides with the Eukitt Quick-hardening mounting medium (Merck, 03989). All samples were digitalized using Mirax Scan 150 BF/FL (Zeiss, Germany).

Human Lung Tissue. Human lung tissue samples were obtained from healthy areas of lungs from patients undergoing lung resection for carcinoma at Glenfield Hospital, Leicester, U.K. All patients gave written informed consent, and the study was approved by the National Research Ethics Service (reference 10/H0402/12 and 17/EM/0231). Samples obtained were anonymized and coded before use.

Human Lung Tissue Explant Culture Model. Pieces of the human lung tissue (2 mm³) were generated as described previously⁴⁰. The tissue was cultured in DMEM + vehicle control (0.1% DMSO) ± TGF-β1 (10 ng/mL) as described⁴⁰ or DMEM + TGF-β1 (10 ng/mL) + 6h (0.41 and 4.1 μM) or vehicle control (0.1% DMSO). The tissue was collected on day 7 for RNA extraction.

RNA extraction was performed as described previously.⁴⁰ The tissue was dissociated using a Precellys 24 tissue homogenizer (Bertin Technologies, Montigny-le Bretonneux, France), and total RNA was purified using the automated QIAcube with RNeasy Fibrosis Mini kit (Qiagen, CA) according to the manufacturer's instructions. RNA integrity was assessed with a Bioanalyzer 2100 system (Agilent, CA), and RIN values >8 were accepted as suitable for PCR profiling. RNA concentrations were then measured using a Nanodrop 2000 (Labtech International, East Sussex, U.K.).

Quantitative real-time PCR (qRT-PCR) was used to measure mRNA expression levels of α-smooth muscle actin (αSMA), collagen types I and III, and fibronectin using a Quantstudio 5 Real-Time PCR machine (Applied Biosystems). Primer sequences for collagen types I and III and αSMA have previously been described by Roach et al.⁸⁷ Qiagen QuantiTect primer assays (QT00038024) were used for fibronectin, and Taqman assays for HDAC6 (Hs00997427_m1) were acquired from Thermo Fisher. Gene expression was quantified using Brilliant SYBR Green QRT-PCR 1-Step master mix (Stratagene, the Netherlands). All expression data were normalized to β2-microglobulin using QuantiTect primer assay primers (Qiagen, Germany), HS_B2M_1_SG, and corrected using the reference dye ROX. PCR products were run on 1.5% agarose gel to confirm the product size, and each product was sequenced to confirm the specificity of the primers. The relative expression was calculated using the 2–ΔΔCt method.

Solubility and Chemical Stability Studies. **HPLC Analysis of Compounds 6d and 6h.** For the HPLC analysis, a Chromolith HPLC column RP-18 was employed. The runs were performed by gradient elution starting from a mixture 0% MeCN (0.1% TFA as the phase modifier) in H₂O (0.1% TFA as the phase modifier) to 20% MeCN (0.1% TFA) in H₂O (0.1% TFA) in 4 min and then up to 50% MeCN (0.1% TFA) in H₂O in 3 min. The flow speed was set at 0.8 mL/min, and the temperature was maintained at 25 °C. The volume of injection of the sample was 10 μL, and the wavelength selected for the detection was 254 nm. The retention times obtained following this protocol for compounds 6d and 6h were 6.7 and 6.4 min, respectively.

Solubility Assay and Chemical Stability at 25 °C. A stock solution for each tested compound was prepared by dissolving the sample in DMSO to a final concentration of 10 mM. From the stock solution, three samples were prepared: one was used as the standard solution and the other two as the test solutions at pH 3.0 and pH 7.4. The concentration of these solutions was 250 μM with a DMSO content of 2.5% (v/v). The standard solution was prepared by dilution of the stock solution in PBS solution (MeCN/water, 60:40), the dilution of the stock solution in 50 mM acetic acid afforded the sample solution at pH

3.0, and the dilution of the stock solution in 50 mM aqueous PBS afforded the sample solution at pH 7.4. These suspensions/solutions were sealed and left for 24 h at 25 °C under orbital shaking to achieve “pseudothermodynamic equilibrium”. After that time, the solutions were filtered using PTFE filters and successively diluted 1:2 with the buffer solution used for the preparation of the samples. Then, they were analyzed by HPLC/UV/ DAD using UV detection at 254 nm for quantitation. Solubility was calculated by comparing areas of the sample and the standard

$$S = \frac{A_{\text{smp}} \times \text{FD} \times C_{\text{st}}}{A_{\text{st}}}$$

S = solubility of the compound (μM); A_{smp} = UV area of the sample solution; FD = dilution factor (2); C_{st} = standard concentration (250 μM); and A_{st} = UV area of the standard solution.

For each sample, the analysis was performed in triplicate, and the solubility result reported was obtained from the average of the three values. The same sample solutions were prepared to evaluate the chemical stability of the compounds after 24 h at 25 °C and analyzed by HPLC/UV/DAD using UV detection at 254 nm for quantitation. Stability was calculated by comparing the area of the peak at T₀ with the area of the peak of the same solution after 24 h. A stability percentage value was calculated by this method at pH 3.0 and pH 7.4 for each compound by applying the following formula

$$\% \text{ remaining} = \frac{AC_{24}}{AC_{T_0}} \times 100$$

AC₂₄ = area of the sample after 24 h at 25 °C; AC_{T₀} = area of the sample at T₀. For each sample, the analysis was performed in triplicate and the stability result reported was obtained from the average of the three values.

Analysis of In Vitro Metabolic Stability of 6d and 6h in HLM. The tested compound (6d or 6h), dissolved in MeCN, was incubated at 37 °C at 5 μM concentration in 100 mM phosphate buffer (pH 7.4) with 0.5 mg/mL rat and human liver microsomal proteins as previously reported.⁸⁸ CYP-dependent reactions were started by addition of NADPH-GS (2 mM NADPH), 66 mM glucose-6-phosphate, 0.4 U/mL glucose-6-phosphate dehydrogenase to 66 mM MgCl₂. Reactions were terminated at regular time intervals (overall range 0–60 min) by adding 1 mL of MeCN. All incubations were performed in triplicate. HPLC analysis was performed on a Shimadzu Prominence apparatus equipped with a Chromolith HPLC column RP-18 and coupled with a UV–vis detector, set at λ = 254 nm. The analysis was carried out as described above. The intrinsic clearance (CL_{int}) was calculated by the equation

$$CL_{\text{int}} = \frac{k(\text{min}^{-1}) \times [V]}{[P]}$$

where *k* is the rate constant for the depletion of the substrate, *V* is the volume of incubation in μL, and *P* is the amount of microsomal proteins as reported elsewhere.⁴³

Cytotoxicity and Mutagenicity Assays. **Materials.** Dulbecco's modified Eagle's medium, trypsin solution, and all of the solvents used for cell culture were purchased from Lonza (Switzerland). Mouse immortalized fibroblasts NIH3T3 were purchased from American Type Culture Collection. The mutagenicity assay was supplied by Biologik s.r.l. (Trieste, Italy).

Cell Cultures and Cytotoxicity Assays. NIH3T3 cells were utilized for cytotoxicity experiments. Cells were maintained in DMEM at 37 °C in a humidified atmosphere containing 5% CO₂. The culture media were supplemented with 10% fetal calf serum (FCS), 1% L-glutamine–penicillin–streptomycin solution, and 1% MEM nonessential amino acid solution. Once at the confluence, cells were washed with 0.1 M PBS, taken up with the trypsin–EDTA solution, and then centrifuged at 1000 rpm for 5 min. The pellet was resuspended in the medium solution (dilution 1:15). The stock solution for each compound was prepared in pure DMSO and diluted with the complete culture medium. The solution/suspension obtained was then added to the cell monolayer.

Cell viability after 24 h of incubation with the different concentrations of each test compound was evaluated by neutral red uptake by the procedure previously reported.⁸⁹ Data processing included the Student's *t*-test with *p* < 0.05 taken as the significance level. First, the following solutions were prepared to determine the percentage of viable cells:

1. Neutral red (NR) stock solution: 0.33 g of NR dye powder in 100 mL of sterile H₂O
2. NR medium: 1.0 mL of NR stock solution + 99.0 mL routine culture medium prewarmed to 37 °C
3. NR desorb solution: 1% glacial acetic acid solution + 50% ethanol + 49% H₂O

At the end of incubation, the routine culture medium was removed from each well, and cells were carefully rinsed with 1 mL of prewarmed D-PBS. Multiwells were then gently blotted with paper towels. The NR medium (1.0 mL) was added to each well and further incubated at 37 °C, 95% humidity, and 5.0% CO₂ for 3 h. The cells were checked during NR incubation for NR crystal formation. After incubation, the NR medium was removed, and cells were carefully rinsed with 1 mL of prewarmed D-PBS. Then, the PBS was decanted and blotted from the wells and 1 mL of NR desorb solution was added to each sample. Multiwells were then put on a shaker for 20–45 min to extract NR from the cells and form a homogeneous solution. During this step, the samples were covered to protect them from light. After 5 min, the multiwells were removed from the plate shaker and the absorbance was read at 540 nm by a UV/visible spectrophotometer (Lambda 25, PerkinElmer).

Mutagenicity Assay: Ames Test. The TA100 and TA98 strains of *Salmonella Typhimurium* and the S9 fraction were utilized for the mutagenicity assay. Approximately 107 bacteria were exposed to six concentrations of each test compound, as well as a positive and a negative control, for 90 min in a medium containing sufficient histidine to support approximately two cell divisions. After 90 min, the exposure cultures were diluted with the pH indicator medium lacking histidine and aliquoted into 48 wells of a 384-well plate. Within two days, cells that have undergone reversion to His grew into colonies. Metabolism by the bacterial colonies reduced the pH of the medium, changing the color of that well. This color change can be detected visually or by a microplate reader. The number of wells containing revertant colonies were counted for each dose and compared to a zero-dose control. Each dose was tested in six replicates. The test was performed both with and without the S9 fraction.

Toxicity Screening of 6h in Zebrafish Larvae. All experiments with in-house wild-type zebrafish larvae (*Danio rerio*) were performed according to ethical exemptions granted by the UCD Animal Research Ethics Committee, University College Dublin (AREC-Kennedy). No animals were used as per European Union Directive 2010/63/EU; larval forms of zebrafish that are not independently feeding and free-living are not classified as animals. Zebrafish larval experiments were performed with approval from the UCD Animal Research Ethics Committee, Ireland. Wild-type (Tübingen) larvae were reared in embryo medium (0.137 M NaCl, 5.5 mM Na₂HPO₄, 5.4 mM KCl, 1.3 mM CaCl₂, 0.44 mM KH₂PO₄, 1.0 mM MgSO₄, and 4.2 mM NaHCO₃, conductivity 1200 μS, pH 7) containing methylene blue at 28.5 °C under a 14 h light/10 h dark cycle (parameters measured in the zebrafish facility for the year 2018: the pH, temperature, and conductivity were reported).⁹⁰ Adult zebrafish were maintained in a recirculating water system at 28 °C under a 14 h light/10 h dark cycle and fed daily with brine shrimp and dry pellet food. Wild-type zebrafish larvae were obtained by incrosses of wild-type adults. The embryos were raised and treated until 3 days old with either increasing concentrations (1, 10, 25, 50, and 100 μM) of compound **6h** or 0.1% DMSO (vehicle control) for 2 days. Four larvae were placed per well in 400 μL of respective drug concentrations prepared in embryo media. Eight larvae were used in total per treatment group, and the experiment was performed in a 48-well plate. The visual behavioral assay—optokinetic reflex assay—was performed 2 days post-treatment as described previously⁹⁰ to determine the effect of compound **6h** on visual function.

Isolated Rat Heart Preparation and Perfusion. All animal care and experimental protocols conformed to the European Union Guidelines for the Care and Use of Laboratory Animals (European Union Directive 2010/63/EU) and were approved by the Italian Department of Health (666/2015-PR). Male Sprague–Dawley rats (350 g; Charles River Italia, Calco, Italy; *n* = 5) were used for this experiment. Rats were anesthetized (ip) with a mixture of Zoletil 100 (7.5 mg kg⁻¹ tiletamine and 7.5 mg kg⁻¹ zolazepam; Virbac Srl, Milano, Italy) and Xilor (4 mg kg⁻¹ xylazine; Bio 98, San Lazzaro, Italy) containing heparin (5000 U/kg), decapitated, and bled. The hearts, spontaneously beating, were rapidly explanted and mounted on a Langendorff apparatus for retrograde perfusion via the aorta at a constant flow rate of 10 mL/min with the Krebs–Henseleit solution of the following composition (mM): NaCl 118, KCl 4.7, CaCl₂ 2.5, MgSO₄ 1.2, NaHCO₃ 25, KH₂PO₄ 1.2, glucose 11.5, Na pyruvate 2, and EDTA 0.5, bubbled with a 95% O₂–5% CO₂ gas mixture (pH 7.4), and kept at 37 °C, as described elsewhere.⁹¹ The hearts were allowed to equilibrate for at least 20 min before drug exposure. Heart contractility was measured as left ventricle pressure (LVP) by means of a latex balloon, inserted into the left ventricle via the mitral valve and connected to a pressure transducer (BLPR, WPI, Berlin, Germany). The balloon was inflated with deionized water from a microsyringe until a left ventricular end diastolic pressure of 10 mmHg was obtained. Alterations in the coronary perfusion pressure (CPP), arising from changes in coronary vascular resistance, were recorded by the pressure transducer (BLPR, WPI, Berlin, Germany) placed in the inflow line.⁹² A surface electrocardiogram (ECG) was recorded at a sampling rate of 1 kHz by means of two steel electrodes, one placed on the apex and the other on the left atrium of the heart. The ECG analysis included the following measurements: RR (cycle length), HR (frequency), PQ (atrioventricular conduction time), QRS (intraventricular conduction time), and QT (overall action potential duration). LVP, CPP, and ECG were recorded with a digital PowerLab data acquisition system (PowerLab 8/30; ADInstruments, Castle Hill, Australia) and analyzed by Chart Pro for Windows software (PowerLab; ADInstruments, Castle Hill, Australia). LVP was calculated by subtracting the left ventricular diastolic pressure from the left ventricular systolic pressure.⁴⁸ As the QT interval is affected by heart rate changes (e.g., it shortens with rapid heart rate), Bazett's formula (QTc = QT/(RR)^{1/2}) was routinely used to avoid confounding effects. Compound **6h** was dissolved in DMSO. Solvents failed to alter the response of the preparations (data not shown).

Statistical Analysis. Data are reported as mean ± SEM; *n* (indicated in parentheses) represents the number of rat hearts. Analysis of data was accomplished using GraphPad Prism version 5.04 (GraphPad Software). Statistical analyses and significance as measured by repeated measures ANOVA (followed by Dunnett's post-test or Friedman test) were obtained using GraphPad InStat version 3.06 (GraphPad Software). In all comparisons, *P* < 0.05 was considered significant.

■ ASSOCIATED CONTENT

Supporting Information

The Supporting Information is available free of charge at <https://pubs.acs.org/doi/10.1021/acs.jmedchem.1c00184>.

Figure S1, HPLC separation of the racemic mixture (±)-**25b**; Table S1, Relative MM energies (ΔE_{MM}), electronic energies (E_{QM} and ΔE_{QM}), free energies (*G* and ΔG), and corresponding Boltzmann populations (χ) for the conformers of (S)-**25b**; Table S2, Oscillator strengths (f_j), rotational strengths in dipole length formalism (R_j), and excitation wavelengths (λ_j) for the conformers of (S)-**25b**; Table S3, X-ray crystallographic data collection and refinement statistics for the zfHDAC6–**6h** complex; Figures S2–S15, Docking studies of compounds **6a–m**; Figure S16, Isolation of human airway basal cells; Figure S17, Bronchosphere generation blocked by compounds

6a, 6d, 6h, and 6l; ^1H , ^{13}C NMR spectra and HPLC purity of final compounds (\pm)-6a–m (PDF)

Molecular formula strings (CSV)

Recommended compound characterization checklist (XLSX)

Recommended compound characterization checklist (XLS)

Accession Codes

The atomic coordinates and crystallographic structure factors of the HDAC6 complex with inhibitor 6h has been deposited in the Protein Data Bank (www.rcsb.org) with accession code 6V79. Authors will release the atomic coordinates and experimental data upon article publication.

AUTHOR INFORMATION

Corresponding Authors

Giuseppe Campiani – Department of Biotechnology, Chemistry and Pharmacy, DoE Department of Excellence 2018-2022, University of Siena, 53100 Siena, Italy; orcid.org/0000-0001-5295-9529; Phone: (+39) 0577 232239; Email: campiani@unisi.it

Stefania Butini – Department of Biotechnology, Chemistry and Pharmacy, DoE Department of Excellence 2018-2022, University of Siena, 53100 Siena, Italy; orcid.org/0000-0002-8471-0880; Phone: (+39) 0577 234161; Email: butini3@unisi.it

Authors

Caterina Cavella – Department of Biotechnology, Chemistry and Pharmacy, DoE Department of Excellence 2018-2022, University of Siena, 53100 Siena, Italy

Jeremy D. Osko – Roy and Diana Vagelos Laboratories, Department of Chemistry, University of Pennsylvania, Philadelphia, Pennsylvania 19104-6323, United States

Margherita Brindisi – Department of Biotechnology, Chemistry and Pharmacy, DoE Department of Excellence 2018-2022, University of Siena, 53100 Siena, Italy; Present Address: Department of Excellence of Pharmacy, University of Naples Federico II, Via D. Montesano, 49, Naples 80131, Italy; orcid.org/0000-0001-9119-3773

Nicola Relitti – Department of Biotechnology, Chemistry and Pharmacy, DoE Department of Excellence 2018-2022, University of Siena, 53100 Siena, Italy; Present Address: IRBM Science Park, Via Pontina km 30,600, 00071 Pomezia, Rome, Italy; orcid.org/0000-0001-9783-8966

Simone Brogi – Department of Pharmacy, University of Pisa, 56126 Pisa, Italy; orcid.org/0000-0001-9375-6242

A. Prasanth Saraswati – Department of Biotechnology, Chemistry and Pharmacy, DoE Department of Excellence 2018-2022, University of Siena, 53100 Siena, Italy

Stefano Federico – Department of Biotechnology, Chemistry and Pharmacy, DoE Department of Excellence 2018-2022, University of Siena, 53100 Siena, Italy; orcid.org/0000-0002-7478-6128

Giulia Chemi – Department of Biotechnology, Chemistry and Pharmacy, DoE Department of Excellence 2018-2022, University of Siena, 53100 Siena, Italy; Present Address: Wellcome Centre for Anti-Infectives Research, Drug Discovery Unit, Division of Biological Chemistry and Drug Discovery, University of Dundee, DD1 5EH Dundee, United Kingdom; orcid.org/0000-0002-3868-6752

Samuele Maramai – Department of Biotechnology, Chemistry and Pharmacy, DoE Department of Excellence 2018-2022, University of Siena, 53100 Siena, Italy; orcid.org/0000-0001-7499-6961

Gabriele Carullo – Department of Biotechnology, Chemistry and Pharmacy, DoE Department of Excellence 2018-2022, University of Siena, 53100 Siena, Italy; orcid.org/0000-0002-1619-3295

Benedikt Jaeger – Klinik für Pneumologie, Medizinische Hochschule Hannover, Hannover 30625, Germany

Alfonso Carleo – Klinik für Pneumologie, Medizinische Hochschule Hannover, Hannover 30625, Germany

Rosaria Benedetti – Department of Precision Medicine, University of Campania Luigi Vanvitelli, 80138 Naples, Italy; orcid.org/0000-0001-5517-5519

Federica Sarno – Department of Precision Medicine, University of Campania Luigi Vanvitelli, 80138 Naples, Italy

Stefania Lamponi – Department of Biotechnology, Chemistry and Pharmacy, DoE Department of Excellence 2018-2022, University of Siena, 53100 Siena, Italy

Paola Rottoli – Specialization School of Respiratory Diseases, Department of Medical Sciences, Surgery and Neurosciences, Centro didattico Le Scotte, University of Siena, 53100 Siena, Italy

Elena Bargagli – Department of Medical Sciences, Surgery and Neurosciences, Respiratory Diseases Unit, AOUS, Centro didattico Le Scotte, University of Siena, 53100 Siena, Italy

Carlo Bertucci – Department of Pharmacy and Biotechnology, University of Bologna, Bologna 40126, Italy

Daniele Tedesco – Department of Pharmacy and Biotechnology, University of Bologna, Bologna 40126, Italy; Present Address: Institute for Organic Synthesis and Photoreactivity (ISOF), National Research Council (CNR), via Piero Gobetti 101, 40129 Bologna, Italy; orcid.org/0000-0003-2585-7791

Daniel Herp – Institute of Pharmaceutical Sciences, Albert-Ludwigs-Universität Freiburg, 79104 Freiburg, Germany

Johanna Senger – Institute of Pharmaceutical Sciences, Albert-Ludwigs-Universität Freiburg, 79104 Freiburg, Germany

Giovina Ruberti – Institute of Biochemistry and Cell Biology (IBBC), National Research Council (CNR), 00015 Monterotondo (Rome), Italy; orcid.org/0000-0003-2367-9709

Fulvio Saccoccia – Institute of Biochemistry and Cell Biology (IBBC), National Research Council (CNR), 00015 Monterotondo (Rome), Italy

Simona Saponara – Department of Life Sciences, University of Siena, I-53100 Siena, Italy

Beatrice Gorelli – Department of Life Sciences, University of Siena, I-53100 Siena, Italy

Massimo Valoti – Department of Life Sciences, University of Siena, I-53100 Siena, Italy

Breádan Kennedy – UCD School of Biomolecular and Biomedical Science, UCD Conway Institute, University College Dublin, D04 V1W8 Dublin, Ireland; orcid.org/0000-0001-7991-4689

Husvinee Sundaramurthi – UCD School of Biomolecular and Biomedical Science, UCD Conway Institute, University College Dublin, D04 V1W8 Dublin, Ireland

Manfred Jung – Institute of Pharmaceutical Sciences, Albert-Ludwigs-Universität Freiburg, 79104 Freiburg, Germany; orcid.org/0000-0002-6361-7716

Katy M. Roach – Department of Respiratory Sciences, University of Leicester, UK, Institute of Lung Health and NIHR Leicester BRC-Respiratory, LE5 4PW Leicester, U.K.

Lucia Altucci – Department of Precision Medicine, University of Campania Luigi Vanvitelli, 80138 Naples, Italy

Peter Bradding – Department of Respiratory Sciences, University of Leicester, UK, Institute of Lung Health and NIHR Leicester BRC-Respiratory, LE5 4PW Leicester, U.K.

David W. Christianson – Roy and Diana Vagelos Laboratories, Department of Chemistry, University of Pennsylvania, Philadelphia, Pennsylvania 19104-6323, United States;

orcid.org/0000-0002-0194-5212

Sandra Gemma – Department of Biotechnology, Chemistry and Pharmacy, DoE Department of Excellence 2018-2022, University of Siena, 53100 Siena, Italy; orcid.org/0000-0002-8313-2417

Antje Prasse – Klinik für Pneumologie, Medizinische Hochschule Hannover, Hannover 30625, Germany

Complete contact information is available at:

<https://pubs.acs.org/10.1021/acs.jmedchem.1c00184>

Author Contributions

^{|||}S.G. and A.P. joined as Co-senior Authors.

Notes

The authors declare no competing financial interest.

ACKNOWLEDGMENTS

The authors thank the Regione Toscana-IT grant HIDE-IPF (Bando Salute 2018) and NIH for grant GM49758 (D.W.C.) in support of this research. This research was also funded by AIRC-17217; Campania Regional Government Technology Platform Lotta alle Patologie Oncologiche iCURE-B21C17000030007; “Epigenetic Hallmarks of Multiple Sclerosis” (acronym Epi-MS) (id: 415, Merit Ranking Area ERC LS) in VALERE 2019 Program; V:ALERE 2020—“CIRCE” D.R. n. 138 del 17/02/2020 Program; Campania Regional Government FASE2: IDEAL; MIUR, Proof of Concept-EPICUREPOC01_00043-B64I19000290008; and P.O.R. CAMPANIA Campania ESF Regional Operational Programme 2014/2020 Axis III-B27D18001070006. This work is based on the research conducted at the Northeastern Collaborative Access Team beamlines, which are funded by the National Institute of General Medical Sciences of the National Institutes of Health (P30 GM124165). This research used resources of the Advanced Photon Source, a U.S. Department of Energy (DOE) Office of Science User Facility operated for the DOE Office of Science by Argonne National Laboratory under Contract No. DE-AC02-06CH11357. Prof. Riccardo Zanasi (Department of Chemistry and Biology, University of Salerno, Italy) kindly provided access to the computing cluster used to perform MM and QM calculations for the stereochemical characterization of compound **25b**. The authors thank K. Schmidt-kunz for technical assistance in IC₅₀ determination.

ABBREVIATIONS

ABC, airway basal cell; AIBN, azobisisobutyronitrile; BAL, bronchoalveolar lavage; CL_{int}, intrinsic clearance; CPP, coronary perfusion pressure; DCM, dichloromethane; DMSO, dimethyl sulfoxide; ECD, electronic circular dichroism; ECG, electrocardiogram; EMT, epithelial–mesenchymal transition; HDAC, histone deacetylase; HDACi, HDAC inhibitor; HLM, human liver microsomal; ILDs, interstitial lung diseases; IPF,

idiopathic pulmonary fibrosis; k, apparent decay constant; LVP, left ventricle pressure; NBS, N-bromosuccinimide; NMO, 4-methylmorpholine N-oxide; NRU, neutral red uptake; PQ, atrioventricular conduction time; QRS, intraventricular conduction time; RR, cycle length; t_{1/2}, half-life time; TD-DFT, time-dependent density functional theory; TGF- β 1, transforming growth factor β 1; THF, tetrahydrofuran; ZBG, zinc-binding group; zfhHDAC6, zebrafish HDAC6

REFERENCES

- (1) Richeldi, L.; Collard, H. R.; Jones, M. G. Idiopathic Pulmonary Fibrosis. *Lancet* **2017**, 389, 1941–1952.
- (2) Bargagli, E.; Piccioli, C.; Rosi, E.; Torricelli, E.; Turi, L.; Piccioli, E.; Pistolesi, M.; Ferrari, K.; Voltolini, L. Pirfenidone and Nintedanib in Idiopathic Pulmonary Fibrosis: Real-Life Experience in an Italian Referral Centre. *Pulmonology* **2019**, 25, 149–153.
- (3) Selman, M.; King, T. E., Jr.; Pardo, A. Idiopathic Pulmonary Fibrosis: Prevailing and Evolving Hypotheses about Its Pathogenesis and Implications for Therapy. *Ann. Intern. Med.* **2001**, 134, 136–151.
- (4) Chakraborty, S.; Chopra, P.; Ambi, S. V.; Dastidar, S. G.; Ray, A. Emerging Therapeutic Interventions for Idiopathic Pulmonary Fibrosis. *Expert Opin. Invest. Drugs* **2014**, 23, 893–910.
- (5) Richeldi, L.; du Bois, R. M.; Raghu, G.; Azuma, A.; Brown, K. K.; Costabel, U.; Cottin, V.; Flaherty, K. R.; Hansell, D. M.; Inoue, Y.; Kim, D. S.; Kolb, M.; Nicholson, A. G.; Noble, P. W.; Selman, M.; Taniguchi, H.; Brun, M.; Le Maulf, F.; Girard, M.; Stowasser, S.; Schlenker-Herceg, R.; Disse, B.; Collard, H. R. Efficacy and Safety of Nintedanib in Idiopathic Pulmonary Fibrosis. *N. Engl. J. Med.* **2014**, 370, 2071–2082.
- (6) King, T. E.; Bradford, W. Z.; Castro-Bernardini, S.; Fagan, E. A.; Glaspole, I.; Glassberg, M. K.; Gorina, E.; Hopkins, P. M.; Kardatzke, D.; Lancaster, L.; Lederer, D. J.; Nathan, S. D.; Pereira, C. A.; Sahn, S. A.; Sussman, R.; Swigris, J. J.; Noble, P. W. A Phase 3 Trial of Pirfenidone in Patients with Idiopathic Pulmonary Fibrosis. *N. Engl. J. Med.* **2014**, 370, 2083–2092.
- (7) Brindisi, M.; Saraswati, A. P.; Brogi, S.; Gemma, S.; Butini, S.; Campiani, G. Old but Gold: Tracking the New Guise of Histone Deacetylase 6 (HDAC6) Enzyme as a Biomarker and Therapeutic Target in Rare Diseases. *J. Med. Chem.* **2020**, 63, 23–39.
- (8) Wang, X. X.; Wan, R. Z.; Liu, Z. P. Recent Advances in the Discovery of Potent and Selective HDAC6 Inhibitors. *Eur. J. Med. Chem.* **2018**, 143, 1406–1418.
- (9) Roche, J.; Bertrand, P. Inside HDACs with More Selective HDAC Inhibitors. *Eur. J. Med. Chem.* **2016**, 121, 451–483.
- (10) Yang, F.; Zhao, N.; Ge, D.; Chen, Y. Next-Generation of Selective Histone Deacetylase Inhibitors. *RSC Adv.* **2019**, 9, 19571–19583.
- (11) Chuang, D. M.; Leng, Y.; Marinova, Z.; Kim, H. J.; Chiu, C. T. Multiple Roles of HDAC Inhibition in Neurodegenerative Conditions. *Trends Neurosci.* **2009**, 32, 591–601.
- (12) Landucci, E.; Brindisi, M.; Bianciardi, L.; Catania, L. M.; Daga, S.; Croci, S.; Frullanti, E.; Fallerini, C.; Butini, S.; Brogi, S.; Furini, S.; Melani, R.; Molinaro, A.; Lorenzetti, F. C.; Imperatore, V.; Amabile, S.; Mariani, J.; Mari, F.; Ariani, F.; Pizzorusso, T.; Pinto, A. M.; Vaccaro, F. M.; Renieri, A.; Campiani, G.; Meloni, I. iPSC-Derived Neurons Profiling Reveals GABAergic Circuit Disruption and Acetylated α -Tubulin Defect Which Improves after HDAC6 Treatment in Rett Syndrome. *Exp. Cell Res.* **2018**, 368, 225–235.
- (13) Ropero, S.; Esteller, M. The Role of Histone Deacetylases (HDACs) in Human Cancer. *Mol. Oncol.* **2007**, 1, 19–25.
- (14) Qin, H. T.; Li, H. Q.; Liu, F. Selective Histone Deacetylase Small Molecule Inhibitors: Recent Progress and Perspectives. *Expert Opin. Ther. Pat.* **2017**, 27, 621–636.
- (15) Mai, A.; Massa, S.; Rotili, D.; Cerbara, I.; Valente, S.; Pezzi, R.; Simeoni, S.; Ragno, R. Histone Deacetylation in Epigenetics: An Attractive Target for Anticancer Therapy. *Med. Res. Rev.* **2005**, 25, 261–309.
- (16) Lyu, X.; Hu, M.; Peng, J.; Zhang, X.; Sanders, Y. Y. HDAC Inhibitors as Antifibrotic Drugs in Cardiac and Pulmonary Fibrosis. *Ther. Adv. Chronic Dis.* **2019**, 10, No. 204062231986269.

- (17) Shan, B.; Yao, T. P.; Nguyen, H. T.; Zhuo, Y.; Levy, D. R.; Klingsberg, R. C.; Tao, H.; Palmer, M. L.; Holder, K. N.; Lasky, J. A. Requirement of HDAC6 for Transforming Growth Factor- β -Induced Epithelial-Mesenchymal Transition. *J. Biol. Chem.* **2008**, *283*, 21065–21073.
- (18) Valenzuela, C.; Torrisi, S. E.; Kahn, N.; Quaresma, M.; Stowasser, S.; Kreuter, M. Ongoing Challenges in Pulmonary Fibrosis and Insights from the Nintedanib Clinical Programme. *Respir. Res.* **2020**, *21*, No. 7.
- (19) Thiery, J. P.; Sleeman, J. P. Complex Networks Orchestrate Epithelial–Mesenchymal Transitions. *Nat. Rev. Mol. Cell Biol.* **2006**, *7*, 131–142.
- (20) Zavadil, J.; Böttinger, E. P. TGF- β and Epithelial-to-Mesenchymal Transitions. *Oncogene* **2005**, *24*, 5764–5774.
- (21) Conforti, F.; Davies, E. R.; Calderwood, C. J.; Thatcher, T. H.; Jones, M. G.; Smart, D. E.; Mahajan, S.; Alzetani, A.; Havelock, T.; Maher, T. M.; Molyneaux, P. L.; Thorley, A. J.; Tetley, T. D.; Warner, J. A.; Packham, G.; Ganesan, A.; Skipp, P. J.; Marshall, B. J.; Richeldi, L.; Sime, P. J.; O'Reilly, K. M. A.; Davies, D. E. The Histone Deacetylase Inhibitor, Romidepsin, as a Potential Treatment for Pulmonary Fibrosis. *Oncotarget* **2017**, *8*, 48737–48754.
- (22) Korfei, M.; Stelmaszek, D.; MacKenzie, B. A.; Skwarna, S.; Chillappagari, S.; Bach, A. C.; Ruppert, C.; Saito, S.; Mahavadi, P.; Klepetko, W.; Fink, L.; Seeger, W.; Lasky, J. A.; Pullamsetti, S. S.; Krämer, O. H.; Guenther, A. Comparison of the Antifibrotic Effects of the Pan-Histone Deacetylase-Inhibitor Panobinostat versus the IPF-Drug Pirfenidone in Fibroblasts from Patients with Idiopathic Pulmonary Fibrosis. *PLoS One* **2018**, *13*, No. e0207915.
- (23) Wang, Z.; Chen, C.; Finger, S. N.; d/o Kwajah, M. M. S.; Jung, M.; Schwarz, H.; Swanson, N.; Lareu, R. R.; Raghunath, M. Suberoylanilide Hydroxamic Acid: A Potential Epigenetic Therapeutic Agent for Lung Fibrosis? *Eur. Respir. J.* **2009**, *34*, 145–155.
- (24) Saito, S.; Zhuang, Y.; Shan, B.; Danchuk, S.; Luo, F.; Korfei, M.; Guenther, A.; Lasky, J. Tubastatin Ameliorates Pulmonary Fibrosis by Targeting the TGF β -PI3K-Akt Pathway. *PLoS One* **2017**, *12*, No. e0186615.
- (25) Bruserud, O.; Stapnes, C.; Ersvær, E.; Gjertsen, B.; Rynningen, A. Histone Deacetylase Inhibitors in Cancer Treatment: A Review of the Clinical Toxicity and the Modulation of Gene Expression in Cancer Cells. *Curr. Pharm. Biotechnol.* **2007**, *8*, 388–400.
- (26) Thomas, E. A. Focal Nature of Neurological Disorders Necessitates Isotype-Selective Histone Deacetylase (HDAC) Inhibitors. *Mol. Neurobiol.* **2009**, *40*, 33–45.
- (27) Yoon, S.; Kang, G.; Eom, G. H. HDAC Inhibitors: Therapeutic Potential in Fibrosis-Associated Human Diseases. *Int. J. Mol. Sci.* **2019**, *20*, 1329.
- (28) Brindisi, M.; Senger, J.; Cavella, C.; Grillo, A.; Chemi, G.; Gemma, S.; Cucinella, D. M.; Lamponi, S.; Sarno, F.; Iside, C.; Nebbioso, A.; Novellino, E.; Shaik, T. B.; Romier, C.; Herp, D.; Jung, M.; Butini, S.; Campiani, G.; Altucci, L.; Brogi, S. Novel Spiroindoline HDAC Inhibitors: Synthesis, Molecular Modeling and Biological Studies. *Eur. J. Med. Chem.* **2018**, *157*, 127–138.
- (29) Brindisi, M.; Cavella, C.; Brogi, S.; Nebbioso, A.; Senger, J.; Maramai, S.; Ciotta, A.; Iside, C.; Butini, S.; Lamponi, S.; Novellino, E.; Altucci, L.; Jung, M.; Campiani, G.; Gemma, S. Phenylpyrrole-Based HDAC Inhibitors: Synthesis, Molecular Modeling and Biological Studies. *Future Med. Chem.* **2016**, *8*, 1573–1587.
- (30) Saccoccia, F.; Brindisi, M.; Gimmelli, R.; Relitti, N.; Guidi, A.; Saraswati, A. P.; Cavella, C.; Brogi, S.; Chemi, G.; Butini, S.; Papoff, G.; Senger, J.; Herp, D.; Jung, M.; Campiani, G.; Gemma, S.; Ruberti, G. Screening and Phenotypical Characterization of Schistosoma Mansoni Histone Deacetylase 8 (SmHDAC8) Inhibitors as Multistage Antischistosomal Agents. *ACS Infect. Dis.* **2020**, *6*, 100–113.
- (31) Saraswati, A. P.; Relitti, N.; Brindisi, M.; Osko, J. D.; Chemi, G.; Federico, S.; Grillo, A.; Brogi, S.; McCabe, N. H.; Turkington, R. C.; Ibrahim, O.; O'Sullivan, J.; Lamponi, S.; Ghanim, M.; Kelly, V. P.; Zisterer, D.; Amet, R.; Hannon Barroeta, P.; Vanni, F.; Ulivieri, C.; Herp, D.; Sarno, F.; Di Costanzo, A.; Saccoccia, F.; Ruberti, G.; Jung, M.; Altucci, L.; Gemma, S.; Butini, S.; Christianson, D. W.; Campiani, G. Spiroindoline-Capped Selective HDAC6 Inhibitors: Design, Synthesis, Structural Analysis, and Biological Evaluation. *ACS Med. Chem. Lett.* **2020**, *11*, 2268–2276.
- (32) Relitti, N.; Saraswati, A. P.; Chemi, G.; Brindisi, M.; Brogi, S.; Herp, D.; Schmidtkunz, K.; Saccoccia, F.; Ruberti, G.; Ulivieri, C.; Vanni, F.; Sarno, F.; Altucci, L.; Lamponi, S.; Jung, M.; Gemma, S.; Butini, S.; Campiani, G. Novel Quinolone-Based Potent and Selective HDAC6 Inhibitors: Synthesis, Molecular Modeling Studies and Biological Investigation. *Eur. J. Med. Chem.* **2021**, *212*, No. 112998.
- (33) Hai, Y.; Christianson, D. W. Histone Deacetylase 6 Structure and Molecular Basis of Catalysis and Inhibition. *Nat. Chem. Biol.* **2016**, *12*, 741–747.
- (34) Chakrabarti, A.; Oehme, I.; Witt, O.; Oliveira, G.; Sippl, W.; Romier, C.; Pierce, R. J.; Jung, M. HDAC8: A Multifaceted Target for Therapeutic Interventions. *Trends Pharmacol. Sci.* **2015**, *36*, 481–492.
- (35) Ho, T. C. S.; Chan, A. H. Y.; Ganesan, A. Thirty Years of HDAC Inhibitors: 2020 Insight and Hindsight. *J. Med. Chem.* **2020**, *63*, 12460–12484.
- (36) Potts, P. R.; Yu, H. The SMC5/6 Complex Maintains Telomere Length in ALT Cancer Cells through SUMOylation of Telomere-Binding Proteins. *Nat. Struct. Mol. Biol.* **2007**, *14*, 581–590.
- (37) Prasse, A.; Binder, H.; Schupp, J. C.; Kayser, G.; Bargagli, E.; Jaeger, B.; Hess, M.; Rittinghausen, S.; Vuga, L.; Lynn, H.; Violette, S.; Jung, B.; Quast, K.; Vanaudenaerde, B.; Xu, Y.; Hohlfeld, J. M.; Krug, N.; Herazo-Maya, J. D.; Rottoli, P.; Wuyts, W. A.; Kaminski, N. BAL Cell Gene Expression Is Indicative of Outcome and Airway Basal Cell Involvement in Idiopathic Pulmonary Fibrosis. *Am. J. Respir. Crit. Care Med.* **2019**, *199*, 622–630.
- (38) Prasse, A.; Carleo, A.; Jaeger, B.; Schupp, J.; Rottoli, P.; Wuyts, W.; Kaminski, N. BAL Cell Transcriptome Predicts Survival in IPF and Can Be Used to Gauge and Model Treatment Effects Interfering with the TGF- β Pathway. *Eur. Respir. J.* **2018**, *52*, No. OA5359.
- (39) Jaeger, B.; Schupp, J. C.; Plappert, L.; Terwolbeck, O.; Kayser, G.; Engelhard, P.; Adams, T. S.; Zweigerdt, R.; Kempf, H.; Lienenklaus, S.; Garrels, W.; Nazarenko, I.; Jonigk, D.; Wygrecka, M.; Klatt, D.; Schambach, A.; Kaminski, N.; Prasse, A. Airway Basal Cells Show a Dedifferentiated KRT17^{high} Phenotype and Promote Fibrosis in Idiopathic Pulmonary Fibrosis. *bioRxiv* **2020**, DOI: 10.1101/2020.09.04.283408.
- (40) Roach, K. M.; Sutcliffe, A.; Matthews, L.; Elliott, G.; Newby, C.; Amrani, Y.; Bradding, P. A Model of Human Lung Fibrogenesis for the Assessment of Anti-Fibrotic Strategies in Idiopathic Pulmonary Fibrosis. *Sci. Rep.* **2018**, *8*, No. 342.
- (41) Gemma, S.; Camodeca, C.; Brindisi, M.; Brogi, S.; Kukreja, G.; Kunjir, S.; Gabellieri, E.; Lucantoni, L.; Habluetzel, A.; Taramelli, D.; Basilio, N.; Gualdani, R.; Tadini-Buoninsegni, F.; Bartolommei, G.; Moncelli, M. R.; Martin, R. E.; Summers, R. L.; Lamponi, S.; Savini, L.; Fiorini, I.; Valoti, M.; Novellino, E.; Campiani, G.; Butini, S. Mimicking the Intramolecular Hydrogen Bond: Synthesis, Biological Evaluation, and Molecular Modeling of Benzoxazines and Quinazolines as Potential Antimalarial Agents. *J. Med. Chem.* **2012**, *55*, 10387–10404.
- (42) Grillo, A.; Chemi, G.; Brogi, S.; Brindisi, M.; Relitti, N.; Fezza, F.; Fazio, D.; Castelletti, L.; Perdoni, E.; Wong, A.; Lamponi, S.; Pecorelli, A.; Benedusi, M.; Fantacci, M.; Valoti, M.; Valacchi, G.; Micheli, F.; Novellino, E.; Campiani, G.; Butini, S.; Maccarrone, M.; Gemma, S. Development of Novel Multipotent Compounds Modulating Endocannabinoid and Dopaminergic Systems. *Eur. J. Med. Chem.* **2019**, *183*, No. 111674.
- (43) Williamson, B.; Wilson, C.; Dagnell, G.; Riley, R. J. Harmonised High Throughput Microsomal Stability Assay. *J. Pharmacol. Toxicol. Methods* **2017**, *84*, 31–36.
- (44) Xu, Q.; Liu, C.; Zang, J.; Gao, S.; Chou, C. J.; Zhang, Y. Discovery of a Novel Hybrid of Vorinostat and Riluzole as a Potent Antitumor Agent. *Front. Cell Dev. Biol.* **2020**, *8*, 454.
- (45) Skipper, P. L.; Tannenbaum, S. R.; Thilly, W. G.; Furth, E. E.; Bishop, W. W. Mutagenicity of Hydroxamic Acids and the Probable Involvement of Carbamoylation. *Cancer Res.* **1980**, *40*, 4704–4708.

- (46) Shen, S.; Kozikowski, A. P. Why Hydroxamates May Not Be the Best Histone Deacetylase Inhibitors—What Some May Have Forgotten or Would Rather Forget? *ChemMedChem* **2016**, *11*, 15–21.
- (47) Caballero, M. V.; Candiracci, M. Zebrafish as Toxicological Model for Screening and Recapitulate Human Diseases. *J. Unexplored Med. Data* **2018**, *3*, 4.
- (48) Fusi, F.; Durante, M.; Gorelli, B.; Perrone, M. G.; Colabufo, N. A.; Saponara, S. MC225, a Novel Probe for P-Glycoprotein PET Imaging at the Blood–Brain Barrier: In Vitro Cardiovascular Safety Evaluation. *J. Cardiovasc. Pharmacol.* **2017**, *70*, 405–410.
- (49) Brindisi, M.; Maramai, S.; Gemma, S.; Brogi, S.; Grillo, A.; Di Cesare Mannelli, L.; Gabellieri, E.; Lamponi, S.; Saponara, S.; Gorelli, B.; Tedesco, D.; Bonfiglio, T.; Landry, C.; Jung, K.-M.; Armirotti, A.; Luongo, L.; Ligresti, A.; Piscitelli, F.; Bertucci, C.; Dehouck, M.-P.; Campiani, G.; Maione, S.; Ghelardini, C.; Pittaluga, A.; Piomelli, D.; Di Marzo, V.; Butini, S. Development and Pharmacological Characterization of Selective Blockers of 2-Arachidonoyl Glycerol Degradation with Efficacy in Rodent Models of Multiple Sclerosis and Pain. *J. Med. Chem.* **2016**, *59*, 2612–2632.
- (50) Halgren, T. A. MMFF VI. MMFF94s Option for Energy Minimization Studies. *J. Comput. Chem.* **1999**, *20*, 720–729.
- (51) Irvine, C. A. *Spartan '02*; Wavefunction, Inc., 2002.
- (52) Frisch, M. J.; Trucks, G. W.; Schlegel, H. B.; Scuseria, G. E.; Robb, M. A.; Cheeseman, J. R.; Scalmani, G.; Barone, V.; Mennucci, B.; Petersson, G. A.; Nakatsuji, H.; Caricato, M.; Li, X.; Hratchian, H. P.; Izmaylov, A. F.; Bloino, J.; Zheng, G.; Sonnenberg, J. L. D. *J. Gaussian09*, revision D.01; Gaussian, Inc.: Wallingford CT, 2010.
- (53) Grimme, S. Semiempirical GGA-Type Density Functional Constructed with a Long-Range Dispersion Correction. *J. Comput. Chem.* **2006**, *27*, 1787–1799.
- (54) Weigend, F.; Ahlrichs, R. Balanced Basis Sets of Split Valence, Triple Zeta Valence and Quadruple Zeta Valence Quality for H to Rn: Design and Assessment of Accuracy. *Phys. Chem. Chem. Phys.* **2005**, *7*, 3297–3305.
- (55) Weigend, F. Accurate Coulomb-Fitting Basis Sets for H to Rn. *Phys. Chem. Chem. Phys.* **2006**, *8*, 1057–1065.
- (56) Tomasi, J.; Mennucci, B.; Cancès, E. The IEF Version of the PCM Solvation Method: An Overview of a New Method Addressed to Study Molecular Solutes at the QM Ab Initio Level. *J. Mol. Struct.: THEOCHEM* **1999**, *464*, 211–226.
- (57) Perdew, J. P.; Burke, K.; Ernzerhof, M. Generalized Gradient Approximation Made Simple. *Phys. Rev. Lett.* **1996**, *77*, 3865–3868.
- (58) Adamo, C.; Barone, V. Toward Reliable Density Functional Methods without Adjustable Parameters: The PBE0 Model. *J. Chem. Phys.* **1999**, *110*, 6158–6170.
- (59) Stephens, P. J.; Harada, N. ECD Cotton Effect Approximated by the Gaussian Curve and Other Methods. *Chirality* **2009**, *22*, 229–233.
- (60) Osko, J. D.; Christianson, D. W. Methods for the Expression, Purification, and Crystallization of Histone Deacetylase 6-Inhibitor Complexes. In *Methods in Enzymology*; Elsevier, 2019; Vol. 626, pp 447–474.
- (61) Winn, M. D.; Ballard, C. C.; Cowtan, K. D.; Dodson, E. J.; Emsley, P.; Evans, P. R.; Keegan, R. M.; Krissinel, E. B.; Leslie, A. G. W.; McCoy, A.; et al. Overview of the CCP4 Suite and Current Developments. *Acta Crystallogr., Sect. D: Biol. Crystallogr.* **2011**, *67*, 235–242.
- (62) Battye, T. G. G.; Kontogiannis, L.; Johnson, O.; Powell, H. R.; Leslie, A. G. W. IMOSFLM: A New Graphical Interface for Diffraction-Image Processing with MOSFLM. *Acta Crystallogr., Sect. D: Biol. Crystallogr.* **2011**, *67*, 271–281.
- (63) Evans, P. R.; Murshudov, G. N. How Good Are My Data and What Is the Resolution? *Acta Crystallogr., Sect. D: Biol. Crystallogr.* **2013**, *69*, 1204–1214.
- (64) McCoy, A. J.; Grosse-Kunstleve, R. W.; Adams, P. D.; Winn, M. D.; Storoni, L. C.; Read, R. J. Phaser Crystallographic Software. *J. Appl. Crystallogr.* **2007**, *40*, 658–674.
- (65) Emsley, P.; Lohkamp, B.; Scott, W. G.; Cowtan, K. Features and Development of Coot. *Acta Crystallogr., Sect. D: Biol. Crystallogr.* **2010**, *66*, 486–501.
- (66) Adams, P. D.; Afonine, P. V.; Bunkóczi, G.; Chen, V. B.; Davis, I. W.; Echols, N.; Headd, J. J.; Hung, L.-W.; Kapral, G. J.; Grosse-Kunstleve, R. W. PHENIX: A Comprehensive Python-Based System for Macromolecular Structure Solution. *Acta Crystallogr., Sect. D: Biol. Crystallogr.* **2010**, *66*, 213–221.
- (67) Chen, V. B.; Arendall, W. B.; Headd, J. J.; Keedy, D. A.; Immormino, R. M.; Kapral, G. J.; Murray, L. W.; Richardson, J. S.; Richardson, D. C. MolProbity: All-Atom Structure Validation for Macromolecular Crystallography. *Acta Crystallogr., Sect. D: Biol. Crystallogr.* **2010**, *66*, 12–21.
- (68) Millard, C. J.; Watson, P. J.; Celardo, I.; Gordiyenko, Y.; Cowley, S. M.; Robinson, C. V.; Fairall, L.; Schwabe, J. W. R. Class I HDACs Share a Common Mechanism of Regulation by Inositol Phosphates. *Mol. Cell* **2013**, *51*, 57–67.
- (69) Brogi, S.; Fiorillo, A.; Chemi, G.; Butini, S.; Lalle, M.; Ilari, A.; Gemma, S.; Campiani, G. Structural Characterization of Giardia Duodenalis Thioredoxin Reductase (GTrxR) and Computational Analysis of Its Interaction with NBDHEX. *Eur. J. Med. Chem.* **2017**, *135*, 479–490.
- (70) Paolino, M.; Brindisi, M.; Vallone, A.; Butini, S.; Campiani, G.; Nannicini, C.; Giuliani, G.; Anzini, M.; Lamponi, S.; Giorgi, G.; Sbardella, D.; Ferraris, D. M.; Marini, S.; Coletta, M.; Palucci, I.; Minerva, M.; Delogu, G.; Pepponi, I.; Goletti, D.; Cappelli, A.; Gemma, S.; Brogi, S. Development of Potent Inhibitors of the Mycobacterium Tuberculosis Virulence Factor Zmp1 and Evaluation of Their Effect on Mycobacterial Survival inside Macrophages. *ChemMedChem* **2018**, *13*, 422–430.
- (71) Wu, R.; Lu, Z.; Cao, Z.; Zhang, Y. Zinc Chelation with Hydroxamate in Histone Deacetylases Modulated by Water Access to the Linker Binding Channel. *J. Am. Chem. Soc.* **2011**, *133*, 6110–6113.
- (72) Zhou, J.; Wu, R.; Luo, H.-B. Inhibition Mechanism of SAHA in HDAC: A Revisit. *Phys. Chem. Chem. Phys.* **2015**, *17*, 29483–29488.
- (73) Ganai, S. A.; Farooq, Z.; Bandy, S.; Altaf, M. In Silico Approaches for Investigating the Binding Propensity of Apigenin and Luteolin against Class I HDAC Isoforms. *Future Med. Chem.* **2018**, *10*, 1925–1945.
- (74) Pottel, J.; Therrien, E.; Gleason, J. L.; Moitessier, N. Docking Ligands into Flexible and Solvated Macromolecules. 6. Development and Application to the Docking of HDACs and Other Zinc Metalloenzymes Inhibitors. *J. Chem. Inf. Model.* **2014**, *54*, 254–265.
- (75) Bieliauskas, A. V.; Weerasinghe, S. V. W.; Negmeldin, A. T.; Plüm, M. K. H. Structural Requirements of Histone Deacetylase Inhibitors: SAHA Analogs Modified on the Hydroxamic Acid. *Arch. Pharm. Chem. Life Sci.* **2016**, *349*, 373–382.
- (76) Heltweg, B.; Dequiedt, F.; Verdin, E.; Jung, M. Nonisotopic Substrate for Assaying Both Human Zinc and NAD⁺-Dependent Histone Deacetylases. *Anal. Biochem.* **2003**, *319*, 42–48.
- (77) Wegener, D.; Wirsching, F.; Riester, D.; Schwienhorst, A. A Fluorogenic Histone Deacetylase Assay Well Suited for High-Throughput Activity Screening. *Chem. Biol.* **2003**, *10*, 61–68.
- (78) Heltweg, B.; Trapp, J.; Jung, M. In Vitro Assays for the Determination of Histone Deacetylase Activity. *Methods* **2005**, *36*, 332–337.
- (79) Marek, M.; Shaik, T. B.; Heimbürg, T.; Chakrabarti, A.; Lancelot, J.; Ramos-Morales, E.; Da Veiga, C.; Kalinin, D.; Melesina, J.; Robaa, D.; Schmidtkunz, K.; Suzuki, T.; Holl, R.; Ennifar, E.; Pierce, R. J.; Jung, M.; Sippl, W.; Romier, C. Characterization of Histone Deacetylase 8 (HDAC8) Selective Inhibition Reveals Specific Active Site Structural and Functional Determinants. *J. Med. Chem.* **2018**, *61*, 10000–10016.
- (80) Copeland, R. A. *Reversible Inhibitors*; Wiley Online Books; 2000. <https://doi.org/doi:10.1002/0471220639.ch8>.
- (81) Raghu, G.; Collard, H. R.; Egan, J. J.; Martinez, F. J.; Behr, J.; Brown, K. K.; Colby, T. V.; Cordier, J.-F.; Flaherty, K. R.; Lasky, J. A.; Lynch, D. A.; Ryu, J. H.; Swigris, J. J.; Wells, A. U.; Ancochea, J.; Bours, D.; Carvalho, C.; Costabel, U.; Ebina, M.; Hansell, D. M.; Johkoh, T.; Kim, D. S.; King, T. E.; Kondoh, Y.; Myers, J.; Müller, N. L.; Nicholson, A. G.; Richeldi, L.; Selman, M.; Dudden, R. F.; Griss, B. S.; Protzko, S. L.; Schünemann, H. J. An Official ATS/ERS/JRS/ALAT Statement: Idiopathic Pulmonary Fibrosis: Evidence-Based Guidelines for

Diagnosis and Management. *Am. J. Respir. Crit. Care Med.* **2011**, *183*, 788–824.

(82) Idiopathic Pulmonary Fibrosis: Diagnosis and Treatment. *Am. J. Respir. Crit. Care Med.* **2000**, *161*, 646–664.

(83) American Thoracic Society/European Respiratory Society International Multidisciplinary Consensus Classification of the Idiopathic Interstitial Pneumonias. *Am. J. Respir. Crit. Care Med.* **2002**, *165*, 277–304.

(84) Prasse, A.; Binder, H.; Schupp, J. C.; Kayser, G.; Bargagli, E.; Jaeger, B.; Hess, M.; Rittinghausen, S.; Vuga, L.; Lynn, H.; Violette, S.; Jung, B.; Quast, K.; Vanaudenaerde, B.; Xu, Y.; Hohlfeld, J. M.; Krug, N.; Herazo-Maya, J. D.; Rottoli, P.; Wuyts, W. A.; Kaminski, N. BAL Cell Gene Expression Is Indicative of Outcome and Airway Basal Cell Involvement in Idiopathic Pulmonary Fibrosis. *Am. J. Respir. Crit. Care Med.* **2019**, *199*, 622–630.

(85) Hackett, N. R.; Butler, M. W.; Shaykhiev, R.; Salit, J.; Omberg, L.; Rodriguez-Flores, J. L.; Mezey, J. G.; Strulovici-Barel, Y.; Wang, G.; Didon, L.; Crystal, R. G. RNA-Seq Quantification of the Human Small Airway Epithelium Transcriptome. *BMC Genomics* **2012**, *13*, 82.

(86) Prasse, A.; Pechkovsky, D. V.; Toews, G. B.; Jungraithmayr, W.; Kollert, F.; Goldmann, T.; Vollmer, E.; Müller-Quernheim, J.; Zissel, G. A Vicious Circle of Alveolar Macrophages and Fibroblasts Perpetuates Pulmonary Fibrosis via CCL18. *Am. J. Respir. Crit. Care Med.* **2006**, *173*, 781–792.

(87) Roach, K. M.; Duffy, S. M.; Coward, W.; Feghali-Bostwick, C.; Wulff, H.; Bradding, P. The K⁺ Channel KCa3.1 as a Novel Target for Idiopathic Pulmonary Fibrosis. *PLoS One* **2014**, *9*, No. e85244.

(88) D'Elia, P.; De Matteis, F.; Dragoni, S.; Shah, A.; Sgaragli, G.; Valoti, M. DP7, a Novel Dihydropyridine Multidrug Resistance Reverter, Shows Only Weak Inhibitory Activity on Human CYP3A Enzyme(S). *Eur. J. Pharmacol.* **2009**, *614*, 7–13.

(89) Lamponi, S.; Aloisi, A. M.; Bonechi, C.; Consumi, M.; Donati, A.; Leone, G.; Rossi, C.; Tamasi, G.; Ghiandai, L.; Ferrini, E.; Fiorenzani, P.; Ceccarelli, I.; Magnani, A. Evaluation of in Vitro Cell and Blood Compatibility and in Vivo Analgesic Activity of Plant-Derived Dietary Supplements. *J. Integr. Med.* **2019**, *17*, 213–220.

(90) Sundaramurthi, H.; Roche, S. L.; Grice, G. L.; Moran, A.; Dillion, E. T.; Campiani, G.; Nathan, J. A.; Kennedy, B. N. Selective Histone Deacetylase 6 Inhibitors Restore Cone Photoreceptor Vision or Outer Segment Morphology in Zebrafish and Mouse Models of Retinal Blindness. *Front. Cell Dev. Biol.* **2020**, *8*, 689.

(91) Pessina, F.; Gamberucci, A.; Chen, J.; Liu, B.; Vangheluwe, P.; Gorelli, B.; Lorenzini, S.; Spiga, O.; Trezza, A.; Sgaragli, G.; Saponara, S. Negative Chronotropism, Positive Inotropism and Lusitropism of 3,5-Di-*t*-Butyl-4-Hydroxyanisole (DTBHA) on Rat Heart Preparations Occur through Reduction of RyR₂ Ca²⁺ Leak. *Biochem. Pharmacol.* **2018**, *155*, 434–443.

(92) Ferrara, A.; Fusi, F.; Gorelli, B.; Sgaragli, G.; Saponara, S. Effects of Freeze-Dried Red Wine on Cardiac Function and ECG of the Langendorff-Perfused Rat Heart. *Can. J. Physiol. Pharmacol.* **2014**, *92*, 171–174.